IEKP-KA/2014-16

Comparative studies of Monte Carlo event generation in leading order and next-to-leading order for the CMS collaboration

Marco Alexander Harrendorf

Master Thesis

At the Department of Physics
Institut für Experimentelle Kernphysik (IEKP)

Referee:	Prof. Dr. Ulrich Husemann
Second referee:	Prof. Dr. Thomas Müller

Karlsruhe, 18 December 2014

This page intentionally left blank.

Accepted by the first referee of the master thesis.
Karlsruhe, 18 December 2014

. . . .
(**Prof. Dr. Ulrich Husemann**)

This page intentionally left blank.

I declare that I have developed and written the enclosed thesis completely by myself, and have not used sources or means without declaration in the text.

Karlsruhe, 18 December 2014

. . . .
(**Marco Alexander Harrendorf**)

This page intentionally left blank.

Contents

This page intentionally left blank.

1. Introduction

The topic of this master thesis will be the modelling of the pp $\rightarrow t\bar{t}$ and the pp $\rightarrow t\bar{t}H$ processes in particle collisions in the Compact Muon Solenoid (CMS) detector at the Large Hadron Collider (LHC) by event generation. It is part of the research of the Compact Muon Solenoid (CMS) Collaboration.

Event generation is the most powerful tool for validating the Standard Model of particle physics by predicting how particles and physics processes should behave if our current concept of nature is accurate. The comparison of simulation data generated with event generators with data from real particle detectors leads both to better understanding of the physics processes under study themselves and to either a verification or extension of the Standard Model. Emphasis in this thesis lies on event generation studies using Monte Carlo (MC) methods and on comparisons of event generation done in leading order (LO) and next-to-leading order (NLO) of perturbation theory. Different Monte Carlo event generators and various parameter sets were employed in this context. In many cases the tools of the CMS software framework (CMSSW) were used during the event generation step and also during the subsequent analysis step. In addition, further event samples were produced by using the event generators in combination with some tools developed in our group.

In the following section, chapter 2, the motivation for the studies presented on the subsequent pages will be discussed, including common practices in particle physics research. In chapter 3 the theoretical foundations of the Standard Model of particle physics are presented: First, the particles themselves are introduced and in the second subsection the three known interactions of the Standard Model are explained. The subject of interest in chapter 4 is the Monte Carlo event generation itself. The chapter includes an introduction into the historical background of the Monte Carlo method, the theoretical principles of event generation by applying Monte Carlo methods and the steps needed in event generation. The various types of event generators are explained briefly. Moreover, the chapter gives a short overview of the merging techniques used in this thesis to combine LO or NLO matrix element event generators with the parton showers contained in general-purpose Monte Carlo (GPMC) event generators and about the parameters and scales which are important for such a merging. In chapter 5 a brief account of the experimental basics is given, which begins with comments on the European Organization for Nuclear Research (CERN), the Large Hardon Collider (LHC) and the Compact Muon Solenoid (CMS) detector, for which the analyses following in the last chapters were carried out. The topic of chapter 6 are cross section calculations in LO and NLO of the pp $\rightarrow t\bar{t}H$ process, and in chapter 7, a comparison of LO and NLO event generation of the pp $\rightarrow$ $t\bar{t}$+jets process and the pp $\rightarrow$ $t\bar{t}H$+jets process will be the subject of interest. A comparison between event samples of the pp $\rightarrow$ $t\bar{t}$+jets process generated by LO and NLO matrix element generators merged with the parton shower of GPMC event generators and measurement data obtained by the CMS detector in 2012 follows in chapter 8. In chapter 9 a summary and outlook will be given to conclude this thesis, while additional material can be found in the appendix.

2. Motivation

In elementary particle physics the task to fulfill is to test theoretical models, essentially the Standard Model of particle physics. Proving these models or finding deviations from them, which could lead to physics beyond the Standard Model and a new theoretical understanding of nature, is achieved by applying a sequence of steps (called analysis chain) which is shown in figure 2.1.

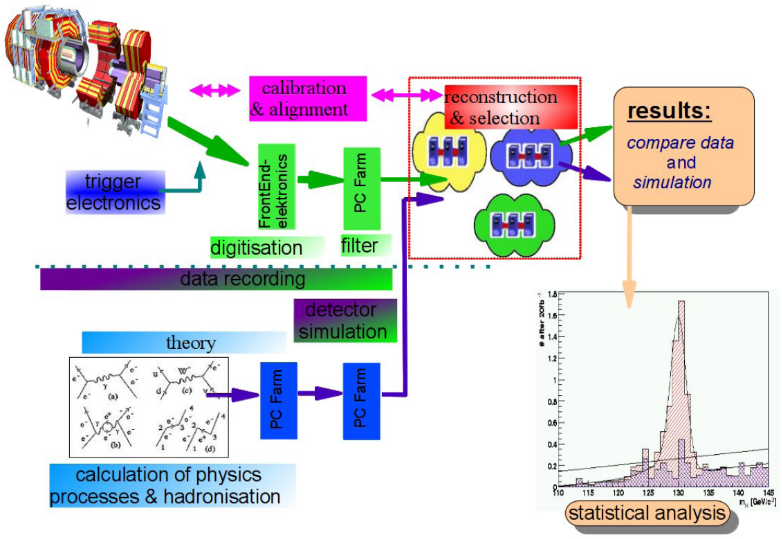

Figure 2.1: Typical analysis chain in elementary particle physics: The analysis chain can be divided in measurement data taking by using a particle detector, generation of event samples based on theoretical models which are further processed by a detector simulation, reconstruction and selection of events contained in the obtained measurement and simulation data, and comparison between measurement data and simulation data in a statistical analysis. Taken from [Qua2013c]

The analysis chain can be divided into several parts:

1a. Measurement data taking by using a particle detector

The measurement data are obtained from a particle detector and have intrinsic uncertainties caused by the detector acceptance, efficiency, and calibration.

1b. Generation of event samples

Simulated event samples are generated by event generators making use of theoretical models (e.g. the Standard Model of particle physics). They only have theoretical uncertainties after the generation step. Furthermore, in order to maintain comparability to the measured data, the detector acceptance and efficiencies have to be taken into account by applying a detector simulation to the generated event samples. Due to convolution of the event samples with the resolution of the detector further uncertainties arise.

2. Reconstruction and selection of events

The events of the measurement data as well as the event of the simulation data undergo the same reconstruction and selection steps to be comparable in a successive analysis.

3. Comparison between measurement and simulation data by making use of a statistical analysis

A comparison between measurement data and simulation data after the reconstruction and selection step can provide first results. However, often the deviation between the two datasets is so small that a more sophisticated statistical analysis is needed to extract underlying physics. Deviations occuring in the statistical analysis can be a clear sign of New Physics or lead to the exclusion of some theoretical models.

Monte Carlo (MC) event generators are applied to generate event samples using theoretical models, as already outlined in part 1b, which are then compared to the measurement data obtained from particle detectors (see part 1a). Both data sets are important ingredients of the analysis chain and in former times the uncertainties of the subsequent statistical analysis were often mainly determined by the uncertainties of the measurement data. However, as a result of progress in measurement techniques and in the development of particle detectors, the uncertainties of the measurement data have been reduced so much that also reducing the uncertainties resulting from theoretical models and introduced by the use of simulation data becomes more and more important. Until now mostly event generators which describe the hard scattering process of a particular physics process in leading order (LO) of perturbation theory have been applied to generate LO event samples. In the recent years new developments and achievements in the field of event generation have made it feasible to use matrix element generators describing the hard scattering process in next-to-leading order (NLO) and combine them with the parton showers of LO GPMC event generators, so that NLO event samples can be obtained. These NLO event samples promise smaller theoretical uncertainties and a better description of the measurement data due to considering the higher-order corrections in the perturbation theory. For that reason, it is a particularly important project in elementary particle physics at the moment to implement the new NLO event generators, to make use of their most advanced techniques, and to test and validate the NLO event generation since the statistical analysis would strongly benefit from improvements in the event generation step.

In the Compact Muon Solenoid (CMS) collaboration the rather old LO matrix element generator MadGraph5 and the LO general-purpose Monte Carlo (GPMC) event generator Pythia6 were used by default to generate event samples of the $\mathrm{pp} \rightarrow \mathrm{t\bar{t}}$ process and of the $\mathrm{pp} \rightarrow \mathrm{t\bar{t}H}$ process required for the analysis of the Run 1 (2010-2012) measurement data of the Large Hadron Collider. In more detail, the $\mathrm{pp} \rightarrow \mathrm{t\bar{t}}$+jets process was simulated by using the MadGraph5 matrix element generator matched with the Pythia6 GPMC event generator. In contrast to that, the $\mathrm{pp} \rightarrow \mathrm{t\bar{t}H}$ process was only described by using the Pythia6 GPMC event generator. In this context it must be said that the pp $\rightarrow t\bar{t}H$ process is an important process to study at the Large Hadron Collider (LHC) since it allows a model-independent measure of the Top-Higgs-Yukawa coupling. However, in contrast to most other Higgs production channels the pp $\rightarrow t\bar{t}H$ process has a very small cross section $\sigma_{t\bar{t}H}$ and it is plagued by backgrounds difficult to determine, with the pp $\rightarrow t\bar{t}$ process being the largest background. A good example of the aforementioned importance to reduce the uncertainty of the simulation data and the corresponding event samples, especially in the pp $\rightarrow t\bar{t}$+jets analysis and the pp $\rightarrow t\bar{t}H$ analysis, is given in figure 2.2. Here the normalised differential $t\bar{t}$ production cross section as a function of the number of jets is represented at a center-of-mass energy of $\sqrt{s} = 7$ TeV obtained in the "measurement of jet multiplicity distributions in $t\bar{t}$ production in p + p collisions at $\sqrt{s} = 7$ TeV" [CMS2014] is shown. It can be clearly seen in subfigure 2.2b that the systematic uncertainties of the LO event sample generated by using the MadGraph5 matrix element event generator matched to the Pythia6 GPMC event generator are of the same order of magnitude as the uncertainties of the measurement data. This analysis of the normalised differential $t\bar{t}$ production cross section as a function of the number of jets will be used later to benchmark NLO event generators with measurement data obtained at a center-of-mass energy of $\sqrt{s} = 8$ TeV.

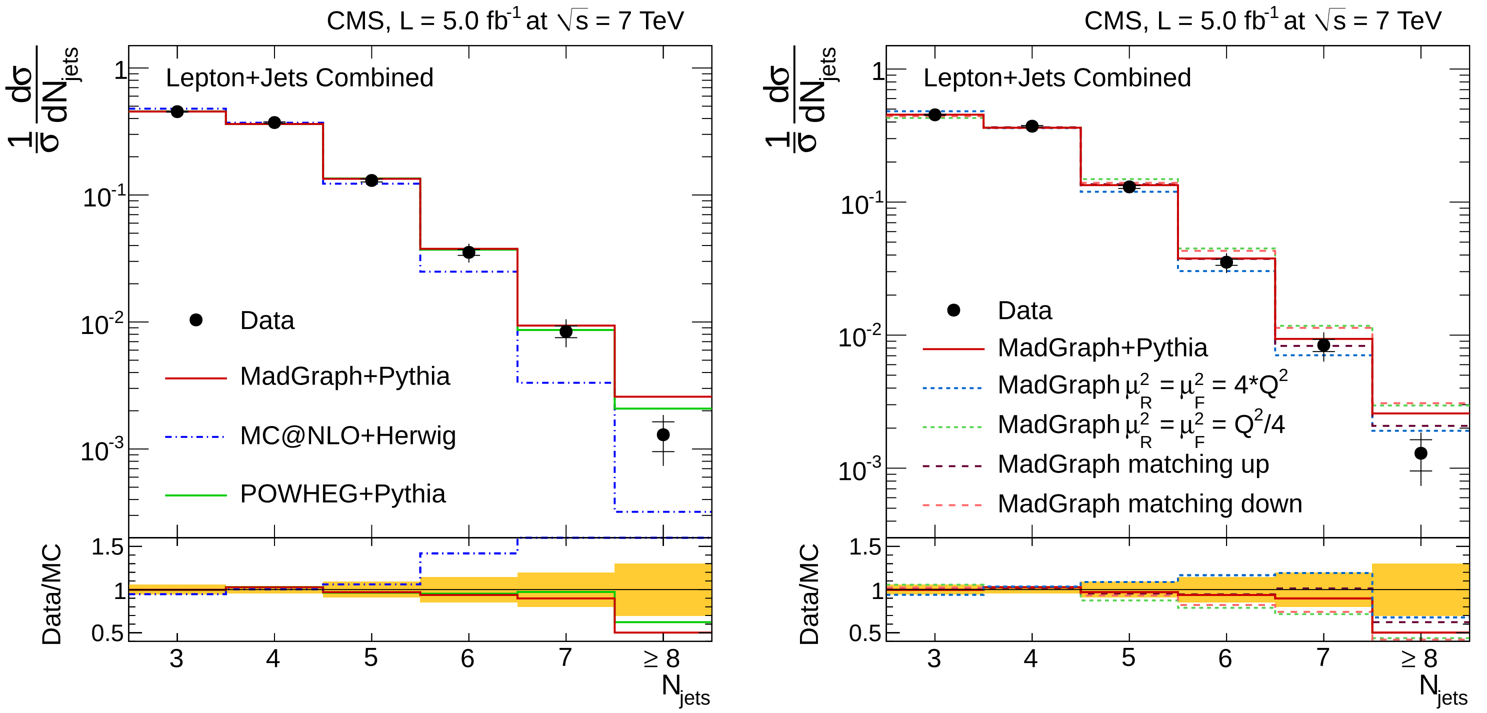

(a) Comparison of measurement data and event samples

(b) Comparison of measurement data and varied LO event sample

Figure 2.2: The normalised differential $t\bar{t}$ production cross section as a function of the number of jets in the lepton+jets channel: The measurement data is compared to predictions from MadGraph5+Pythia6, MC@NLO+Herwig, and POWHEG Box+ Pythia6 (left plot), as well as from MadGraph5+Pythia6 with varied renormalisation and factorization scales, and merging scales (right plot). The inner (outer) error bars indicate the statistical (combined statistical und systematic) uncertainty. The shaded band corresponds to the combined statistical and systematic uncertainty. Taken from [CMS2014]

The CMS collaboration, knowing the various benefits and the few drawbacks of the LO event generators, considers to use NLO event generators for the production of the pp $\rightarrow t\bar{t}$+jets and the pp $\rightarrow t\bar{t}H$ event samples required for the analysis of the Run 2 (Start

2015) measurement data due to the possible improvements of the analysis by the use of NLO event generators. However, before making a decision if either the LO MadGraph5 matrix element generator or the NLO aMC@NLO matrix element generator will be used by default in combination with the Pythia8 GPMC event generator, which supersedes the Pythia6 event generator, a testing and validation campaign was started. The comparisons between LO and NLO event generation, which are described in this thesis and which also include a determination of the normalised differential $t\bar{t}$ production cross section as a function of the number of jets similar to [CMS2014], while using NLO event samples, are part of this ongoing testing and validation campaign. Lastly, it is worth mentioning that a more specific motivation will be given in each chapter.

3. The Standard Model of particle physics

The Standard Model of particle physics (SM) is a theory which unifies the electromagnetic, weak, and strong nuclear interactions and it is based on quantum field theories and local gauge symmetries. In the mid-1970s and the early 1980s the current formulation of SM was finalized upon the experimental confirmation of

- **the existence of quarks** by discovering the J/ψ meson [Aub1974] [Aug1974] and thereby proving the existence of a fourth quark, the charm quark.
- **the correctness of the electroweak theory** [Bil1982] by the discovery of neutral currents in neutrino scattering [Has1973a] [Has1973b] [Has1974] and later by the discovery of the $W^{\pm}$ gauge bosons [Arn1983] [Ban1983] and the Z gauge boson [Arn1983b] [Bag1983].

The Standard Model of particle physics is regarded as the most successful theory of nature in history due to its capability of providing experimentally testable predictions whose correctness could later be verified. For example the discovery of

- **the top quark**, which was predicted 1973 as the up-type quark of the third generation of quarks by Makoto Kobayashi and Toshihide Maskawa to explain the observed violation of the CP symmetry in kaon decay [Kob1973] and which was discovered 1995 at the Tevatron accelerator at Fermi National Acccelerator Laboratory (FNAL) by the CDF and DØ collaborations [Abe1995] [Aba1995].
- **the tau neutrino**, which was postulated as the neutral partner of the tau in the third generation of leptons after the detection of the tau [Per1975] in the mid-1970s and which was discovered 2000 at FNAL by the DONUT collaboration [DON2000] while directing the Tevatron proton beam into a fixed target.
- **the Higgs boson**, which was theorized by Robert Brout, Francois Englert [Eng1964], Peter Higgs [Hig1964a] [Hig1964b], Gerald Guralnik, Carl Richard Hagen, and Tom Kibble [Gur1964] in 1964 and discovered 2012 at the Large Hadron Collider (LHC) by the ATLAS [ATL2012] and CMS [CMS2012a] collaboration.

However, even the huge success of the Standard Model in predicting new particles could not mask the fact that the Standard Model has its limitations and leaves some phenomena unexplained: Being an inherently incomplete theory, the Standard Model lacks the description and explanation of the fourth important interaction observed in nature, gravity.

Additionally there exists no verified and widely accepted way to implement the theory of general relativity into the Standard Model up to now. Furthermore, the Standard Model seems to be a limiting case of a more general theory due to several reasons:

- Observation of dark matter and dark energy in the universe which is not explained by the Standard Model of particle physics.
- Observation that the matter and antimatter asymmetry in the universe is much larger than predicted by the Standard Model of particle physics.
- Neutrinos are massless in the Standard Model, but neutrino oscillations require that neutrinos have small masses.
- The hierarchy problem, a large discrepancy between the strengths of the weak interaction and gravity, hereby among others the question arises why the weak force is 10^{32} times stronger than the force of gravity.
- 19 to 28 free parameters (depending on the counting method) occur in the Standard Model, which is considered unacceptable for a theory of everything.

3.1 Elementary particles in the Standard Model

All known ordinary matter is composed of few elementary particles, which are described in the Standard Model and which can be classified according to their spin into the so-called fermions and bosons. Fermions are particles with half-integer spins, such as $\frac{\hbar}{2}$, $\frac{3\hbar}{2}$, ..., while particles with integer spins, such as $\hbar$, $2\hbar$, ... are known as bosons.[1] In contrast to the bosons, fermions obey the Pauli exclusion principle, meaning that two identical fermions cannot simultaneously occupy the same quantum state. Fermions include elementary particles such as leptons and quarks, but also the subatomic protons and neutrons as well as some atoms. The leptons are all spin $\frac{1}{2}$ fermions and form three generations with one charged lepton (electron, muon, or tau) and a neutral lepton (electron neutrino, muon neutrino, or tau neutrino) respectively. The six quarks in the Standard Model are spin $\frac{1}{2}$ fermions, too, and are also paired in three generations (up quark, down quark; charm quark, strange quark; top quark, bottom quark) – with six flavours in total (see figure 3.1). Additionally, every lepton and every quark has an associated antiparticle with the same mass and opposite charge-like quantum numbers. Due to the electroweak interaction every quark, every antiquark, and all charged leptons have an electric charge which is specified in figure 3.2. The quarks and antiquarks obeying the strong interaction carry in addition a colour charge. A pair of a quark and such a corresponding antiquark with opposite colour

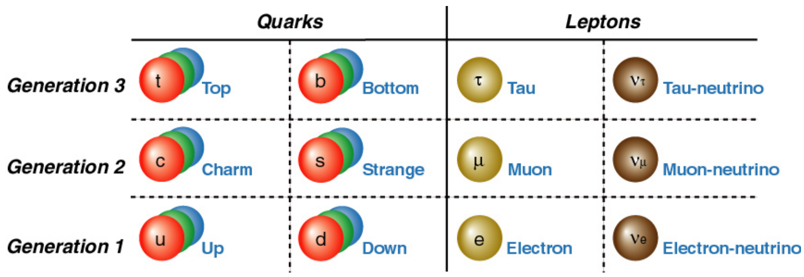

Figure 3.1: Quarks and leptons. Taken from [Cer2001]

charge can compose a so-called meson, which is a composite boson due to its integer spin. Moreover, it is a hadron as a consequence of being a composite particle held together by the

[1] In the following natural units will be used in which the reduced Planck constant $\hbar$ and the speed of light c are set to $\hbar = c = 1$.

strong force. Another class of hadrons exists in which three quarks or antiquarks compose a so-called baryon or antibaryon respectively. In contrast to the mesons the baryons and antibaryons belong to the class of fermions. An overview about the classification of elementary particles and composite particles by their spin is given in table 3.1.

Table 3.1: Classification of elementary particles and composite particles by their spin

	Bosons	Fermions
Fundamental	Photon, W^+, W^-, Z^0, Gluons, H^0	Leptons (e^-, ν_e,...), Quarks (u, d,...)
Hadron	Mesons (Pions, Kaons,...)	Baryons (Proton, Neutron,...)

3.2 Types of interactions

Beside the classification according to the spin, the elementary particles in the Standard Model can be classified according to their role in interactions described in more detail in the subsequent sections: The leptons take part only in the electromagnetic and weak interaction, while quarks also undergo the strong interaction. Furthermore, the Standard Model recognizes four gauge bosons (γ, W^+/W^-, Z^0, g) which mediate the interactions.

- The photon for the electromagnetic interaction,
- W^+, W^-, and Z^0 boson for the weak interaction,
- and gluons for the strong interaction,

all with spin one. Additionally the Standard Model includes the Higgs boson H^0, which is an uncharged spin zero particle and causes the mass of the W^+, W^-, and Z^0 boson by interacting with them. It is also the cause that both the quarks and the charged leptons acquire mass via Yukawa couplings. The figure 3.2 gives an overview about all the fundamental fermions and bosons of the Standard Model of particle physics. Furthermore, it is shown which kind of interaction a particle is subject to and which gauge boson is exchanged due to this interaction: The gluon as the gauge boson of the strong interaction is exchanged only by quarks and antiquarks while the photon of the electromagnetic interaction is exchanged with all charged particles and the W and Z bosons as mediators of the weak interaction are exchanged with every fermion. It remains to note that the Higgs boson is the smallest possible quantum excitation of the Higgs field and that it interacts with all particles which have mass due to either the Higgs mechanism in the case of the gauge bosons or the Yukawa interaction in the case of the massive fermions.

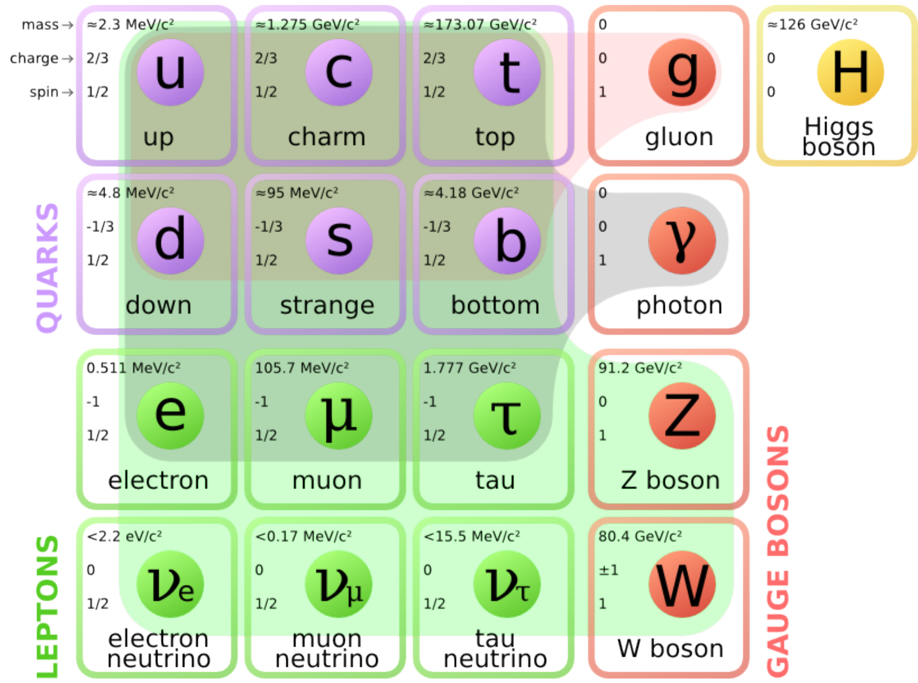

Figure 3.2: Fundamental fermions and bosons of the Standard Model of particle physics: The antiparticles of the leptons and quarks, the antileptons and antiquarks, are neglected for presentation purposes. The mass, the electric charge and the spin is specified in the top left corner of each particle. Furthermore, the interactions a particle obeys is shown by coloured areas (Red colour: Strong interaction, Dark blue colour: Electromagnetic interaction, Green colour: Weak interaction). Adapted work, based on [Mis2014]

3.2.1 Electromagnetic interaction

The electromagnetic interaction is described by the theory of Quantum Electro dynamics (QED) [Tom1946] [Sch1948] [Fey1949b]. The mediator of the electromagnetic interaction is the massless photon which couples to electrically charged particles allowing them to form bounding states. Since the photon is massless and does not carry electric charge itself, the range of the electromagnetic field is infinite. However, the field strength decreases with increasing distance according to the inverse square law which is in contrast to the behaviour of the strong interaction in which the field strength increases with distance (see figure 3.5 for a comparison). The coupling constant of the electromagnetic interaction is the fine-structure constant α which is roughly 100 times smaller than the coupling constant of the strong interaction α_S.

3.2.2 Weak interaction

The weak interaction is described by the theory of Quantum Flavour dynamics (QFD) [Fri1977]. Nevertheless, this term is seldom used since the weak interaction can be better understood in terms of the Electroweak Theory (EWT) [Bil1982] in which the electromagnetic interaction and weak interaction are unified. Due to its coupling to all particles with a so-called weak isospin and weak hypercharge the weak interaction affects all the fermions of the Standard Model as well as the Higgs boson while two types of weak interaction can be distinguished: The flavour- and charge-changing weak interaction caused by the exchange of the electrically charged W^+ and W^- bosons and the neutral-current interaction which conserves the flavour and charge of the involved particles and is mediated by the neutral charged Z^0 boson. All three gauge bosons of the weak interaction can couple to themselves and have a mass resulting in a short-range and a small field-strength of the weak interaction. The coupling constant of the weak interaction is some orders of magnitude smaller than the coupling constant of the electromagnetic interaction and strong coupling which explains the name of this interaction.

3.2.3 Strong interaction

The strong interaction is described by the non-abelian theory of Quantum Chromodynamics (QCD). Its gauge bosons are gluons of which 8 types with different colour-charge-states (combination of colour and anticolour) can be found. The gluons can couple to the quarks and antiquarks carrying colour charge, which results in the formation of hadrons. Furthermore, the gluons can couple to themselves since they carry colour charge (see figure 3.3).

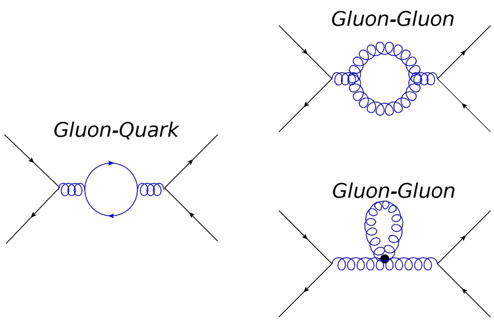

Figure 3.3: Visualization of the gluon coupling with quarks and of the gluon self-coupling: The coupling of gluons with quark (referred to as Gluon-Quark) by the creation of a quark-antiquark pair and the gluon self-coupling (referred to as Gluon-Gluon) is shown in blue colour. The Feynman diagrams were created by using Jaxodraw [Bin2004].

This gives rise to a few unique phenomena of QCD: In contrast to the electromagnetic field the field of the strong interaction can be visualized by a flat tube (compare both fields in figure 3.4) and its field strength is increasing with distance.

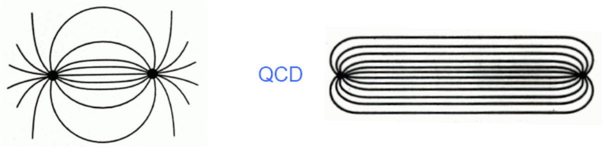

Figure 3.4: Visualization of the fields of the electromagnetic and strong interaction: The field of the electromagnetic interaction described by QED has the shape of a dipole while the field of the strong interaction described by QCD can be visualized by a flat tube. Taken from [Hus2011]

This dependency of the field strength and the corresponding coupling constant α_S on the energy scale and the distance can also be observed for the electromagnetic interaction and is called running of the coupling constant α_S or α in the case of the strong or electromagnetic interaction, respectively. However, due to the self-coupling of the gluons the coupling constant of the strong interaction α_S shows the opposite behaviour of the fine-structure constant α of the electromagnetic interaction (see figure 3.5 for a comparison). The coupling constant α_S of the strong interaction and the strong interaction itself increases when the energy is decreased corresponding to an increased distance between the interacting partons. When the distance between two originally interacting partons becomes large the strength of the field becomes so high that the creation of a quark-antiquark pair by the exchanged gluons is favoured over a further increase in field strength. This is known as fragmentation and leads to the phenomenon of confinement which states that single quarks can never be observed in nature because the formation of hadrons designated as hadronization is always favoured. Another phenomenon due to the behaviour of the strong coupling constant α_S resulting from the gluon self-coupling is asymptotic freedom. With higher energy and shorter distance between the interacting partons the value of the strong coupling constant diminishes, so that the strong interaction between the partons becomes negligible and the partons bound in a hadron behave like free particles. This is also the reason why perturbation theory can be applied to describe hard hadron-hadron scattering processes while the hadronization taking place at low energies cannot be described by perturbative approaches.

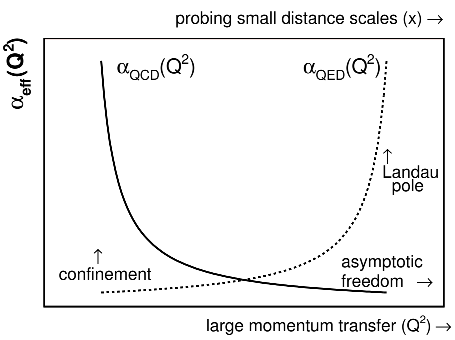

Figure 3.5: Running of the coupling constants: The behaviour of the strong coupling constant α_S (designated here as α_{QCD}) and of the electromagnetic coupling constant α (designated here as α_{QED}) in dependency of the momentum transfer Q^2 is shown. The strong coupling constant α_S behaves different due to the self-coupling of the gluons leading to the phenomena of confinement and asymptotic freedom. Taken from [Gro2006]

4. Monte Carlo event generation

In this chapter the fundamentals of Monte Carlo event generation will be explained. At first an introduction to the Monte Carlo method which constitutes the foundation of the subsequently described event generation will be given. Next, the theoretical principles of Monte Carlo event generation and the steps in the event generation will be presented. This is followed by a discussion of the various types of event generators and the matching and merging techniques used to combine a matrix element event generator with the parton shower of a general-purpose Monte Carlo (GPMC) event generator. A description of scale parameters and selection criteria applied in event generation will conclude this chapter.

4.1 The Monte Carlo method

The Monte Carlo (MC) method is a numerical method to solve mathematical problems by means of modelling random variables [Sob1991] using pseudo or quasi random numbers. One can say that Georges-Louis Leclerc - Comte de Buffon used it the first time ever in 1733 [Buf1733] when he threw needles on a sheet of paper to determine the value of π by counting how many times the needles of length l intersected with equally spaced parallel lines l units apart. However Nicholas Metropolis and Stanislaw Ulam were the first to publish a theoretical essay about "The Monte Carlo method" [Met1949] in 1949. Prior to this breakthrough, Ulam was working in the US nuclear weapons program helping to improve the weapon design and seeking for a way to calculate the neutron diffusion in fissionable material by numerical methods [Ric1947]. After Ulam's breakthrough John von Neumann programmed one of the first computers, ENIAC, to carry out Monte Carlo calculations immediately afterwards. It is worth noting that the name giver for this method was the identically named casino because it was well-known that Ulam's uncle often tried his luck there and the method is based on probability just like gambling.

4.1.1 Applications of the Monte Carlo method

Today the Monte Carlo method is used in a wide range of fields due to its versatility. It is suitable for all procedures which can be modeled and have a sequence dependent upon random factors. Furthermore it lends itself well for all mathematical tasks which can be described by a probability model, where it is used to explore the quantitative properties of such models with stochastic elements. In various scientific subdisciplines such as the following ones the Monte Carlo method is applied:

- Particle and neutron physics: Without the Monte Carlo method large portions of quantitative analysis of particle and neutron physics would be unthinkable of. On the one hand, Monte Carlo simulations are used to predict measurement results which are later compared to the measured data. On the other hand, variables which can not determined by a direct measurement are estimated with these simulations. Furthermore, Monte Carlo integration is employed for solving higher-dimensional integrals which one can find in many parts of these subdisciplines.
- Solid-state physics: In solid-state physics the Monte Carlo method is well suited to tackle physical questions which cannot be solved in closed form but rather need a numerical approach, if no more appropiate solving methods exist.
- Queueing theory: In queueing theory Monte Carlo simulations are used for dealing with queueing problems. For example, it is possible to estimate the utilization rates of a telephone hotline as a function of the number of telephones on the basis of data collected.
- Game theory: In Game theory the Monte Carlo method can be employed, among other use cases, for the simulation of single individuals' choices in a interdependent decision situation. Hence the outcome of the decision can be predicted.
- Econometrics and statistics: Monte Carlo simulations are an important tool in the field of econometrics and statistics since they allow – based on theoretical economic models and empirical findings – to make statements about the future performance, such as the future price developments on the stock exchange.

4.1.2 Categorization and uncertainty budget of the Monte Carlo method

Irrespective of the fact that the Monte Carlo method is very versatile in use it can be divided in two parts:

- Monte Carlo Integration, and
- Monte Carlo Simulation.

In both areas the Monte Carlo method is applied for numerical problem solution. Therefore the result has a certain degree of uncertainty, even though the statistical uncertainty can be reduced by increasing the underlying statistical sample. The uncertainty can be estimated when pseudo random numbers are used with the law of large numbers and with the Koksma-Hlawka inequality [Kok1942] [Hla1961] [Hla1971] if one makes use of quasi random numbers. In contrast to the uniformly distributed pseudo random numbers which are generated by a pseudo random number generator, the quasi random numbers are produced by using a low-discrepancy sequence which has the property that for all possible values of N, its subsequence $x_1, \ldots, x_N$ has a low discrepancy.

4.1.3 Monte Carlo Integration

The Monte Carlo method is frequently applied to solve numerical integrals of higher dimensionality. For integrals of up to three dimensions there are other numerical integration methods like the trapezoidal rule or the Gaussian quadrature which gain the desired accuracy faster. However Monte Carlo integration has one outstanding feature in contrast to many of the other methods: The uncertainty of its integration result decreases independently of the dimension of the integration space and depends only on the number N of sample points used for the integration. When one relies on pseudo random numbers – obeying the law of large numbers – for the integration, the uncertainty is approximately proportional to $\mathcal{O}\left(\frac{1}{\sqrt{N}}\right)$ while the uncertainty decreases faster with up to a complexity

of $\mathcal{O}\left(\frac{1}{N}\right)$ given that quasi random numbers are used. Though applying quasi random numbers is not always possible, the approach to calculate an integral with the help of the Monte Carlo method is the same as for pseudo random numbers:
For the approximation of an d-dimensional integral

$$\int_{[x',x'']^d} f(\vec{u})\ d\vec{u}$$

of a function $f(\vec{u})$ in the value range from x' to x'' N grid points $\vec{y}_N$ are randomly chosen for which the function value $f(\vec{y}_N)$ is evaluated. The numerical value of the integral is then given by adding up the single function values and dividing the result by the number of sample points N:

$$\int_{[x',x'']^d} f(\vec{u})\ d\vec{u} \cong \frac{1}{N}\sum_{n=1}^{N} f(\vec{y}_N).$$

A realization of such a Monte Carlo integration is schematically shown in figure 4.1 for two-dimensional integration. In this illustration, the size of the area with the blue contour is the value searched for. It is computed by drawing grid points, counting the number of points inside the blue area (displayed in orange color) and the number of points in the known black area (displayed in red color) to determine their ratio, and by multiplication of the obtained ratio with the size of the black area.

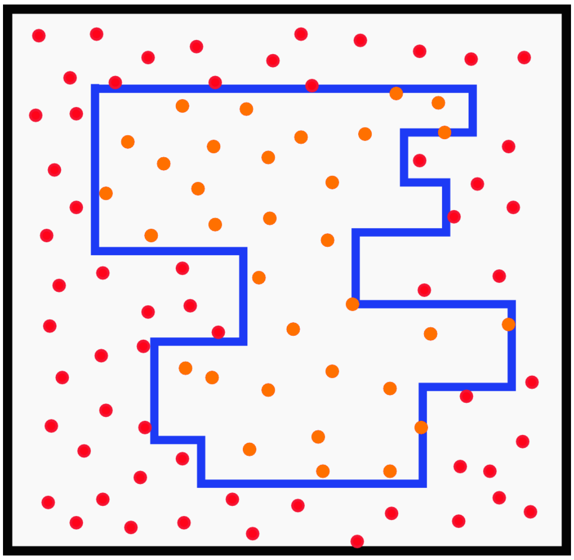

Figure 4.1: Schematical representation of a Monte Carlo integration: The blue area – which corresponds to the unknown integration space – is placed inside of a known black area. Grid points are randomly drawn inside the black area and the number of points in the blue and black area is counted to obtain the ratio between both areas. Afterwards the integral is given by the product of the obtained ratio and the size of the black area.

4.1.4 Monte Carlo Simulation

The calculation algorithm used in the Monte Carlo simulation consists of the following steps: As a first step the simulation problem has to be defined and to be realized as a random trial experiment. Then the random experiment must be repeated many times before a statistical analysis can be carried out.
An advantage of a Monte Carlo simulation is the possibility to start with a very simple simulation model, that can be successively extended until the desired simulation accuracy is reached.

4.1.5 Use of Monte Carlo methods for event generation

As can be seen in the subsequent sections, the event generation in particle physics involves multi-dimensional integrations and, therefore, the only choice is to make use of the Monte Carlo integration. Furthermore, if event samples should be compared to measurement data it is required to take the acceptance and efficiences of a particle detector into account by simulating the detector with a Monte Carlo simulation.

4.2 Theoretical principles of Monte Carlo event generation

4.2.1 Fermis golden rule of quantum mechanics

According to the Standard Model of particle physics every elementary particle and every composite particle can be described by a quantum eigenstate $|\phi\rangle$. Furthermore the electromagnetic, weak, and strong interactions acting on these states can be represented by three different quantum operators or Hamiltonians $\hat{H}$.
The Hamiltonian $\hat{H}$ can be split into diagonal contribution H_0 and a perturbation $\hat{H}'$

$$\hat{H} = H_0 + \lambda \hat{H}',$$

if the perturbation $\hat{H}'$ and the corresponding parameter λ is sufficiently small. The transition probability $T_{i \to f}$ from one eigenstate $|\phi_i\rangle$ to another eigenstate $|\phi_f\rangle$ is related to the matrix element $\mathcal{M} = \left\langle \phi_f \middle| \hat{H}' \middle| \phi_i \right\rangle$ of this perturbation $\hat{H}'$ and can be described by Fermis golden rule using perturbation theory:

$$T_{i \to f} = \frac{2\pi}{\hbar} \left| \left\langle \phi_f \middle| \hat{H}' \middle| \phi_i \right\rangle \right|^2 \rho.$$

Here ρ is the density of final-states or, in other words, the number of final-states per unit of energy. The transition probability $T_{i \to f}$ is also called decay probability, because it is related to the mean life time τ of a decay from the initial-eigenstate $|\phi_i\rangle$ to the final-eigenstate $|\phi_f\rangle$ like the decay of a muon μ to $e^- \overline{\nu}_e \nu_\mu$.

$$\tau \left(\mu^- \to e^- \overline{\nu}_e \nu_\mu \right) \propto \frac{1}{\left| \mathcal{M} \left(\mu^- \to e^- \overline{\nu}_e \nu_\mu \right) \right|^2}.$$

4.2.2 Feynman diagrams, matrix elements, and cross section calculation

In 1949 Richard Feynman – using the novel knowledge gained from quantum electro dynamics – developed a pictorial representation scheme, the so-called Feynman diagrams, to describe scattering processes in particle physics [Fey1949b]. Since this scheme represents the perturbative transition from an initial to a final quantum state, it could later be extended to depict further interactions of particles and was adopted in other fields of physics. Nowadays Feynman diagrams are used as a convenient way to describe a perturbative contribution to the transition amplitude of a quantum mechanical field theory instead of showing both the underlaying probability amplitudes and the rather complicated path integrals.
In particle physics Feynman diagrams represent rules [Wei1964] derived from the Lagrangian of the Standard Model. The in- and outgoing lines in such a Feynman diagram (see figure 4.2) represent the wave functions of actually occuring, on-shell elementary particles. Each external line depicts four momentum, and spin of a particle. Beside the external lines, also vertices, and inner lines (propagators) occur in a Feynman diagram: Each point where three or more lines meet displays an interaction point, which is called vertex. This vertex is associated with one of the three fundamental interactions, so that

it represents either an electromagnetic interaction vertex, a weak interaction vertex, or a strong interaction vertex. The vertex factor can be derived from the corresponding interaction term in the Lagrangian.
Inner lines correspond to the propagators of the quantum field theory and resemble virtual particles. These particles are allowed to be off-shell because the propagator does not vanish, even if combinations of momentum and energy forbidden by classical mechanics occur. Nonetheless also virtual particles must obey the law of conservation of momentum and energy, except whenever the virtual particles participate in a closed loop. The momentum and energy of virtual particles in closed loops is partly unconstrained, because only the total momentum and energy of the particles in the loop must be conserved. Calculating Feynman diagrams with loops can therefore be difficult because the loop integral can diverge. Accordingly, regularization procedures that are compatible with the structure of the applied quantum field theories are needed. By this so-called renormalization of the theory the basic parameters are redefined in a way that the integral originating from the propagator becomes finite and calculable.
It shall also be noted that Feynman diagrams describe a physical process by a space-time approach. For this reason, one of the two axes is used to show the time coordinate while the other axis represents the space. For example in figure 4.2 the scattering process ($e^+e^- \to \mu^+\mu^-$) is drawn and the time scale runs in horizontal direction from the initial-state ($e^+ + e^-$) on the left side to the final-state ($\mu^+ + \mu^-$) on the right side. The vertex of the initial-state is connected with the final-state by a electromagnetic propagator (γ). Additionally the wave functions of the particles, the vertex factors and the propagator terms are stated in the diagram.

One can derive the matrix element $\mathcal{M}$ for the above-mentioned scattering process by

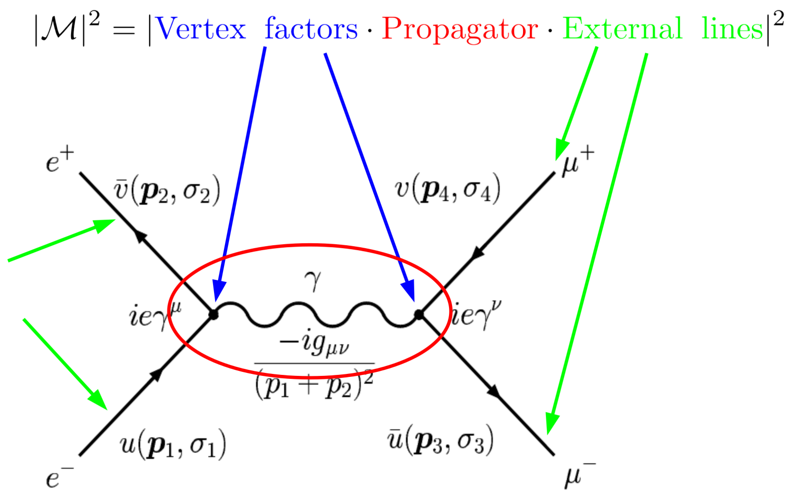

Figure 4.2: Feynman diagram of the ($e^+e^- \to \mu^+\mu^-$) scattering process: The external lines represent the wave functions of the scattered elementary particles. The two vertices are connected by the electromagnetic propagator corresponding to a virtual photon. Note that the time runs in horizontal direction. Taken from [Qua2013b]

using Feynman rules [Wei1964]:

$$-i\mathcal{M} = [\overline{u}(\mathbf{p}_3, \sigma_3)\,(ie\gamma^\nu)\,v(\mathbf{p}_4, \sigma_4)]\,\frac{-ig_{\mu\nu}}{(p_1+p_2)^2}\,[\overline{v}(\mathbf{p}_2, \sigma_2)\,(ie\gamma^\mu)\,u(\mathbf{p}_1, \sigma_1)]\,.$$

Using the abbrevations $u_1 \equiv u(\mathbf{p}_1, \sigma_1)$ and $v_4 \equiv v(\mathbf{p}_4, \sigma_4)$ one can obtain

$$\mathcal{M} = \frac{e^2}{(p_1+p_2)^2}\,[\overline{u}_3\gamma_\mu v_4]\,[\overline{v}_2\gamma^\mu u_1]\,.$$

More generally, the formula for the differential cross section $d\sigma$ of a $2 \to n$ scattering process is given by:

$$d\sigma = \frac{1}{u_\alpha}\frac{1}{2E_1}\frac{1}{2E_2}\overline{|\mathcal{M}|^2}\,(2\pi)^4\,\delta^4\left(p_1 + p_2 - p_1' - \cdots - p_n'\right)\sum_{i=1}^{n}\frac{d^3p_i'}{(2\pi)^3\,2E_i'}.$$

Herein the energies and momenta of the n final-state particles are marked by a apostrophe and the following abbrevation was used for the relative velocity of the two initial-state particles

$$u_\alpha = \frac{\sqrt{(p_1 \cdot p_2)^2 - m_1^2 m_2^2}}{E_1 E_2}.$$

Consequently, the cross section σ of a scattering between the initial-eigenstate $|\phi(e^+e^-)\rangle$ and the final-eigenstate $|\phi(\mu^+\mu^-)\rangle$ is connected with the squared sum of the matrix element $\mathcal{M}$ derived from the Feynman diagram shown above by the following relation.

$$\sigma\left(e^+e^- \to \mu^+\mu^-\right) \propto \left|\mathcal{M}\left(e^+e^- \to \mu^+\mu^-\right)\right|^2.$$

The cross section σ is a measure of the frequency of a scattering process and is stated in units of area. Typically the unit barn ($1\,\text{barn} = 10^{-28}\,\text{m}^2$) is used. The cross section is also closely related to the event rate $\frac{dN}{dt}$ of a specific process measured by a particle detector:

$$\frac{dN}{dt} = \sigma \cdot \mathcal{L}.$$

Herein $\mathcal{L}$ is the time-dependent luminosity, which is a characteristic quantity of the particle accelerator. Often the time-independent integrated luminosity $\int \mathcal{L}\; dt$ is also used.
By using the following relation and with the knowledge of the integrated luminosity $\int \mathcal{L}\; dt$ the theoretical estimation of the cross section σ can be connected with the measurement of the number of events N for a specific process:

$$N = \sigma \cdot \int \mathcal{L}\; dt.$$

4.2.3 Differences between leading-order and next-to-leading order

An leading-order (LO) cross section calculation represents the lowest order of perturbation theory which can be made use of. It takes only matrix elements of leading-order (LO) and corresponding LO Feynman diagrams – which are also called Born level Feynman diagrams – into account. Obviously, a more complete description of the physical process can be achieved by using higher orders in perturbation theory and accordingly higher-order matrix elements and Feynman diagrams. For example, by using the next-to-leading order (NLO) matrix elements and Feynman diagrams for a physical process like $\mathrm{pp} \to \mathrm{t\bar{t}H}$, one would expect a more complete description of the physical process due to the additional terms in the perturbation series. Furthermore in regard to this example, it is assumed that the dependency on the NLO K-factor $k_{\mathrm{NLO}} = \frac{\sigma_{\mathrm{t\bar{t}H,NLO}}}{\sigma_{\mathrm{t\bar{t}H,LO}}}$, which is used to scale an LO cross section of the $\mathrm{pp} \to \mathrm{t\bar{t}H}$ process $\sigma_{\mathrm{t\bar{t}H,LO}}$ to a NLO cross section $\sigma_{\mathrm{t\bar{t}H,NLO}}$ and which is derived from theory, is smaller because at the moment LO event samples are still used in the CMS collaboration which are scaled to a NLO cross section. From a more general point of view, using NLO instead of LO is also advantageous due to the decrease in the scale dependency: One knows that in NLO the change of the strong coupling constant α_S in relation to the scale variable is significantly smaller than in LO. However, due to the additional perturbation terms a NLO computation is more difficult and was not possible in a general and automated way until 2007 when with "CutTools [...] a program implementing the OPP reduction method to compute one-loop amplitudes" [Oss2007a] was released. This program allows to compute the one-loop path integrals occurring in NLO which correspond to the so-called virtual Feynman diagrams which have one loop in the propagator. Besides the (LO) Born level and the virtual Feynman diagrams, so-called real emission Feynman diagrams come into play. These real emission diagrams contain either Feynman diagrams with initial-state radiation (ISR) or with final-state radiation (FSR). All three kinds of diagrams are shown for the above-mentioned $t\bar{t}H$ process in picture 4.3. A consequence of

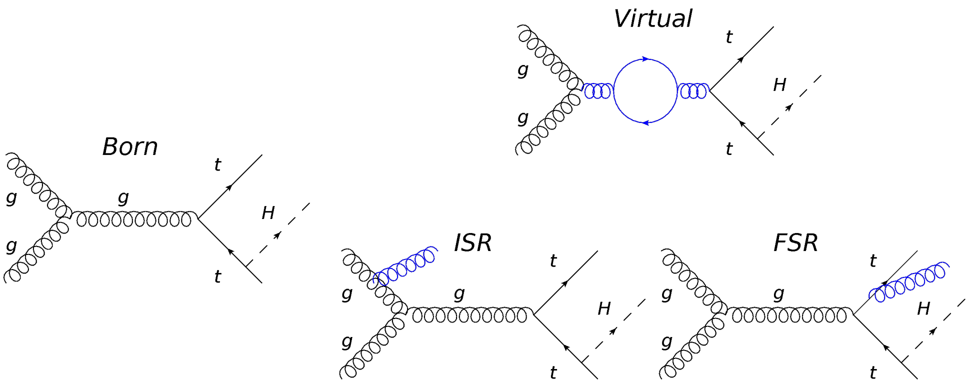

Figure 4.3: The three different kinds of NLO Feynman diagram topologies for the example of the $t\bar{t}H$ process: One example of a Born level Feynman diagram is shown on the left side, one example of a virtual Feynman diagram is shown in the upper right corner while examples of an initial-state radiation (ISR) and of a final-state radiation (FSR) Feynman diagram are shown in the lower right corner. The Feynman diagrams were created by using Jaxodraw [Bin2004].

the additional virtual Feynman diagrams in NLO is that the matrix elements $\mathcal{M}_{\mathrm{Born}}$ of the Born level diagrams and the matrix elements $\mathcal{M}_{\mathrm{Virtual}}$ of the virtual Feynman diagrams interfere with each other. Hence the NLO differential hard scattering cross section $d\sigma_{\mathrm{NLO}}$ which is proportional to the squared sum of the matrix elements $|\mathcal{M}_{\mathrm{NLO}}|^2$ depends also on further terms originating from the higher order of perturbation:

$$d\sigma_{\mathrm{NLO}} \propto \quad |\mathcal{M}_{\mathrm{NLO}}|^2 = |\mathcal{M}_{\mathrm{Born}}|^2 + 2\Re\left(\mathcal{M}_{\mathrm{Born}} \cdot \mathcal{M}_{\mathrm{Virtual}}\right) + |\mathcal{M}_{\mathrm{ISR}} + \mathcal{M}_{\mathrm{FSR}}|^2 .$$

One should also mention the drastically increased computation time in NLO due to huge amount of additional matrix elements including the more complex real emissions and loops. As an example: The pp $\rightarrow$ $t\bar{t}H$+0/1/2jets process in LO has 1338 (independent) Feynman diagrams, while in NLO 49 866 (independent) Feynman diagrams have to be taken into account (which is roughly a factor of 40). Due to this it takes approximately 100 times longer to generate a NLO event than an LO event.

4.2.4 Parton distribution function

Parton distribution functions (PDF) are used to describe in a non-perturbative way the structure of hadrons like protons. Hadrons are composite particles which are formed by partons, quarks and gluons (see also chapter 3.1). The valence quarks of the hadron define the type of the hadron and exchange gluons as carriers of the strong interaction which hold the quarks together. Furthermore, due to the time-energy uncertainty principle and the properties of the strong interaction gluons can have enough energy to create virtual quark-antiquark pairs, which are called sea quarks and which can also participate in interactions.

This internal structure of hadrons can be probed in (deep-inelastic) scattering experiments

(see e.g. [Geh1999]) and it is important to understand that depending on the energy scale Q or resolution scale Q, as it is also called, of the interaction between the hadron and its scattering partner the structure of the hadron is resolved: At a low energy scale Q the hadron appears to be a fundamental particle in the interaction while for a higher energy scale Q the internal structure of the hadron becomes more apparent and the interaction happens with a single parton of the hadron. Consequently, in high energy scattering processes each of the partons in the hadron carries its own momentum fraction of the hadron which can be described by a probability function. More precisely, the parton distribution function $f_i(x, Q)$ of a hadron corresponds to the probability to find a parton of type i, having a longitudinal momentum fraction x, inside the hadron at an energy scale Q.
It is obvious that these distributions are especially important for QCD processes at the LHC due to the high momentum transfer in the scattering process and the resulting interactions between single partons originating from the colliding hadron beams. However, the parton distribution functions have been measured at lower energy scales Q in the above-mentioned deep-inelastic scattering experiments or in other experiments like proton-nucleon fixed target experiments as well as at former colliders like the HERA and Tevatron collider. Therefore, they were then evolved to higher energy scales Q by making use of the DGLAP evolution equations ([Dok1977], [Gri1972], [Alt1977]) which allow to determine the change of the parton density in relation to the energy scale variation. Various parton distribution functions are publicly available from different groups like the CTEQ Collaboration [Pum2002] or the NNPDF [NNP2013] Collaboration. They mostly differ by the measurement data which was taken into account and how the parton distributions were parametrized and evolved to higher energy scales Q.
An example of the CTEQ6M parton distribution function at two scales $Q = 2\,\text{GeV}$ and $Q = 100\,\text{GeV}$ is shown in figure 4.4. Herein the parton densities $f_i(x, Q)$ are displayed in dependency of the momentum fraction x for the given energy scale Q. One can see that the parton densities are quite different between the two energy scales Q and that the gluons become more dominating for higher energy scales Q. A more detailed description of the evolution of the parton distribution function is out of the scope of this thesis, but can be found in [Fel2010].

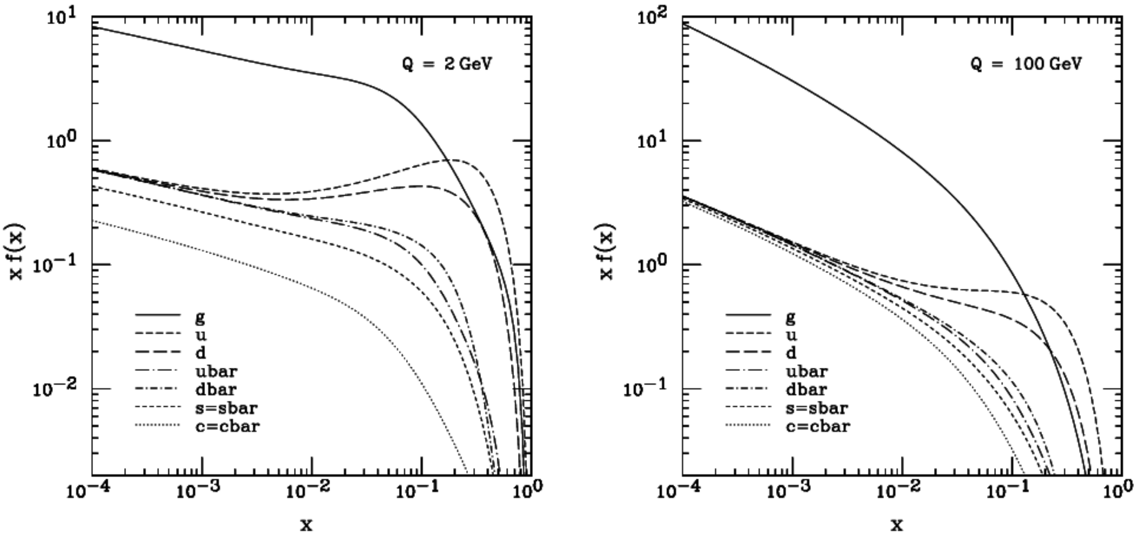

Figure 4.4: The CTEQ6M parton distribution function at two energy scales $Q = 2\,\text{GeV}$ and $Q = 100\,\text{GeV}$: For a given energy scale Q the parton density $f_i(x, Q)$ is displayed in dependency of the momentum fraction x. Taken from [Pum2002]

4.2.5 Factorization theorems

The calculation of high energy cross sections in which Quantum Chromodynamics (QCD) is involved proves to be difficult. These difficulties occur especially at experimentally studied phyiscs processes with a lepton-hadron or hadron-hadron initial state [Col2004]. As a consequence of this it can be concluded that basically every cross section calculation done for the experiments at the Large Hadron Collider (LHC) is affected because either proton-proton collisions or heavy-ion collisions are conducted.
The problems with calculating the cross section or other quantities arise because the general QCD cross section is a combination of short- and long-distance behaviour and cannot be described by (the so-called) perturbative QCD [Col2011] alone. For making use of the methods of perturbative QCD the strong coupling constant α_S has to be small. However, this is only true in high energy interactions or for short-distance interactions like the parton-level hard scattering cross section. Due to color confinement, meaning free quarks and gluons cannot be observed, for long-distance interactions the strong coupling constant α_S is no longer a small parameter and thus these interactions cannot be described with perturbation theory. Since also no non-perturbative methods are known which would be applicable for such long-distance interactions, the only known way to address this problem is to measure their effects and to describe them by empirical models.
Due to this factorization theorems for separating the cross section into two parts were derived: A process dependent short-distance parton cross section which can perturbatively calculated, and a universal empirical model which takes the long-distance interactions into account. To illustrate this, in figure 4.5 the Z^0+jets production by a proton-proton collider is shown together with the schematic representation of the factorization model used for computing the differential hard scattering cross section $d\sigma^{h_1 h_2 \to cd}$.

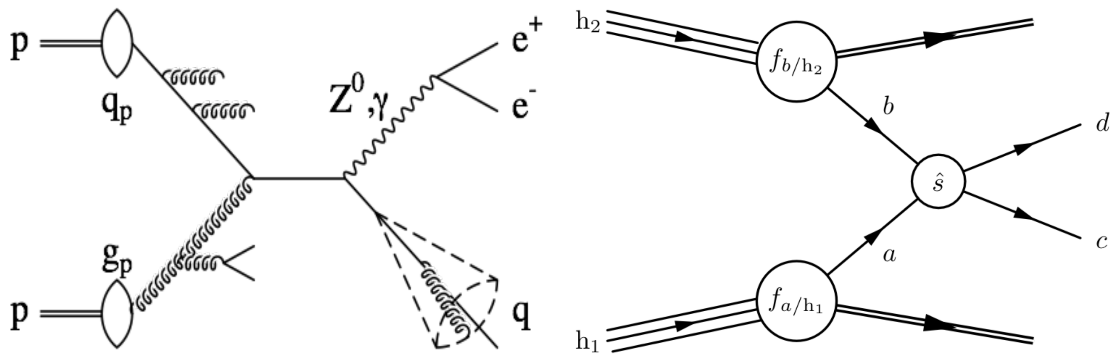

Figure 4.5: Exemplary use of the QCD factorization theorem for the Z+jet production: In the left picture the Z+jet production at a proton-proton collider is shown while in the right picture the schematic representation of the factorization used for the computation of the hard scattering cross section $d\sigma^{h_1 h_2 \to cd}$ is displayed. The cross section $d\sigma^{h_1 h_2 \to cd}$ is splitted in two parts for the computation: A perturbative differential parton level hard scattering cross section $d\sigma^{ab \to cd}(Q^2, \mu_F^2)$ displayed by the interaction vertex $\hat{s}$ and two parton distribution functions $f_{a/h_1}(x_1, \mu_F^2)$ and $f_{b/h_2}(x_2, \mu_F^2)$. Taken from [Geh2013]

Each of the two protons – shown in the left picture – consists of partons from which one participates in the hard interaction while the other partons keep on flying without interference. In the right picture the parton distribution functions $f_{a/h_1}(x_1, \mu_F^2)$ and $f_{b/h_2}(x_2, \mu_F^2)$ are used to describe the probability of finding a parton of type a or b with longitudinal momentum fraction x_1 or x_2 in the corresponding hadron while the factorization scale μ_F^2 is set to a specific value. These parton distribution functions described in section 4.2.4 are process-independent, however not calculable in perturbation theory, hence they must be determined from data. The two colliding partons in the left picture are represented in the right figure by a hard interaction vertex $\hat{s} = Q^2$ that corresponds to a differential parton level hard scattering cross section $d\sigma^{ab\to cd}(Q^2, \mu_F^2)$. This differential cross section $d\sigma^{ab\to cd}(Q^2, \mu_F^2)$ can be computed by perturbative QCD. It also depends on the factorization scale μ_F because it only contains hard emissions above the factorization scale μ_F – the parton distribution function contains all other unresolved emission below the factorization scale μ_F. Furthermore the differential cross section $d\sigma^{ab\to cd}(Q^2, \mu_F^2)$ is connected with the virtuality Q^2, which describes the momentum transfer from the hadron to the hard interacting parton. Taking all these factors together the differential hard scattering cross section $d\sigma^{h_1h_2\to cd}$ is given by [Geh2013]:

$$d\sigma^{h_1h_2\to cd} = \int_0^1 dx_1 \int_0^1 dx_2 \sum_{a,b} f_{a/h_1}(x_1, \mu_F^2) f_{b/h_2}(x_2, \mu_F^2) d\sigma^{ab\to cd}(Q^2, \mu_F^2)$$

The aim of cross section computations and event generation is to predict measurable quantities which can be tested by measurements. However the most QCD hard scattering cross sections σ(hard) cannot be measured due to the previously mentioned color confinement. Nonetheless, using a more comprehensive factorization, one can compute, for example, the total cross section σ(total) of the pp $\to$ Z^0+jets process which is acctually measurable. Later, in section 4.3, it will be seen that event generation can be split into various steps and that for every step a single factorization term can be used. In this way a full description of the specific process can be obtained. Here only the hard cross section term is calculated by perturbation theory while all the other terms are based on approximation schemes, non-perturbative techniques and empirical models.

4.2.6 Collinear factorization and Sudakov form factor

An example of the aforementioned factorization theorems is the collinear factorization theorem which is assumed in all Monte Carlo event generators and allows to calculate cross sections in hadron-hadron collisions as the convolution of universal parton distribution functions and the perturbatively calculable hard scattering cross sections [For2012]. The collinear factorization theorem takes advantage of the fact that a matrix element with many legs can be described by a matrix element with less legs by using a branching sequence which starts at the energy scale of the hard fixed-order scattering process and continues all the way down to the non-perturbative region of hadronization.

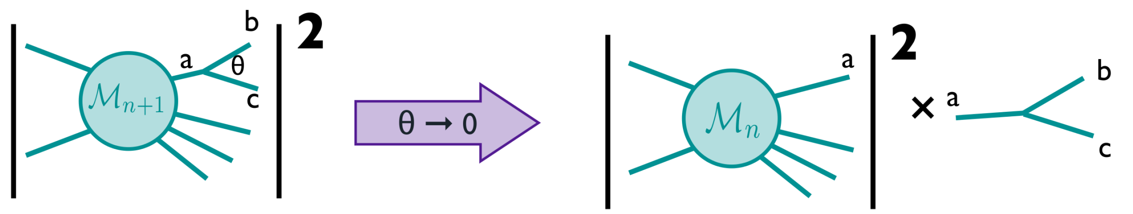

Figure 4.6: Collinear factorization: A matrix element $\mathcal{M}_{n+1}$ with $n+1$ legs can be described by a matrix element $\mathcal{M}_n$ with only n legs and an additional branching term $a \to bc$ if the two partons b and c are only separated by a small angle $\theta \to 0$. Taken from [Mal2012]

Discussing it in more detail and considering the process shown in figure 4.6, the matrix element $\mathcal{M}_{n+1}$ with $n+1$ legs (left side of the picture) can be described by the matrix element $\mathcal{M}_n$ with only n legs and an additional branching term $a \to bc$ (right side) if the two partons b and c are only separated by a small angle $\theta \to 0$. This collinear factorization is justifiable for small angles θ because the contribution to this branching comes from the single parent parton a going on shell. Therefore, the branching of the parton a is related to time scales, which are very long with respect to the hard subprocess, and thus does not change the global picture set up by the hard matrix element process (For example, beside other variables the cross section does not change due to the branching). In the collinear limit an universal collinear factorization procedure of the following form can be applied [Mal2012]

$$|\mathcal{M}_{n+1}|^2 \, d\Phi_{n+1} \approx |\mathcal{M}_n|^2 \, d\Phi_n \frac{dt}{t} dz \frac{d\phi}{2\pi} \frac{\alpha_S}{2\pi} \mathcal{P}_{a\to bc}(z) \quad ,$$

where the matrix element $\mathcal{M}_{n+1}$ with $n+1$ legs and its corresponding phase-space factor $d\Phi_{n+1}$ is related to matrix element $\mathcal{M}_n$ with n legs, its corresponding phase-space factor $d\Phi_n$ and further variables. Herein t defines the so-called evolution variable, z the "energy variable" and ϕ is the azimuthal angle. The evolution variable t represents the hardness of the branching and is chosen differently by different Shower Monte-Carlo (SMC) event generators (see section 4.4.1). For example, beside the angle squared θ^2, the virtuality m^2 of parton a or its transverse momentum squared p_T^2 can be used for the evolution scale t of the parton shower. Alongside the term angular-ordered or p_T-ordered parton shower is often used to make clear which type of evolution scale t was applied for the parton shower. It is important to note that in the collinear limit all the different definitions of the evolution scale t tend to zero and are equal [Mal2012]

$$\frac{d\theta^2}{\theta^2} = \frac{dm^2}{m^2} = \frac{dp_T^2}{p_T^2} \quad .$$

The "energy variable" z enters in the Altarelli-Parisi splitting kernels $P_{i\to jk}$ and states the energy fraction taken by parton b from parton a and thus determines the energy left over for parton c. Consequently, z tends to one if parton c is going soft. The Altarelli-Parisi splitting kernel $P_{i\to jk}$ definition depends on the kind of splitting, either a quark q or gluon g can split in a parton pair (qq, gg, qg and gq), see [Alt2009] for further additional information. The azimuthal angle in the relation above can be chosen to represent the angle between the polarization of parton a and the plane of the branching [Mal2012].
The recipe to treat the first branching by a collinear factorization can be extended to make use of it for a further branching, see figure 4.7. Here an additional branching at a smaller angle $\theta' \ll \theta$ was added and the multiplicity $n+2$ of the orginal matrix element $\mathcal{M}_{n+2}$ was reduced to n by introducing two branching terms $a \to bc$ and $b \to de$.

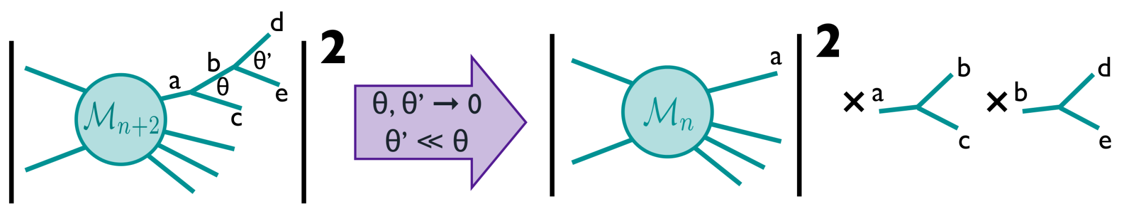

Figure 4.7: Handling an additional branching by using collinear factorization: The recipe to treat the first branching $a \to bc$ by a collinear factorization can be extended to make use of it for a further branching $b \to de$ if the angles θ and θ' are ordered by magnitude. Taken from [Mal2012]

This approach can be repeated for an arbitrary number of further branchings. However, it is important to note two points: For the application of the collinear factorization the branchings have to be ordered by the evolution scale t and by making use of the collinear factorization the probability for the branching does not depend on the past history of the system resulting in neglecting interference effects between the various legs. Keeping this in mind, the differential probability $d\mathcal{P}_{a\to bc}(t)$ for the branching $a \to bc$ between the evolution scales t and $t + dt$ is given by the following equation on the condition that no branching occured before:

$$d\mathcal{P}_{a\to bc}(t) = \sum_{bc} \frac{dt}{t} \int dz \frac{d\phi}{2\pi} \frac{\alpha_S}{2\pi} \mathcal{P}_{a\to bc}(z)$$

Taking advantage of the above equation the differential probability $d\mathcal{P}_{a\nrightarrow bc}(t)$ that parton a does not split between the scales t and $t + dt$ can be easily obtained by

$$d\mathcal{P}_{a\nrightarrow bc} = 1 - d\mathcal{P}_{a\to bc}(t) \quad .$$

The Sudakov form factor $\Delta(Q^2, t)$, which corresponds to the probability that parton a does not branch between scales Q^2 and t at all, can then be obtained by multiplying the individual differential probabilities $d\mathcal{P}_{a\nrightarrow bc}(t_k)$ [Mal2012]:

$$\begin{aligned}
\Delta(Q^2, t) &= \prod_k d\mathcal{P}_{a\nrightarrow bc} \\
&= \prod_k \left[1 - \sum_{bc} \frac{dt_k}{t_k} \int dz \frac{d\phi}{2\pi} \frac{\alpha_S}{2\pi} \mathcal{P}_{a\to bc}(z) \right] \\
&= \exp\left[- \sum_{bc} \int_t^{Q^2} \frac{dt'}{t'} dz \frac{d\phi}{2\pi} \frac{\alpha_S}{2\pi} \mathcal{P}_{a\to bc}(z) \right] \\
&= \exp\left[- \int_t^{Q^2} d\mathcal{P}_{a\to bc}(t') \right]
\end{aligned}$$

In this way, the Sudakov form factor $\Delta(Q^2, t)$ takes all collinear-enhanced real parton emissions at each order in perturbation theory into account due to the consideration of each possible branching. Nevertheless, it also includes further contributions: Virtual (quantum loop) effects of all orders, such effects are included in the probability of not splitting, and unresolvable emissions which contain branchings with a "energy value" z near to one, where the parton c is so soft, that it cannot be resolved [Web2011].
As a summary, the Sudakov form factor $\Delta(Q^2, t)$ is an important quantity used by a parton shower. It gives the probability that a parton originating from the matrix element does not branch between a hard scale Q^2 and an evolution scale t. For this reason, the Sudakov form factor can be used to determine the branching sequence for a given leg in the matrix element while the branching sequence starts at the energy scale of the hard fixed-order perturbative subprocess Q^2 and continues all the way down to the non-perturbative region Q_0^2 in which the hadronization of the partons begins.

4.3 Steps in the event generation process

Monte Carlo event generation is used "to simulate the final states of high-energy collisions in full detail down to the level of individual stable particles. The aim is to generate a large number of simulated collision events, each consisting of a list of final-state particles and their momenta, such that the probability to produce an event with a given list is proportional (approximately) to the probability that the corresponding actual event is produced in the real world." [Web2011]. The event generation for a hadron-hadron collision is normally split into different steps by taking advantage factorization theorems (see section 4.2.5) in use to simulate an event in full detail. An overview about the steps needed to obtain such a complete event is given in figure 4.8. More details about the single steps in the event generation will follow in the subsequent paragraphs. However, the figure 4.8 can already provide a short summary: The Monte Carlo simulation of a single event starts with the computation of the hard subprocess – a matrix element generator like aMC@NLO or POWHEG Box is used for that purpose. During this step the specific matrix element of the event is calculated for the interaction between two highly energetic initial-state constituents, which originate from the colliding particle beams, resulting in a partonic final-state with a few partons, leptons, and / or other fundamental particles with colour charge. Since the fundamental particles and especially the partons are directly defined by the matrix element calculation and, for this reason, have not undergone any further interactions and accordingly no hadronization, the events at this point are called parton-level events. After this step, a SMC event generator like Herwig6, Herwig++, Pythia6, or Pythia8 is in general applied to the events to simulate the emission of further gluons by the involved highly energetic and strongly interacting fundamental particles. Because the newly formed gluons themselves can create further elementary particles and radiate gluons as long as their energy is above the hadronization scale, this results in a parton shower. When the parton reaches the hadronization scale, the coupling of the strong interaction has risen to a point at which colourless hadrons are formed out of the colour charged partons, this is called hadronization. While partons cannot exist individually due to colour confinement the newly generated hadrons, which can be stable or undergo further decay in an additional step, are observable particles. For this reason, events from this stage of event generation are called particle-level events. In strict terms, the event generation is complete at this point. However, due to the limited capabilities of the measurement devices in particle physics a detector simulation and a reconstruction step has to follow. The detector simulation takes into account the specific properties of the particle detector and its measurement methods, while during the reconstruction step the particle objects, which are obtained by the virtual detector, are reconstructed, selected and identified with some algorithms as data. After these steps the simulated events are only comparable with data measured by this specific detector and are called reco-level events due to the previous reconstruction.

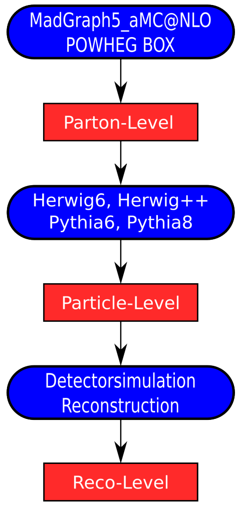

Figure 4.8: Overview about the steps in event generation: See text for further details.

1. The computation of the hard subprocess

As a first step in the event generation the hard subprocess is simulated. The hard process is defined by the collision of two particle beam constituents which interact with each other at a high momentum scale. Thus the strong coupling constant α_S is rather small for this process and the hard subprocess can be described with perturbation theory and by a matrix element which can be illustrated by a Feynman diagram (see section 4.2.2). In this context it is important to understand that the order of perturbation which is taken into account during the computation of the matrix element and the corresponding hard subprocess defines the precision and order of the whole event. For example, if the p + p $\rightarrow$ t$\bar{\text{t}}$+0jet, meaning p + p $\rightarrow$ t$\bar{\text{t}}$ (exclusive), process is studied and the next-to-leading order (NLO) diagrams are included in the matrix element computation, the final event sample will be an exclusive NLO t$\bar{\text{t}}$+0jet event sample. Due to the use of the parton shower in the next event generation step the event sample will then also consist of p + p $\rightarrow$ t$\bar{\text{t}}$+1jet events, which have leading-order (LO) precision.
To describe the computation of the hard subprocess in more detail the collision of two protons – each consisting of partons (quarks and gluons, each with a colour charge) – is (exemplary) illustrated in figure 4.9. From a single proton only one high energetic parton participates in the hard interaction and produces two further outgoing fundamental objects (shown by two red outgoing lines) while the other partons (displayed by two black arrows) of the protons keep flying without participation in the main interaction – however these partons will become important later, because they form the so-called underlying event. The momenta of the colliding partons from the protons are selected by sampling the parton distribution functions (see section 4.2.4) of the proton at the energy scale of the hard subprocess. Convolution with the differential parton scattering cross section and integration over the phase space gives the relevant hard scattering cross section (see section 4.2.2) while at the same time the momentum distributions of the primary produced objects – in the form of a set of representative phase-space points – are obtained. Furthermore, each of the particles occuring in the hard subprocess, which carries a colour charge, will be involved in the subsequent parton shower step [Web2011].

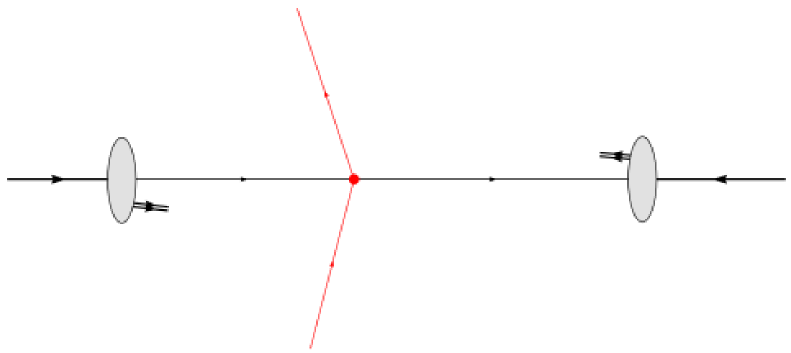

Figure 4.9: The hard subprocess in the event generation process: Two protons (displayed by gray ellipses) collide with each other. Thus one high energetic parton from each proton interacts with the other one in a hard interaction and produce two further fundamental objects (shown by two red outgoing lines). The other partons (displayed by two black arrows) from each proton are unaffected by the collision and keep on flying. Taken from [Gie2012a]

2. The parton shower step

After the hard collision a parton shower is used to evolve the event further. Due to the large momentum transfers during the hard subprocess step the final-state particles obtained from the matrix element have high energies and are accelerated. Due to the acceleration the strongly interacting partons (quarks and gluons) carrying a colour charge can emit QCD radiation in the form of gluons – similar to the electromagnetic shower cascade generated by electrically charged particles. However, in contrast to QED radiation in which the uncharged photons, being the gauge bosons of QED, can produce only pairs of electrons, the gluons, being the gauge bosons of QCD, carry a colour charge themselves and hence can interact among each other by emitting further gluons. This leads to a parton shower which does not stop until the involved partons have decreased their energy by collinear parton splitting and / or soft gluon emission so much that they enter the (closely following) hadronization phase. Different approximation schemes exist to describe the parton shower and, in principle, the showers represent higher-order corrections to the hard subprocess [Web2011]. Accordingly, one can say that by applying a parton shower one can gain an inclusive event sample. However, one should always keep in mind that the parton shower generally produces only low-energy additional radiation due to the collinear parton splitting and soft gluon emission and that for non-collinear parton splitting the parton shower approximation diverges. For this reason, the parton shower can fill phase-space for higher orders of perturbation theory, which are not covered by the matrix element of the hard process, in this way, however, the emission of additional hard radiation is suppressed. Furthermore, a matching or merging (see section 4.5) between the matrix element computation for the hard process and the parton shower is needed, otherwise some parts of the phase-space would be filled twice.
The splitting of partons in the initial-state (before the hard interaction took place) and in the final-state (after the hard interaction) by emitting gluons is schematically illustrated in figure 4.10. Please note that the gluons can also radiate further gluons.

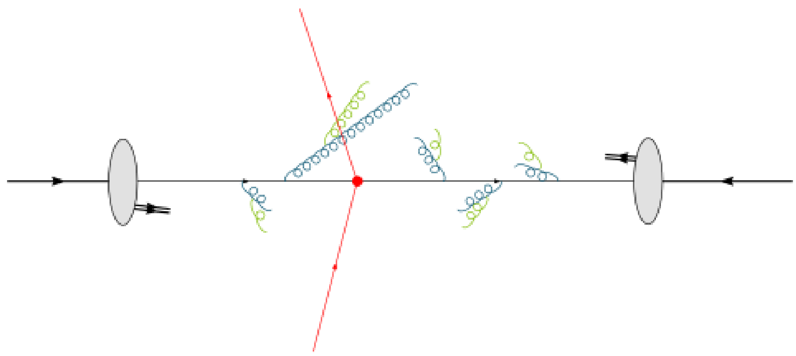

Figure 4.10: The parton shower step during the event generation: Splitting of partons in the initial-state (before the hard interaction shown in red took place) and in the final-state (after the hard interaction) by emitting gluons (displayed in blue color) is shown. The newly emitted gluons (blue color) can radiate further gluons (green color). Taken from [Gie2012b]

3. The hadronization process

During the parton shower the involved partons lose energy by splitting and gluon emission, at the same time the strong coupling constant α_S rises due to the running of the strong coupling constant α_S described in section 3.2.3. In this evolution the dynamics reach a non-perturbative phase and at some point the coupling between the individual colour charged partons becomes so strong that they are bound into colourless hadrons which are observable. This hadronization process begins roughly at an energy of 1 GeV (the exact value depends on the hadronization model) and cannot be described by the non-perturbative techniques currently available. For this reason, hadronization models based on empirical data are needed for the description of this formation of hadrons. Nowadays two commonly used hadronization models exist, which cannot be covered in detail in the context of this thesis, the cluster model [Web1984] and the Lund string model [And2002]. In figure 4.11 the cluster hadronization approach is exemplarily represented: The quarks and gluons from the previous parton shower step form colour neutral clusters with corresponding colour partners (displayed as white ellipsoid objects). In a second step the clusters are rearranged and, if necessary, split into smaller clusters in a way that the clusters have a limited cluster mass and can decay into hadrons (shown in yellow color) using a simple decay model. The hadrons thus produced are the first particles in the event generation process which could theoretically be observed in nature. Anyway, most of this hadrons are in an excited state and have only a short mean life time τ. Due to that only a small fraction of these hadrons is observed by particle detectors while the larger fraction of them decays beforehand.

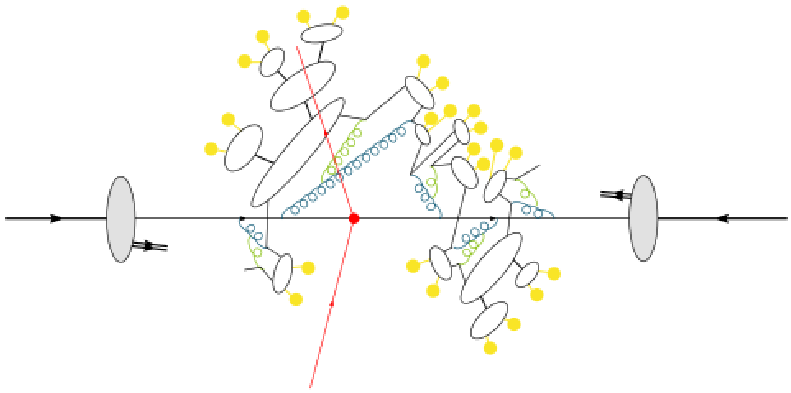

Figure 4.11: The hadronization process in the event generation: Here the cluster hadronization is exemplarily represented. Colourless clusters are formed by colour charged partons which have reached the hadronization scale by parton splitting and soft gluon emission. The clusters are rearranged and, if necessary, split into smaller clusters in a second step before the cluster decays to hadrons which are observable. Taken from [Gie2012d]

4. The hadron decay stage

After the formation of the hadrons a sequential decay stage (see figure 4.12) follows because not all of the newly formed hadrons (shown in yellow) are stable. In this stage the excited und unstable hadrons decay into further hadrons until only long-living or stable hadrons are left over. It is especially important for the simulation of high-energy hadron collisions like the LHC experiments to include almost all possible excited hadronic states and their decay modes, since measurements done in previous experiments indicate that most of the final-state particles originate from these decaying hadrons. In some cases, this means that hadrons and decay modes have to be modelled which are not yet well established experimentally. Furthermore the sum of branching fractions for all decays of a given state must be unity, hence modelling of experimentally non established decay modes may also be required. Likewise one needs to include the momentum distributions and correlations in multiparticle decays and additionally one can take spin correlations into account [Web2011].

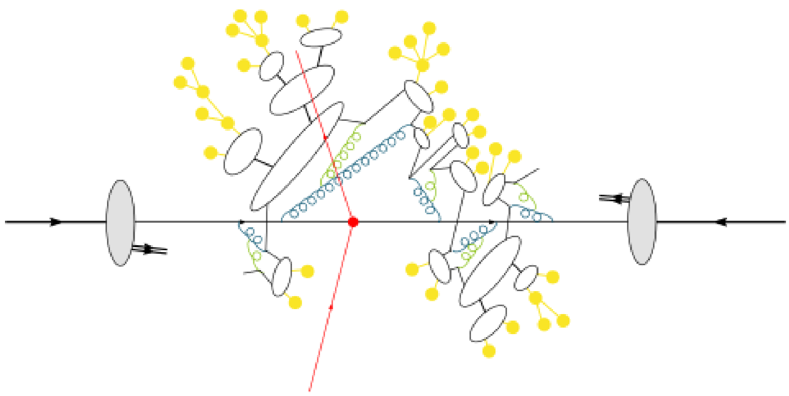

Figure 4.12: The hadron decay stage during the event generation: The excited and unstable hadrons formed in the previous hadronization decay into further hadrons until only long-living or stable hadrons are left over. Taken from [Gie2012d]

5. The consideration of the underlying event

In the previous steps the interactions of the partons, which were part of the colliding proton, but not participating in the hard subprocess, were neglected. As a first approximation it was assumed that these beam remnants keep on flying undisturbed. However they can also split and emit gluons themselves and take part in the hadronization process together with their emitted daughter partons. In figure 4.13 the so-called underlying event is exemplary represented: The primarily undisturbed flying beam remnants (shown in brown colour) consisting of partons can split and emit gluons (blue colour) while they form hadronization clusters (white ellipsoidal objects) – also with the partons originating from the hard subprocess and the subsequent parton shower step – before decaying into additional hadrons (displayed in yellow colour).

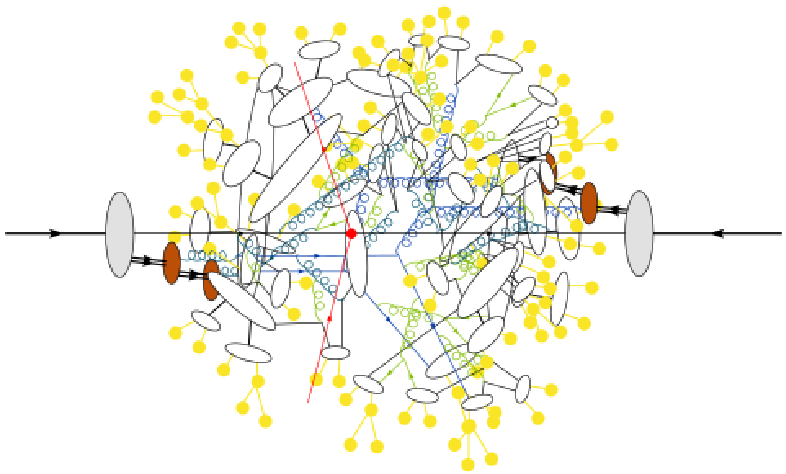

Figure 4.13: The consideration of the underlying event in the event generation process: The beam remnants (shown in brown colour) consisting of partons which do not participate in the hard subprocess (red point) can split and emit gluons (blue gluons) themselves while they form hadronization clusters (white ellipsoidal objects). Such hadronization clusters can also include partons from the hard subprocess and decay into hadrons (yellow colour). Taken from [Gie2012d]

In strict terms, the event generation is complete after the previously described stages. However, in a full analysis the Monte Carlo event generation is continued by the following steps:

6. Detector simulation

Particle detectors which are designed to measure the final-state particles of two colliding highly energetic (hadron) beams cannot directly measure the particles themselves. Instead they make use of interactions between the particles produced during a collision and the purposefully-chosen detector material for indirect detection of the observed particles in detector cells – the final-state particles leave specific tracks and hits in the detector, depending on their properties, while they cross the detector. Furthermore, since the measurement components have only a limited measurement precision and the detector itself in general covers not the whole region, in which particles can be emitted during the collision, this has also to be taken care of in a detector simulation.
Using Monte Carlo techniques the detector and its subcomponents (see section 5.3) are simulated to describe the measurement procedure and results of this specific detector and to gain simulation data which is comparable to the measured data after a reconstruction and identification step was applied to the resulting data. Consequently, it is also notable that after the simulated events undergo a detector simulation they are tailored to a detector and not generally applicable anymore.

7. Reconstruction and identification step

In the first step a particle detector only measures hits of the final-state particles emitted by a collision in the single detector cells of their subdetectors. Afterwards tracks and particle objects can be reconstructed by using the information from the multiple detector cells of the single measurement components while applying reconstruction algorithms which make use of the specific properties of different particle types. In a last step the obtained information of all measurement components is gathered and the particle objects are identified as particles. Particle physicists can then try to use the measurement results to determine the specific process which has happened based on the identified final-state particles. The unique identification of the specific process using the identified final-state particles alone is not possible in most cases and that is why event generators are used: The simulated events which undergo a detector simulation are treated the same way as the measured data from the real detector. However, after the reconstruction and identification step not only the final-state particles are known, but the whole event history is available and it is known which specific physics process took place. For this reason, particle physicists can use simulation data to conclude on unknown initial-states by comparing the final-states of simulations and measurements.

4.4 Types of event generators

Monte Carlo event generators play an essential role in QCD modelling and in data analysis for high-energy physics, “where they are used together with detector simulation to provide a realistic estimate of the detector response to collision events, and in the planning of new experiments, where they are used to estimate signals and backgrounds” [Oli2014]. Different types of event generators exist, however, there are three types of event generators which are used as work horses in the event generation for the LHC and which will be explained in more detail.

4.4.1 GPMC event generators

The so-called general-purpose Monte Carlo (GPMC) event generators allow the complete simulation of high-energy physics processes. For this purpose, the GPMC event generators include low-order (LO and/or NLO) matrix elements for $2 \rightarrow 1$ and $2 \rightarrow 2$ process and follow the parton shower approach, in which the shower evolution has to be independent from the details of the hard scattering and relies only on a few features of the matrix element: The energies and flavours of incoming and outgoing partons in the matrix element as well as the overall energy scale Q^2 of the hard subprocess most be known by the successive parton shower. However, in contrast to the so-called Self-Contained Parton-Shower-Monte-Carlo (SMC) event generators GPMC event generators include beside parton shower algorithms also hadronization models and, therefore, allow to describe physics processes starting from the matrix element up to the hadron formation and hadron decay. Different GPMC event generators can be mainly distinguished by their choice of the evolution scale t, the implemented hadronization and hadron decay models, and the available matrix elements. A more elaborate comparison of the three following GPMC event generators can be found in [Buc2011].

4.4.1.1 Herwig6 and Herwig++

Herwig++ [Bah2008] is a GPMC event generator redeveloped from the ground up and written in C++ which implements functionality from the ThePEG toolkit [Lön2014] and is based on the experience gained with the out-dated Herwig6 event generator [Cor2002] written in Fortran. Both Herwig event generators have implemented a range of hard subprocesses, make use of differently defined angular-ordered parton showers, and use a cluster model of hadronization. However, in Herwig++ a multiple-interaction is directly implemented while Herwig6 has to be interfaced with the separate JIMMY module [But1996]. Furthermore, Herwig++ allows to implement further matrix elements of $2 \rightarrow 2$ processes by making use of an internal matrix element generator [Web2011].

4.4.1.2 Pythia6 and Pythia8

In the last few years Pythia6 [Sjö2006] – written in Fortran – was probably the most frequently used event generator in high-energy particle physics. It is now superseded by the Pythia8 [Sjö2014] event generator which is the actively developed C++ version of Pythia. In both Pythia event generators a wide range of hard-coded subprocesses is available and both apply the Lund string model for hadronization. However, they use different evolution scales t for the parton shower. In Pythia6 the virtuality m^2 or the transverse momentum squared p_T^2 is used as the evolution scale t while Pythia8 uses a dipole shower: A dipole shower is an interesting alternative to the earlier described other parton showers since it also takes soft gluon coherence into account. By using a dipole shower gluon emission is not generated by parton splitting but by splitting of a dipole formed from a pair of partons into two dipoles. Another point worthy of mention is that both event generators contain a highly developed multiple-interaction model for the underlying event [Web2011].

4.4.1.3 Sherpa

Sherpa [Gle2008] written in C++ is the most recent contender amongst the three presented GPMC event generators. Sherpa has two built-in matrix-element generators AMEGIC++ and Comix which allow to generate LO and NLO matrix elements for a wide range of subprocesses and are not limited to $2 \rightarrow 2$ processes. Since the version 2.0.0 Sherpa can also make use of the MEPS@NLO [Hoe2012] [Geh2012] merging between matrix elements and parton shower and can be interfaced to NLO one-loop scattering amplitudes libraries like Blackhat [Ber2013] or OpenLoops [Cas2011] to simulate NLO hard scattering processes.

Sherpa makes use of a dipole showering for the parton shower step and a cluster model for the subsequent hadronization. Additionally, Sherpa contains a multiple-interaction model which is loosely based on that of Pythia [Web2011]. Sherpa stands out among the other two GPMC event generators due to various available matching and merging algorithms such as the CKKW merging prescription [Cat2001] [Kra2002],the CKKW-L merging prescription [Lön2001] [Lav2005], the MLM merging prescription [Man2001] and the MC@NLO matching technique [Fri2002].

4.4.2 ME+PS and NLO+PS event generators

GPMC event generators have a big disadvantage: They rely on parton shower algorithms which are based upon a combination of collinear (small-angle) and soft (small-energy) approximations. This approximation prove to be inaccurate for hard, large-angle emissions. Thus the GPMC event generators make use of so-called Matrix Element Corrections (MEC) [Ben1987] which correct the emission of the hardest jet at large angles in a $2 \rightarrow 1$ or $2 \rightarrow 2$ process. Nevertheless, in the past decade, so-called Matrix Element and Parton Shower matching (ME+PS) event generators together with NLO and Parton Shower matching (NLO+PS) event generators were developed to improve the parton shower description of the hard scattering process and to get rid of the limitation to $2 \rightarrow 1$ and $2 \rightarrow 2$ processes. The main focus of these programs lays on the use of exact matrix elements for the hard subprocess. It is obvious that due to the accurate description of the hard subprocess these generators strive for more advanced techniques for the generation of the matrix elements and the phase space calculation have to be applied resulting in more difficult computations. Furthermore, it is to note that the ME+PS and NLO+PS event generators consider not only the matrix elements for a basic $2 \rightarrow n$ process, but also generate matrix elements for the basic process plus a small number of additional partons. In this way, processes with many jets which are typically required to be well separated and to have large transverse momenta can be described better than with the GPMC generators. However, the matrix element event generators still depend on GPMC generators for the parton shower and hadronization, so that elaborated matching and merging procedures between the matrix element generator and the parton shower are needed (see section 4.5).
In contrast to the ME+PS event generators, the NLO+PS event generators extend the accuracy of the generation of the basic process at NLO in QCD. For this purpose, the NLO+PS event generators contain also real emission and virtual loop matrix elements beside the Born matrix elements. Due to taking the real emission into account NLO+PS event generators produce the hardest additional jet with Born level accuracy even at a large angle for a given basic process [Sjö2012] [Oli2014]. The following two event generators have a ME+PS operation mode as well as a NLO+PS operation mode and are amongst the most frequently used event generators of this type.

4.4.2.1 MadGraph5_aMC@NLO

MadGraph5_aMC@NLO [Alw2014] is a fusion of the LO ME+PS event generator MadGraph5 and the NLO+PS event generator aMC@NLO. It is notable that particular attentation has been devotated to design a fully automated event generator which has the capability of computing Born level and one-loop amplitudes for arbitrary processes and that MadGraph5_aMC@NLO was at the end of 2013 the first public event generator who allowed to perform a NLO computation and optional matching with a GPMC event generator without the need to include further external dependencies [Alw2014].
For this purpose, among other sophisticated tools aMC@NLO makes use of the CutTools program [Oss2007a] to compute one-loop amplitudes representing the most challenging part of a matrix element calculation and of the MC@NLO formalism [Fri2002] to match the NLO matrix element calculation to the parton shower of a GPMC event generator.

The CutTools program implements the OPP reduction method [Oss2007b] which was the first generally applicable method to compute arbitrary one-loop amplitudes at the integrand level. Different interesting techniques have been proposed before (see [Oss2007b] for an overview), however, they faced all the same problems during the calculation of the one-loop amplitudes which the OPP reduction method could finally solve: The very large number of different one-loop Feynman diagrams for processes with more than five involved particles and the appearence of numerical instabilities if no manual tuning of the calculation is done [Oss2007b].
The MC@NLO formalism used in aMC@NLO allows to match the NLO matrix element computation with a parton shower by introducing so-called MC counterterms and a subtraction scheme. These MC counterterms are required because the real emission matrix elements fill parts of the phase-space which are later also filled by the parton shower resulting in an overlap. It is important to understand that this overlap is far more complicated than the so-called double-counting (see section 4.5.1) which occurs by matching of LO subprocesses of different multiplicities to a parton shower. By adding or subtracting these MC counterterms during the computation of the parton-level short-distance cross sections the overlap is taken into account and the parton shower can later be applied to the parton-level events. The necessary MC counterterms can be computed in a process-independent manner, however, they are dependent on the particular parton shower and lead to a specific set of MC subtraction terms for each specific parton shower (More information about the MC@NLO formalism can be found in [Alw2014], [Fri2002], and [Fri2010]).
It remains to mention that due to the MC counterterms event samples generated by aMC@NLO consist of a large number of events with positive weight, but also include a small number of events with negative weights. The ratio of these two event classes depends on the specific process. As a rule of thumb, the fraction of events with negative weight increases for processes with higher multiplicities.
MadGraph5_aMC@NLO can be matched with the GPMC event generators Herwig6, Herwig++, Pythia6, and Pythia8. However, in case of NLO operation mode Pythia6 is not considered a suitable choice due to the missing handling of events with negative weight.
Additionally, MadGraph5_aMC@NLO includes the MadSpin tool [Art2012] for the proper treatment of the decay of parton-level events. If MadSpin is applied to the particle decay spin correlations between the decaying particles are preserved with very good accuracy.
A further outstanding feature of the NLO operation mode of MadGraph5_aMC@NLO is that FxFx merging [Fre2012] can be used to combine exclusive NLO processes with different jet multiplicities like $t\bar{t}$+0jet and $t\bar{t}$+1jet to an inclusive NLO $t\bar{t}$+0/1jets sample (see section 4.5.3 for more details).

4.4.2.2 POWHEG Box

POWHEG Box [Nas2004] [Fri2007] [Ali2010] is a general computer framework for implementing NLO matrix element computations in GPMC event generators and makes use of the POWHEG method [Fri2007]. In the POWHEG method the hardest emission is generated with NLO accuracy at first and independently from the subsequent parton shower which is matched to the matrix element generator part. In this way, also for NLO event generation no subtraction terms are required. The particularity of POWHEG Box is that it cannot be used for arbitrary processes because for each process the LO and NLO matrix element computation of the hard subprocess has to be provided in the form of a program package. A large number of processes of general interest for high-energy physics were implemented and are now available in POWHEG Box (see [Ali2014] for an overview). However, the single processes were implemented by different authors, so the functionality, structure, and user interface of each corresponding program package often differs making it difficult to give generic statements about POWHEG Box at all.
Nevertheless, POWHEG Box has one big advantage in contrast to aMC@NLO: By using

the POWHEG method the NLO computations with POWHEG Box are independent of the successional parton shower, so that POWHEG Box can be interfaced with all GPMC event generators supporting the Les Houches Accord (LHA) for user processes [Boo2001] and Les Houches Event files (LHEF) [Alw2006] as an input.

4.5 Matching and merging

The above-mentioned LO and NLO matrix element event generators (see the ME+PS and NLO+PS section 4.4.2) deliver valid results for a given process when the partons in the hard subprocess are hard (having high energy) and well separated (large angle between them), so that each parton can be resolved in a fixed order calculation. Furthermore, they correctly deal with quantum interference due to the exact description of the process by the matrix elements. They are especially needed for inclusive processes, in which the proper description of exclusive processes with larger multiplicity, meaning with one or more hard additional jets, is important. However, the computation of the matrix elements is expensive and drastically increases for processes with a larger number of partons like in processes with larger multiplicity [Mal2012].
In this respect, the SMC event generators which are part of the GPMC event generators (see section 4.4.1) have an advantage because they are computationally cheap and not limited to any parton multiplicity. Furthermore, they are inclusive up to all orders and needed anyway for the hadronization of the partons generated by the matrix element generators. A limitation of the SMC event generators is that they cannot treat quantum interference effects correctly and are only valid when the partons generated by them are soft (having low energy) and collinear (small angles between them) [Mal2012].
Both of the approaches mentioned before are justified and complementary, so techniques were developed to get the best of both worlds. In the beginning so-called Matrix Element Corrections (MEC) [Ben1987] [Sey1994] were used to improve the GPMC event generators directly. Starting with the development of ME+PS and NLO+PS event generators matrix element matching and matrix element merging methods were developed and put into practical use. The matrix element matching techniques are similar to the MEC, but they are usually used together with NLO corrections like the MC@NLO [Fri2002] and the POWHEG [Fri2007] matching prescription. Furthermore, it is hard to use the MEC and matching techniques in an iterative way to combine exclusive processes with different multiplicities to an inclusive process. In contrast to that, merging techniques like the CKKW [Cat2001] [Kra2002], the CKKW-L [Lön2001] [Lav2005], the MLM [Man2001] and the FxFx [Fre2012] method introduce a resolution criterion slicing the phase-space in two parts: One part which contains processes with hard additional jets is filled by the matrix element generator while the other part containing soft and infrared additional emissions is filled by the SMC generator [Pre2014].
Finally, it should be pointed out that independent of the technique used the main idea of matching or merging is always to let the matrix element describe the hard emissions and let the SMC generator describe the soft and collinear emissions [Lav2008].

4.5.1 Double-counting and overlap

Matching and merging techniques are used to combine a matrix element (ME+PS or NLO+PS) generator with a SMC generator which is part of a GPMC generator. Even in the simplest case of merging exclusive LO processes described by Born level matrix elements and differing only in the multiplicity to an inclusive sample while applying a parton shower problems arise: The additional partons occuring by the LO processes with a multiplicity greater than zero can also be created by the subsequent parton shower resulting in an overlap in the phase-space which is called double-counting. This becomes particularly obvious if one has a look at the Feynman diagrams in figure 4.14. For example, the Feynman diagram of an LO process with multiplicity $n+1$ used by a matrix element generator looks exactly like the Feynman diagram of the same LO process with multiplicity n if one additional branching by a parton shower was taken into account. This is because the parton shower contains all orders starting from the lowest order defined by the matrix element of the LO process with multiplicity zero.

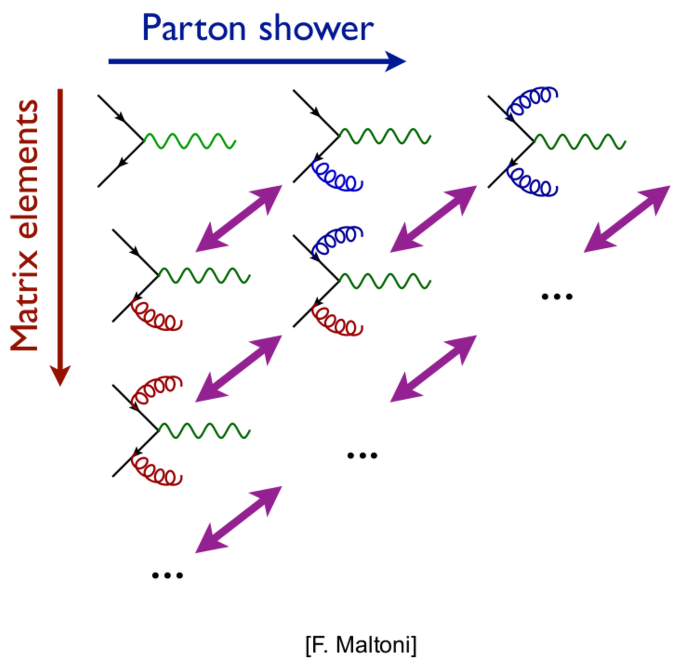

Figure 4.14: Double counting: In the downwards vertical direction Feynman diagrams of LO processes with increasing multiplicity (displayed in red) which are used by matrix element generators are displayed. The horizontal direction shows the Feynman diagrams of the corresponding LO processes with given multiplicity while the number of additional partons created by a parton shower (displayed in blue) is increased. A comparison between diagonal Feynman diagrams shows that they look alike which gives raise to the double-counting called overlap in the phase-space. Taken from [Mal2012]

In this thesis the MLM merging technique (see next section) was applied to respect the double-counting occuring by the combination of exclusive LO processes with different multiplicities to an inclusive sample and the processing of the inclusive sample by a SMC event generator.
The occurence of more complicated overlap must be mentioned as well, e.g when the different matrix elements of a NLO process originating from a NLO+PS generator have to be combined and matched with a SMC generator. Nowadays solution for this matching of a NLO+PS with a SMC event generator exist by the means of the MC@NLO [Fri2002] and POWHEG method [Fri2007] and even a solution for the even more challenging task of combining exclusive NLO samples to an inclusive NLO sample which can be processed by a SMC generator exists in the form of FxFx merging [Fre2012] (see the corresponding section 4.5.3).

4.5.2 MLM merging

MLM merging [Man2001] is in comparison to other common merging methods a quite straight-forward method to match an LO matrix element generator with a parton shower and take double-counting into account: As a first step in the MLM merging scheme, the number of partons in the parton-level event before the shower is determined and a value for the merging scale (see section 4.6.3 for further information) is chosen. Afterwards the event is fed into the SMC event generator, the parton shower is invoked and the partons resulting from the parton shower step are clustered into jets by a k_T algorithm [Cat1993] [Ell1993] like the one implemented in the FastJet [Cac2011] package. The MLM merging algorithm checks then if all matrix element partons can be matched to a partonic jet and accepts events provided by the parton shower only if the single event contains no additional jets above the merging scale. Consequently, the emissions from the parton shower are approximately constrained to be below the merging scale and no modification of the parton shower is necessary [Lav2008] (see the same reference also for a more elaborated description of the MLM merging technique).

4.5.3 FxFx merging

In LO a combination of exclusive (LO) processes differing only in the multiplicities n to an inclusive sample does not result in an overlap beside the aforementioned double-counting. However, in NLO a further overlap arises due to including the additional contributions of the real emissions: The real emission matrix elements contain in comparison to the Born level matrix elements also additional initial-state radiation (ISR) or final-state radiation (FSR). Looking on the corresponding NLO Feynman diagrams of a given NLO process (see figure 4.15) it is clearly evident that a real emission Feynman diagram for the NLO process with multiplicity n appears to be the same as the Born level Feynman diagram of multiplicity $n+1$ when an additional parton was created by a parton shower. This is the reason why in NLO a more elaborate treatment of the occuring double-counting and the additional overlap is required. Furthermore, the merging technique should also prefer the Born level matrix elements associated with processes with larger multiplicity n over the corresponding real emission matrix elements originating from a process with a magnitude smaller multiplicity $n-1$ because this improves the perturbative accuracy of the inclusive process and leads to a better description of hard additional emissions.

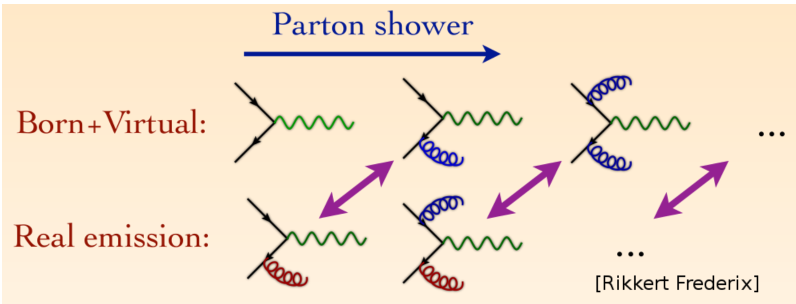

Figure 4.15: FxFx merging: In the upper row the Feynman diagrams of the Born level and virtual loop matrix elements of a NLO process are schematically represented. In the lower row the Feynman diagrams of the real emission matrix elements are shown. Taken from [Fre2013]

A solution to this challenge was found in developing the FxFx merging technique [Fre2012] which can be seen as an enhanced and adopted MLM merging: In an analogous way to the MLM merging a value for the merging scale (see section 4.6.3 for further information) is chosen. However, also the number of final-state partons which occur in the Born level matrix element of the corresponding NLO process n_{current} and the number of final-state partons in the process with the largest multiplicity n_{max} has to be provided for an event. It is important to note that also for an event originating from a real emission matrix element the number of the partons n has to be set to the number of partons in the

Born level matrix elements. Subsequently the event is processed by the parton shower of a GPMC event generator and the resulting partons are clustered into jets by a k_T algorithm [Cat1993] [Ell1993]. Similar to the MLM merging, the algorithm matches then the hardest parton before the parton shower step to the hardest partonic jet, compares the number of partons and partonic jets and accepts events only if no additional partonic jet occurred or if the additional partonic jets are below the merging scale. There is an exception, though, for the process with the largest multiplicity additional partonic jets above the merging scale are allowed. In this way, for all NLO processes, except the process with the largest multiplicity $n_{\max}$, the contribution of real emission matrix elements is suppressed and the hard additional emissions are defined by the corresponding Born level matrix element resulting in the best prediction of hard emission which is achievable. Nevertheless, the real emission matrix elements are important because they provide the correct normalisation of the NLO process due to cancelling of their and the virtual loop matrix element divergent logarithms which occur in the NLO matrix element computation. Furthermore, the real emission matrix elements of the process with the largest multiplicity $n_{\max}$ are used to extend the phase-space covered by the matrix element computations because they behave similar to a Born level matrix element of multiplicity $n_{\max} + 1$.

4.6 Scale parameters and selection criteria in event generation

In the following section scale parameters and selection criteria are listed which are used in the event generators and in this thesis and which are important for a realistic modeling of physics processes.

4.6.1 Renormalization scale

In quantum field theories like QED and QCD ultraviolet (UV) divergences occur due to closed loops of virtual particles in the corresponding Feynman diagrams and to the limited scope of the perturbation approach which is used to describe the hard interactions of these quantum field theories. For the proper treatment of these UV divergences renormalization techniques are used which result in the appearance of a renormalization scale μ_R. Naively, this scale could be an UV cutoff scale splitting the divergent loop integral into two pieces: A finite piece known as radiative correction which includes all effects in the loop up to the renormalization scale μ_R leading to physically measurable effects and a divergent piece which can be incorporated later as a modification of the tree-level propagator and cancels with the counterterms which are also originating by setting an UV cutoff. The parameters involved in the corresponding Feynman diagrams like the strong coupling constant α_S must then also be renormalized. This can be done either by renormalizing the strong coupling constant α_S at a given reference point, it is common to use an energy characteristic of the corresponding process like the invariant mass of the partons created in the hard scattering process, or to define a running of the strong coupling constant $\alpha_S(\mu_R)$ which corresponds to a variable renormalization scale μ_R [Ple2008] [Wal2010].

4.6.2 Factorization scale

In the parton and hadron picture the factorization scale μ_F corresponds to the resolution with which the hadron is being probed. As mentioned in the sections 4.2.2 and 4.2.5 the process dependent short-distance parton cross section of the hard scattering process $d\sigma^{h_1 h_2 \to cd}$ is convolved with the universal parton distribution functions $f_{a/h_1}(x_1, \mu_F^2)$ and $f_{b/h_2}(x_2, \mu_F^2)$ which take the long-distance interactions into account. The short-distance parton cross section $d\sigma^{h_1 h_2 \to cd}$ depends in any finite order in perturbation theory on the factorization scale μ_F and this dependency is usually significant at low orders in perturbation theory. Furthermore, the factorization scale μ_F should be chosen in a way that the collinear (long-distance) physics is included in the parton distribution functions $f_{a/h_1}(x_1, \mu_F^2)$ and $f_{b/h_2}(x_2, \mu_F^2)$, and noncollinear (short-distance) physics in the cross section of the hard scattering process $d\sigma^{h_1 h_2 \to cd}$. For this reason, a characteristic energy scale of the examined process like the invariant mass of the final-state partons is commonly used to set the value of the factorization scale μ_F[Mal2007].

4.6.3 Merging scale

The merging scale Q is a parameter which is used for the matching of a matrix element event generator to a parton shower. As described in section 4.5.1 a double counting can occur because the matrix element generator as well as the parton shower can lead to the radiation of additional partons so that some parts of the phase space are filled twice. By introducing a merging scale Q one defines which part of the phase space is filled by the matrix element computation and which part by the parton shower. To be more precise, additional partons having an energy larger than the merging scale are normally created by the matrix element generator while additional partons with an energy below the merging scale Q are mostly produced by the parton shower. Therefore, the value of the merging scale Q must be chosen carefully: If the value Q is too large the parton shower has to fill parts of the phase-space which cannot be accurately described by the collinear approach of the parton shower. On the other hand, if a too small value of Q is chosen the perturbation theory approach of the matrix element generator is no longer valid.

4.6.4 Matrix element minimum jet transverse momentum selection criterion

During the event generation with MadGraph5_aMC@NLO among other selection criteria the so-called matrix element mininum jet transverse momentum selection criterion $p_{\mathrm{T,\,me}}$ is applied to the generated events. By this selection criterion the generation of additional partons, which have a transverse momentum p_T smaller than the value $p_{\mathrm{T,\,me}}$ and would later lead to partonic jets separated only by a small angle from one of the main jets, by the matrix element event generator is suppressed. In this way only additional partons which are hard (having large energy and/or a large angle) and can be accurately described by fixed-order perturbation theory are resolved during the matrix element computation and generated by the matrix element event generator. In this way, the softer additional partons are included in the other final-state partons and can be taken of later by the parton shower which better describes the collinear factorization of soft partons.

4.6.5 Analysis level selection criteria

In this thesis different selection criteria on analysis level, meaning applying the selection criteria after event generation and during the successive analysis, will be applied to the following variables and will be written in the corresponding abbreviated form:

- $p_{\mathrm{T,\,ana}}$: Selection criterion for the transverse momenta p_T of the jets occuring in the corresponding events
- $|\eta|_{\mathrm{ana}}$: Selection criterion for the pseudo rapidity η of the jets occuring in the corresponding events

It is important to note that by making use of such selection criteria not whole events from the sample are discarded, but single jets which are considered as too soft will be neglected during the analysis of an event and the study of the whole event sample.

5. Experimental basics

In this chapter a short overview about experimental basics will be given. The European Organization for Nuclear Research (CERN), the Large Hadron Collider (LHC), and the Compact Muon Solenoid (CMS) detector will be presented.

5.1 The European Organization for Nuclear Research (CERN)

"At CERN, the European Organization for Nuclear Research, physicists and engineers are probing the fundamental structure of the universe" [Cer2014a].
CERN, named the European Council for Nuclear Research at the time, was founded as a provisional body in 1952. The aim of this foundation was to establish a world-class research organization in Europe with the concentration on fundamental physics research in the field of nuclear physics, which was at that time a most promising and rising research topic and which was later superseded by the field of particle physics. After only two years CERN was founded in 1954 in the northwest suburbs of Geneva on the border between France and Switzerland (see figure 5.1). Over the following 60 years CERN became a world-class research organization and manifested its position as the world's largest particle physics laboratory: CERN not only has over 2500 staff members, mostly scientists and engineers, but hosts also over 12000 fellows, associates, students, users and apprentices from over 20 member states and other associate states [Cer2014b].
Following its founding purpose CERN's research activities are mostly focused on providing purpose-built particle accelerators and detectors together with other infrastructure which is needed for high-energy physics research in the field of particle physics. At the moment – among other impressive experiments and accelerators hosted or operated by CERN – the Large Hardon Collider (LHC) particle accelerator and its related detectors (ALICE, ATLAS, CMS, and LHCb) stand out.

5.2 The Large Hadron Collider (LHC)

The Large Hadron Collider (LHC) is part of CERN's accelerator complex and the last element of CERN's main accelerator chain (see figure 5.2) in which a succession of machines is used to accelerate either protons or lead ions to increasingly higher energies. The proton beam from the previous machine is injected into the next accelerator machine, which increases the energy of the beam and injects the beam into the next machine. The beam is handled like this until the beam is finally injected into the Large Hadron Collider

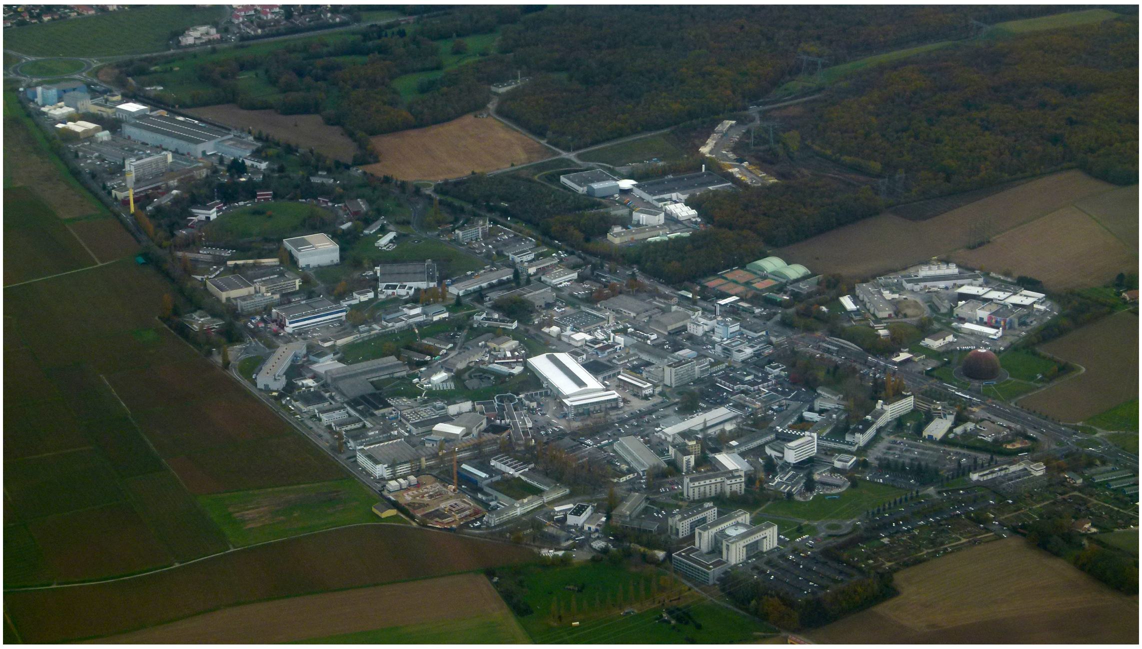

Figure 5.1: CERN's main site: Looking from Switzerland towards France. Taken from [Brü2012]

(LHC) "the world's largest and most powerful particle accelerator. It first started up on 10 September 2008, and remains the latest addition to CERN's accelerator complex. The LHC consists of a 27-kilometre ring of superconducting magnets with a number of accelerating structures to boost the energy of the particles along the way" [Cer2014c]. The protons in each of the two beams in the LHC can reach a record energy of up to 7 TeV, while the lead ions can reach an energy of up to 2.76 TeV/u.
In the Run 1 of the LHC, which lasted roughly from March 2010 to December 2012, the protons reached an energy of either 3.5 TeV (2010 and 2011) or of 4 TeV (2012), which corresponds – due to the two head-on colliding proton beams – to a center-of-mass energy of either $\sqrt{s} = 7$ TeV or $\sqrt{s} = 8$ TeV. During the Run 2, which is going to start mid of 2015, the protons are expected to reach an energy of 6.5 TeV at first. Later the energy of the proton beams shall be increased to 7 TeV, so that in the end the LHC reaches its design maximum center-of-mass energy of $\sqrt{s} = 14$ TeV.
The two beams circulate in the LHC in well-defined bunches, so that under nominal operating conditions the approximately 10^{11} protons in each of the 2808 bunches can be accelerated by radio frequency (RF) acceleration. Hereby the protons in the bunch gain additional energy when they pass through an accelerating cavity at the same time when the radio frequency field has the correct orientation [Cer2009]. Furthermore the synchronized radio frequency field helps to keep the particle beam bunched: Faster than average protons in a bunch reach the microwave cavities while the increasing radio frequency field has not yet reached its maximum. As a result they will not gain as much energy as protons reaching the microwave cavities at the right moment and thus will be slowed down approaching the average speed of the bunch. Also slow protons which reach the cavity after the maximum of the radio frequency field passed it will be decelerated. Thus, they completely lose contact with the bunch and consequently have to be removed from the beam.
At certain collision points – the LHC is divided in 8 sectors and has in total 8 collision points — one of the four major particle detectors of the LHC (ALICE, ATLAS, CMS, and LHCb) is placed. At this spot the two beams cross each other so that some of the protons (or lead ions) from a bunch of each beam will collide. While the single beam particles undergo an interaction, energy is converted into matter and elementary particles will be

created out of energy of the colliding particles. The detectors will detect the elementary particles and their corresponding decay products with their highly sophisticated detector components and allow physicists to draw conclusions about the underlying physics process.

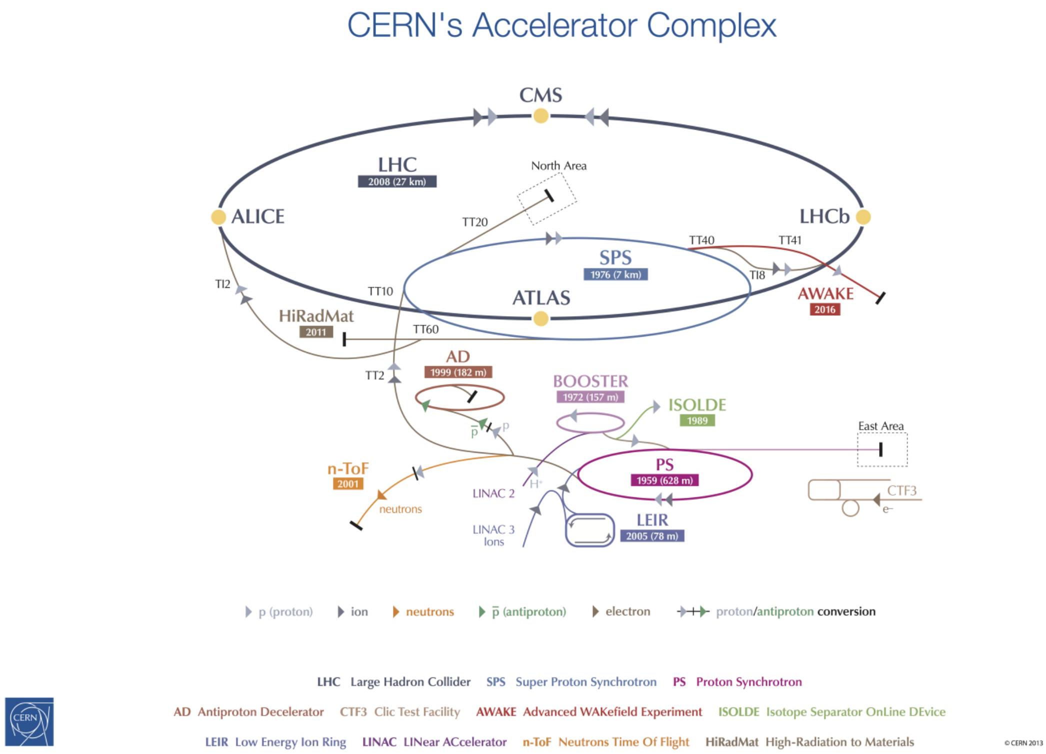

Figure 5.2: CERN's accelerator complex: The Large Hadron Collidier (LHC) is the last and most powerful accelerator in the main accelerator chain. The two beams, which are accelerated in the LHC up to a center-of-mass energy of $\sqrt{s} = 14$ TeV, are transfered from the Super Proton Synchrotron (SPS), which itselfs gets its beam from a chain of smaller accelerators. Taken from [Cer2013]

5.3 The Compact Muon Solenoid (CMS) detector

The Compact Muon Solenoid (CMS) detector is a general-purpose detector which is located at point 5 of CERN's Large Hadron Collider. It is operated by the independent CMS collaboration and competing with the other general-purpose detector, the ATLAS detector. These two detectors differ significantly and the CMS detector possesses some unique features:

The design around a solenoid

All of the detector's measurement components – except the muon chambers – are located inside of a strong magnet. More precisily the coil of superconducting wire with an overall length of 13 metres and a diameter of 7 metres [Tay2011], which forms the solenoid, is "the largest magnet of its type ever constructed" [Tay2011] and has a magnetic field ranging from 2 Tesla in the outer detector parts to 4 Tesla in the detector core. This design was chosen to allow an accurate measurement of charged particles' momenta by determing the curvature of the charged particle's track inside the magnetic field.

The compactness of the detector

The CMS detector is called compact because in contrast to its enormous weight of 14,000 tonnes it has a rather small overall size (15 metres in diameter and 21.5 metres in length) for a high-energy particle detector [CMS2013].

The muon detection system

The CMS detector has an outstanding muon detection system, which was specifically constructed to be sensitive to the $Z \to ZZ^* \to 4\mu$ signature. The $H \to \mu\mu$ channel was expected to be one of the most promising channels for finding the Higgs boson – as predicted in the Standard Model. This assumption has proven to be true in 2012, when the CMS collaboration together with the ATLAS collaboration could claim the discovery of a Higgs-like boson while both used the $H \to ZZ$ and the $H \to \gamma\gamma$ channel the discovery of a Higgs-like boson.

In more detail the CMS detector consists of the following measurement and analysis components (see figure 5.3):

In the innermost part of the multilayered CMS detector the tracking system, made of silicon pixel and strip detectors, is placed. Using the accurate position measurements of passing charged particles by these detectors physicists can reconstruct particle tracks. Furthermore the transverse momenta p_T of charged particles can be determined with a precision of up to $\frac{\Delta p_T}{p_T} \approx 0.005 + 0.15 p_T$ (p_T in TeV) [CMS1996] due to the deflection of the charged particles by the lorentz force in the magnetic solenoid field.
The next detector components are used to measure the energy of the particles formed during the collision and their successive decay products. In the electromagnetic calorimeter the vast majority of the electrons and photons – both obeying the electromagnetic force – interact with the scintillator detector material made of lead tungstate crystals and produce an electromagnetic shower which can be used to determine their energy with a resolution better than 0.6 % if the electrons and photons have energies greater than 75 GeV [CMS1996].
The subsequently positioned hadronic calorimeter can measure the energy, arrival time and position of hadrons, particles made of quarks and gluons and obeying the strong force defined already in section 3.2.3. Its design and coverage of pseudorapidities of up to $|\eta| < 5$ [CMS1996] forces basically every strongly interacting particle to deposit its energy in the hadronic calorimeter. To achieve this, alternating layers of dense copper absorbers and

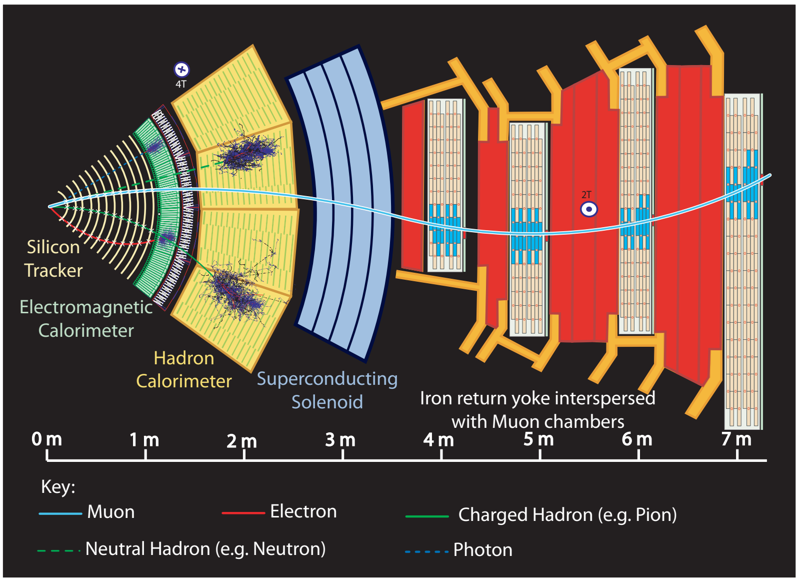

Figure 5.3: Schematic illustration of the CMS measurement components: The tracker detection system in the innermost part of the CMS detector is shown on the left side. The outer parts of the detector are shown on the right side. Note that all detector measurement systems – except the muon chambers – are located inside of the solenoid. Taken from [Bar2011]

tiles of plastic scintillator are used. In the absorber layer the incoming particles produce a shower of emerging particles detected by the adjacent scintillator detectors.
All of the aforementioned detector components are located inside of the solenoid, which is placed around the hadronic calorimeter.
Outside of the solenoid four identical layers of muon stations – interspersed with the iron return yoke – are placed. Apart from just weakly interacting, non-charged particles like neutrinos, only muons can penetrate several metres of absorber material and consequently reach the muon stations. Due to the iron return yoke there still is a strong magnetic field, which bends the tracks of the electrically charged muons and thus allows to determine their momenta in a second independent measurement with 100 μm precision in position and better than 1 mradin direction in the barrel [CMS1996]. The first measurement of the muon momentum was already done by the tracker.
A specialized trigger system which consists of an electronic pre-stage built inside of the detector and a high level trigger stage which is formed by a fast and purposefully programmed computer cluster in the first floor of the CMS detector building completes the CMS detector. This two-stage trigger system is required due to the huge amount of data generated during the normal operation phase of the LHC. The CMS is built to detect events at a proton beam crossing frequency of 40 MHz. The electronic Level-1 Triggers (L1T) reduces the 40 MHz event rate to less than 100 kHz while the subsequent High Level Triggers (HLT) reduces the amount of events further so that an output rate of about 400 Hz is achieved resulting in a passable amount of measurement data which is stored in purposefully designed data storage centers [Kla2012].

6. Cross section calculations of the pp $\rightarrow$ t$\bar{\text{t}}$H process in LO and NLO using aMC@NLO

In this chapter calculations of the cross section $\sigma_{\mathrm{t\bar{t}H}}$ of the pp $\rightarrow$ t$\bar{\text{t}}$H process with aMC@NLO using fixed-order perturbation theory in leading order (LO) and next-to-leading order (NLO) together with the use of different parton distribution function sets (PDFs) at various center-of-mass energies ($\sqrt{s}$ = 7, 8, 13, 14 TeV) will be shown. After a motivation and an overview about the techniques used for the cross section calculations a general outline of the results of these cross section calculations will follow. Subsequently, the results will be discussed in more detail, before conclusions are given.

6.1 Motivation

Up to now the default sample used for the study of the pp $\rightarrow$ t$\bar{\text{t}}$H process in CMS is generated by Pythia6 in LO and a NLO K-factor k_{NLO} is used to scale the LO cross section $\sigma_{\mathrm{t\bar{t}H,LO}}$ of the LO event sample to the value of a NLO cross section $\sigma_{\mathrm{t\bar{t}H,NLO}}$ introducing scale uncertainties which have to be considered during the analysis.
Furthermore, it is well known that the LO cross sections $\sigma_{\mathrm{t\bar{t}H,LO}}$ calculated for different parton distribution function sets a long time ago [Rai1979] [Ng1984] [Kun1984] [Gun1991] [Mar1991] differ quite a lot because of the running of the strong coupling constant α_S. In more detail, in LO the value of the strong coupling constant α_S changes significantly with the given energy scale and every parton distribution function set makes use of its own implementation of the strong coupling constant α_S. In contrast to that, in NLO the change of the strong coupling constant α_S is only small, so it is expected that in NLO the difference of the cross sections $\sigma_{\mathrm{t\bar{t}H,NLO}}$ obtained from different parton distribution function sets is reduced leading to a smaller uncertainty due to the parton distribution function set which has to be taken into account for the analysis. Moreover, the NLO K-factor k_{NLO} used for the scaling of the LO cross section $\sigma_{\mathrm{t\bar{t}H,LO}}$ of an LO pp $\rightarrow$ t$\bar{\text{t}}$H event sample to the value of the NLO cross section $\sigma_{\mathrm{t\bar{t}H,NLO}}$ with a value of $k_{\mathrm{NLO}} = \frac{\sigma_{\mathrm{t\bar{t}H}}(\mathrm{NLO})}{\sigma_{\mathrm{t\bar{t}H}}(\mathrm{LO})} \approx 1.2$ [LHC2011] is quite large and previous studies [Bee2001] [Rei2001] [Bee2002] [Daw2002] [Fre2011] have already shown that the residual scale uncertainty decreased from $\mathcal{O}(50\%)$ in LO to an order of only $\mathcal{O}(10\%)$ in NLO "signalling a significant improvement of the theoretical prediction at NLO" [LHC2011].
Another interesting topic to study is the production mechanisms of t$\bar{\text{t}}$H: At Tevatron

energies ($\sqrt{s}$ up to 2 TeV) the cross section $\sigma_{\mathrm{t\bar{t}H}}$ and the production of $\mathrm{t\bar{t}H}$ should be dominated by the quark-antiquark annihilation (combination of $\mathrm{\bar{q}q} \to \mathrm{t\bar{t}H}$ and $\mathrm{q\bar{q}} \to \mathrm{t\bar{t}H}$) while at LHC energies (7 TeV $< \sqrt{s} <$ 14 TeV) gluon fusion $\mathrm{gg} \to \mathrm{t\bar{t}H}$ should be the dominant mechanism [Bee2002]. In this context, it is noteworthy that there should be no difference between the quark-antiquark annihilation cross section $\sigma_{\mathrm{t\bar{t}H}}(\mathrm{q\bar{q}})$ and the antiquark-quark annihilation cross section $\sigma_{\mathrm{t\bar{t}H}}(\mathrm{\bar{q}q})$ since both production processes can be described with the same s-channel matrix elements and are equal for a pp collision.

6.2 Program setup for calculation

The cross sections presented in this chapter were computed either with the LO or NLO operation mode of the most current version of aMC@NLO, which is part of the MadGraph5_aMC@NLO event generator version 2.2.2. If not stated otherwise the default values and parameters of this MadGraph5_aMC@NLO version have been used.
However, in all cases the value of the mass of the top quark m_t and the value of the corresponding Yukawa coupling of the top quark $y_{m_t}$was readjusted to $m_t = 172.5\,\mathrm{GeV}$ and $y_{m_t} = 172.5\,\mathrm{GeV}$, respectively, this is in accordance with the values chosen by the LHC Higgs Working Group for their studies (see [LHC2011], [LHC2012], and [LHC2013]) which will be used in the next section for a validation of the cross section results gained from aMC@NLO. Furthermore, if a four-flavour scheme (4FS) was applied the mass of the bottom quark m_b and its Yukawa coupling y_{m_b} was set to $m_b = 4.75\,\mathrm{GeV}$ and $y_{m_t} = 172.5\,\mathrm{GeV}$, respectively, corresponding with the choice of parameters in [LHC2011]. In contrast to the calculations referred to in [LHC2011], in a five-flavour (5FS) scheme the mass of the bottom quark m_b was neglected by chosing the "loop_sm-no_b_mass" model instead of the commonly used "loop_sm" in aMC@NLO (see subsection 6.3.1 for more information). Moreover, it is notable that the mass of the Higgs boson m_H was always kept at a value of $m_H = 125\,\mathrm{GeV}$ like given in the default parameter set.
Additionally, the parton distribution function set defined in the default configuration file of aMC@NLO and its associated parameters were changed: Instead of making use of the parton distribution function provided by aMC@NLO the LHAPDF interface [Buc2013] in version 6.1.4 was applied, so that also the error sets of the particular parton distribution were available and the scale and PDF uncertainties could be determined. Either a variable renormalization scale μ_R and factorization scale μ_F was chosen or a fixed value of $\mu_R = \mu_F = m_t + \frac{m_H}{2} = 235\,\mathrm{GeV}$ was applied for both scales in accordance with [LHC2011].
For the cross section calculation the following parton distribution functions were put into use:

- CTEQ66 [Nad2008]
- MSTW2008lo68cl [Mar2009]
- MSTW2008lo68cl_nf4 [Mar2009]
- MSTW2008nlo68cl [Mar2009]
- MSTW2008nlo68cl_nf4 [Mar2009]
- NNPDF23_lo_as_0119_qed [NNP2013]
- NNPDF30_nlo_as_0118 [NNP2014]
- NNPDF30_nlo_as_0118_nf4 [NNP2014]

The above-mentioned 5FS parton distribution functions CTEQ66 [Nad2008], MSTW2008lo68cl [Mar2009], and MSTW2008nlo68cl [Mar2009] were also applied to obtain the results in the publication of the LHC Higgs Working Group [LHC2011] which will later be used for a comparison (see subsection 6.3.1) with aMC@NLO. The publication of the LHC Higgs

Working Group [LHC2011] states also results gained from NNPDF20 [Bal2010] parton distribution functions. However, in the LHAPDF version 6.1.4 [Buc2013] only more recent parton distribution functions of the NNPDF collaboration are available. For the Run 2 Monte-Carlo event generation of the CMS collaboration it is planned to make use of the NNPDF23_lo_as_0119_qed [NNP2013] parton distribution function for the event generation in LO and of the NNPDF30_nlo_as_0118 [NNP2014] parton distribution function for the event generation in NLO, for this reason, these two parton distribution functions were also studied. Furthermore, for a comparison of cross sections, results obtained from a 5FS with results obtained from a 4FS the 4FS parton distribution functions MSTW2008lo68cl_nf4 [Mar2009], MSTW2008nlo68cl_nf4 [Mar2009], and NNPDF30_nlo_as_0118_nf4 [NNP2014] were used for the 4FS cross section calculation. In the appendix A the configuration files used with the aMC@NLO event generator are shown for the 4FS as well as the 5FS together with a more technical explanation of the varied parameters.

6.3 Results

In the tables 6.2-6.5 and in the tables 6.6-6.9 at the end of this chapter the cross sections $\sigma_{\mathrm{t\bar{t}H}}$ of the pp $\rightarrow$ $\mathrm{t\bar{t}H}$ process obtained with aMC@NLO for different center-of-mass energies ($\sqrt{s}$ = 7, 8, 13, 14 TeV) and parton distribution functions are given.
Beside the total cross section $\sigma_{\mathrm{t\bar{t}H}}$ of the pp $\rightarrow$ $\mathrm{t\bar{t}H}$ process, the tables 6.2-6.5 state the corresponding statistical uncertainty (Stat. unc.), the scale uncertainty (Scale unc.) due to the applied renormalization scale μ_R and factorization scale μ_F, and the uncertainty related to the parton distribution function (PDF unc.) for a given center-mass energy $\sqrt{s}$. Additionally, the tables contain the NLO K-factor k_{NLO} which was calculated dividing the NLO pp $\rightarrow$ $\mathrm{t\bar{t}H}$ cross section $\sigma_{\mathrm{t\bar{t}H,NLO}}$ by the LO pp $\rightarrow$ $\mathrm{t\bar{t}H}$ cross section $\sigma_{\mathrm{t\bar{t}H,LO}}$ ($k_{\mathrm{NLO}} = \frac{\sigma_{\mathrm{t\bar{t}H}}(\mathrm{NLO})}{\sigma_{\mathrm{t\bar{t}H}}(\mathrm{LO})}$).
In the tables 6.6-6.9 the cross sections of the three different production mechanism of $\mathrm{t\bar{t}H}$ and their statistical uncertainties are listed, the cross section of the gluon fusion $\sigma_{\mathrm{t\bar{t}H}}(\mathrm{gg})$, the cross section of the antiquark-quark annihilation $\sigma_{\mathrm{t\bar{t}H}}(\mathrm{\bar{q}q})$, and the cross section of the quark-antiquark annihilation $\sigma_{\mathrm{t\bar{t}H}}(\mathrm{q\bar{q}})$. Moreover, the ratio $\frac{\mathrm{gg}}{\mathrm{q\bar{q}+\bar{q}q}}$ between the two main production mechanisms of gluon fusion and quark-quark annihilation is given in the tables. Some aspects of the results documented in the aforementioned tables will be discussed in more detail in the subsequent subsections.

6.3.1 Comparison between four-flavour, five-flavour scheme results, and results of the LHC Higgs Working Group

For a center-of-mass energy of $\sqrt{s}$ = 7 TeV the cross section calculations were done in a four-flavour (4FS) and a five-flavour (5FS) scheme: In a four-flavour scheme the bottom quark and antiquark is neglected during the computation of the matrix elements by considering only the lighter quarks (up, down, charm, strange) and their associated antiquarks as content of the proton and by setting the bottom quark parton distribution function to zero, or in other words, by using a 4FS parton distribution function. For this reason, bottom partons can only be generated as final-state particles and in a subsequent event generation step the parton shower would have to introduce further bottom quarks and antiquarks during the parton shower and hadron decay step. In a five-flavour scheme the bottom quark and antiquark are already taken into account in the matrix element computation, therefore the definition of the initial-state protons (and other multiparticles like jets not occuring in this calculations) is changed in a way that they also contain bottom partons as possible interacting particles. However, there is an obstacle when a five-flavour scheme is used with aMC@NLO to calculate the cross section $\sigma_{\mathrm{t\bar{t}H}}$ of the pp $\rightarrow$ $\mathrm{t\bar{t}H}$ process, the bottom quarks and antiquarks appearing in the matrix element must be massless. Otherwise the IR divergences between the real emission and virtual matrix elements do not cancel and the cross section cannot be computated. The LO cross section can also not be done with massive bottom partons in the five flavour scheme without further adjusting of parameters in aMC@NLO since inconsistencies in the observed and expected center-of-mass energy of initial-state bottom partons arise during the integration of the matrix elements. The mass of the bottom quarks and antiquarks can be set to zero ($m_b = 0\,\mathrm{GeV}$) with no concern, though, because the parton distribution functions already include the mass of the bottom quark m_b. Nevertheless, the results of the cross section calculations obtained from aMC@NLO for a center-mass-energy $\sqrt{s} = 7$ TeV were compared with results coming from specifically tailored LO and NLO cross section calculations (see [Rai1979], [Ng1984], [Kun1984], [Gun1991], and [Mar1991] for LO results and [Bee2001], [Rei2001], [Bee2002], and [Daw2002] for NLO results) which were published by the LHC Higgs Working Group (see [LHC2011] and [LHC2013]). These calculations were done in a 5FS while massive bottom partons with a mass of $m_b = 4.75\,\mathrm{GeV}$ were taken into account, the mass of the top quark was set to $m_t = 172.5\,\mathrm{GeV}$ and a fixed renormalization and factorization scale of $\mu_R = \mu_F = m_t + \frac{m_H}{2} = 235\,\mathrm{GeV}$ was applied. Table 6.1 gives an extract of these LO and NLO cross section results for a center-of-mass energy of $\sqrt{s} = 7$ TeV and a mass of the Higgs boson of $m_H = 125\,\mathrm{GeV}$. In LO only the cross section $\sigma_{\mathrm{t\bar{t}H,LO}}$ of the $\mathrm{pp} \to \mathrm{t\bar{t}H}$ process is listed, in NLO beside the cross section $\sigma_{\mathrm{t\bar{t}H,NLO}}$ the scale uncertainty (Scale unc.) and the uncertainty due to the parton distribution function (PDF unc.) is stated.

Table 6.1: Extract of the LO and NLO cross section results of the LHC Higgs Working Group [LHC2011] for the $\mathrm{pp} \to \mathrm{t\bar{t}H}$ process and a center-of-mass energy of $\sqrt{s} = 7$ TeV: The cross section $\sigma_{\mathrm{t\bar{t}H}}$ is given either in LO or NLO for a particular parton distribution function (PDF). In NLO is also the scale uncertainty (Scale unc.) and the uncertainty due to the parton distribution function (PDF unc.) stated.

Order LO/NLO	PDF	$\sigma_{\mathrm{t\bar{t}H}}$ [fb]	Scale unc. +	Scale unc. -	PDF unc. +	PDF unc. -
LO	CTEQ66	71.44	–	–	–	–
NLO	CTEQ66	83.94	3.5%	−9.1%	6.3%	−5.3%
LO	MSTW2008lo68cl	87.66	–	–	–	–
NLO	MSTW2008nlo68cl	89.80	3.3%	−9.3%	3.0%	−3.4%
NLO	NNPDF20nlo	87.50	4.1%	−10.2%	4.2%	−4.2%

As mentioned in section 6.2 similar settings were applied to compute the cross sections with aMC@NLO. However, due to using the more recent version 6.1.4 of the LHAPDF interface [Buc2013] not all parton distribution functions used by the LHC Higgs Working Group were available, e.g. instead of the NNPDF20nlo parton distribution function [Bal2010] the newer NNPDF30_nlo_as_0118 and NNPDF30_nlo_as_0118_nf4 [NNP2014] parton distribution functions of the NNPDF collaboration were used.

Nonetheless, a comparison between the cross sections obtained with aMC@NLO and listed in table 6.2 with the cross sections of the LHC Working Group displayed in table 6.1 shows good agreement of the results originating from the same parton distribution function when a fixed renormalization and factorization scale was applied: All results, except the result of the 5FS CTEQ66 LO cross section and of the 4FS MSTW2008lo68cl LO cross section obtained with aMC@NLO, are compatible with each other if one takes a 2σ uncertainty into account. Comparing the results of the LHC Working Group and this thesis in more detail, one finds that the agreement between the results obtained with the MSTW2008 parton distribution functions in a 5FS is the best while the differences for the other two classes

of parton distribution functions are larger. In regard to the NNPDF parton distribution functions this difference can be explained by the use of different parton distribution function sets. The NNPDF23 and NNPD30 parton distribution functions already incorporate recent measurement data from the LHC which is not true for the other parton distribution functions. However, the difference between the results originating from the same CTEQ66 parton distribution function, which are still covered by statistical uncertainties of 2σ in the NLO case, is remarkable, especially because the obtained statistical uncertainties are smaller than the statistical uncertainties of the other two parton distribution function classes. It is also to note that the 5FS cross section results obtained from aMC@NLO by using the MSTW2008 parton distribution functions are in a better agreement with the 5FS cross section results published by the LHC Higgs Working Group than the 4FS results obtained from aMC@NLO which is not unexpected since the two flavour schemes have a different way to order the perturbative expansion and include different parts of the all-order result for the cross section at finite order of perturbation theory (for a more detailed discussion, see [Har2011]). This is the reason why for the other center-of-mass energies ($\sqrt{s}$ = 8, 13, 14 TeV) only the 5FS was used for the calculation of the cross sections. All in all, the results of the cross section calculations done with aMC@NLO seem trustworthy after this comparison with the results of the LHC Higgs Working Group.
Unfortunately, a further comparison with results published by the LHC Higgs Working Group (see [LHC2011] and [LHC2013]) for other center-of-mass energies $\sqrt{s}$ = 8 TeV and $\sqrt{s}$ = 14 TeV was not possible because for these center-of-mass energies only results using the envelope method of the PDF4LHC recommendation [Bot2011] were published and the calculation of these results was based on the combination of results obtained with the CTEQ66 [Nad2008], MSTW2008 [Mar2009], and NNPDF20 [Bal2010] parton distribution function, which is not available in LHAPDF version 6.1.4 [Buc2013].

6.3.2 Examination of the NLO K-factor behaviour as a function of the center-of-mass energy

The NLO K-factor $k_{\mathrm{NLO}} = \frac{\sigma_{\mathrm{t\bar{t}H}}(\mathrm{NLO})}{\sigma_{\mathrm{t\bar{t}H}}(\mathrm{LO})}$ of the pp $\rightarrow$ $\mathrm{t\bar{t}H}$ process which is calcuted by dividing the NLO pp $\rightarrow$ $\mathrm{t\bar{t}H}$ cross section $\sigma_{\mathrm{t\bar{t}H,NLO}}$ by the LO pp $\rightarrow$ $\mathrm{t\bar{t}H}$ cross section $\sigma_{\mathrm{t\bar{t}H,LO}}$ is used up to now in CMS to scale the LO cross section $\sigma_{\mathrm{t\bar{t}H,LO}}$ of an LO pp $\rightarrow$ $\mathrm{t\bar{t}H}$ event sample to the value of the NLO cross section $\sigma_{\mathrm{t\bar{t}H,NLO}}$ introducing scale uncertainties. The more the value of the K-factor k_{NLO} differs from one, the larger the scale uncertainties due to the larger difference between the LO cross section $\sigma_{\mathrm{t\bar{t}H,LO}}$ and the NLO cross section $\sigma_{\mathrm{t\bar{t}H,NLO}}$. For this reason, the K-factor should be either small or the events of the event sample should be directly produced by making use of NLO perturbation theory which would reduce the scale uncertainties in a way that only the quite smaller residual scale uncertainties due to higher orders (NNLO and even higher) would be left.
The cross section results obtained from aMC@NLO and listed in tables 6.2-6.5 show that the value of the NLO K-factor k_{NLO} increases from roughly $k_{\mathrm{NLO}} \approx$ 0.91-1.26 depending on the parton distribution function and on the renormalization and factorization scale chosen in aMC@NLO at a center-of-mass energy of $\sqrt{s}$ = 7 TeV to a value of approximately $k_{\mathrm{NLO}} \approx$ 1.12-1.30 at a center-of-mass energy of $\sqrt{s}$ = 14 TeV. This leads to the conclusion that for higher center-of-mass energies like $\sqrt{s}$ = 13, 14 TeV the generation of events used for the study of the pp $\rightarrow$ $\mathrm{t\bar{t}H}$ process with a NLO+PS event generator is preferable to the event generation with an LO event generator, so the recommendation based on these results of the K-factor behaviour would be to apply NLO+PS event generators for the Run 2 Monte-Carlo production in CMS, where pp $\rightarrow$ $\mathrm{t\bar{t}H}$ event samples at center-of-mass energies of $\sqrt{s}$ = 13, 14 TeV will be needed.

6.3.3 Comparison of scale uncertainties

From the results of the cross section calculations obtained by making use of aMC@NLO and given in tables 6.2-6.5 it is obvious that the scale uncertainties (Scale unc.) of the LO cross sections $\sigma_{\mathrm{t\bar{t}H,LO}}$ are quite larger (roughly a factor of 8-10) than the scale uncertainties of the corresponding NLO cross sections $\sigma_{\mathrm{t\bar{t}H,NLO}}$. Further it is to note that with an increase in center-of-mass energy $\sqrt{s}$ the scale uncertainties of the LO cross sections decrease while the scale uncertainties of the NLO cross sections increase in the vast majority of cases. Moreover, it can be said that the cross section results of the different parton distribution function classes differ quite a lot and that there are also large differences between the results obtained with a variable renormalization and factorization scale and the results obtained with fixed scales. Nonetheless, these differences are covered by the partially large scale uncertainties. Also it is to note that the scale uncertainties of the NNPDF parton distribution function class are almost always the smallest ones in comparison to the two other parton distribution function classes and if one neglects the cross section results at a center-of-mass energy of $\sqrt{s} = 7$ TeV.

6.3.4 Comparison of PDF uncertainties

It is difficult to make generalisations about the uncertainties related to the used distribution function (PDF unc.) which are given in the tables 6.2-6.5. However, it can be stated that the PDF uncertainties are getting smaller with increasing center-of-mass energies $\sqrt{s}$. This behaviour can be explained with the dependency of the parton distribution functions on the gluon distribution functions which depend themselves on the value of the strong coupling constant α_S and the dependency of the parton distribution functions on the quark masses, especially the heavy quark masses. Due to the running of the strong coupling constant α_S and in this regard the smaller variations of the strong coupling constant α_S at higher center-of-mass energies $\sqrt{s}$ the differences of the gluon distribution functions included in the different parton distribution functions of the same parton distribution function error set also diminish since the major difference between the parton distribution functions in the error set is the value of the strong coupling constant α_S. Furthermore, in a high-energy process at center-of-mass energy of $\sqrt{s} \approx$ some TeV even the mass of the heavy quarks becomes more and more neglectable and in this way also the dependency of the parton distribution function on the quark masses becomes smaller leading to decreasing uncertainties related to the parton distribution function. Moreover, the uncertainty of the parton distribution function also depends on the momentum fractions x_1 and x_2 of the colliding partons: At increasing center-of-mass energies $\sqrt{s}$ smaller values of $x_1 \cdot x_2$ are required to generate the $\mathrm{t\bar{t}H}$ final-state leading to smaller uncertainties of the scale since the parton distributions are better known for smaller momentum fractions x. Further it can be said that the LO cross section $\sigma_{\mathrm{t\bar{t}H,LO}}$ results applying the MSTW2008lo68cl parton distribution have the smallest PDF uncertainties of all LO cross sections $\sigma_{\mathrm{t\bar{t}H,LO}}$ while in NLO the PDF uncertainties of the MSTW2008nlo68cl and the NNPDF30 parton distribution function set have a comparable small value, whereby the PDF uncertainties of the NNPDF30 parton distribution function set are a little bit smaller than the uncertainties of the MSTW2008nlo68cl parton distribution function set. It remains to note that the PDF uncertainties originating from the use of the CTEQ66 parton distribution function set are quite high and that there is no big difference of the PDF uncertainties of the LO cross section calculations and the NLO cross section calculations. The latter can be explained by applying the CTEQ66 parton distribution function being an LO parton distribution function set also to the NLO cross section calculations.

6.3.5 Study of the total cross section and the production cross sections

In the tables 6.2-6.5 is the total cross section $\sigma_{\mathrm{t\bar{t}H}}$ of the pp $\rightarrow$ t$\bar{\mathrm{t}}$H process listed in dependency of the center-of-mass energy $\sqrt{s}$ and other important parameters. It is obvious that the total cross section $\sigma_{\mathrm{t\bar{t}H}}$ increases with an increase of the center-of-mass energy $\sqrt{s}$ as expected from theory and already shown by many publications due to the larger phase space (see [Rai1979], [Ng1984], [Kun1984], [Gun1991], [Mar1991], [Bee2001], [Rei2001], [Bee2002], and [Daw2002] as a starting point).
Nevertheless, it is interesting to study in this context the production mechanisms of t$\bar{\mathrm{t}}$H: The publication [Bee2002] has already stated that at Tevatron energies ($\sqrt{s}$ up to 2 TeV) the cross section $\sigma_{\mathrm{t\bar{t}H}}$ and the production of pp $\rightarrow$ t$\bar{\mathrm{t}}$H should be dominated by the quark-antiquark annihilation (combination of $\bar{\mathrm{q}}$q $\rightarrow$ t$\bar{\mathrm{t}}$H and q$\bar{\mathrm{q}}$ $\rightarrow$ t$\bar{\mathrm{t}}$H) while at LHC energies (7 TeV $< \sqrt{s} <$ 14 TeV) gluon fusion gg $\rightarrow$ t$\bar{\mathrm{t}}$H should be the dominant mechanism. However, the results of the ratio $\frac{\mathrm{gg}}{\mathrm{q\bar{q}+\bar{q}q}}$ between the two main production mechanisms of gluon fusion and quark-quark annihilation published by the aforementioned publication [Bee2002] are only given by using the LO cross section calculations $\sigma_{\mathrm{t\bar{t}H,LO}}$, center-of-mass energies of $\sqrt{s}$ = 2, 14 TeV and other values of the Higgs boson mass ($m_H = 120\,\mathrm{GeV},\ 140\,\mathrm{GeV},\ 160\,\mathrm{GeV},\ 180\,\mathrm{GeV}$).
For this reason, the results obtained from aMC@NLO and stated in the tables 6.6-6.9 of the cross section of the gluon fusion $\sigma_{\mathrm{t\bar{t}H}}(\mathrm{gg})$, the cross section of the antiquark-quark annihilation $\sigma_{\mathrm{t\bar{t}H}}(\mathrm{\bar{q}q})$, and the cross section of the quark-antiquark annihilation $\sigma_{\mathrm{t\bar{t}H}}(\mathrm{q\bar{q}})$ complete the knowledge about the pp $\rightarrow$ t$\bar{\mathrm{t}}$H production mechanisms and their dependency on the center-of-mass energy $\sqrt{s}$. In order to give a better overview the ratio $\frac{\mathrm{gg}}{\mathrm{q\bar{q}+\bar{q}q}}$ between the two main production mechanisms of gluon fusion and quark-quark annihilation is additionally given in the tables. It can be clearly seen that this ratio drastically increases with an increase in the center-of-mass energy $\sqrt{s}$ from roughly $\frac{\mathrm{gg}}{\mathrm{q\bar{q}+\bar{q}q}} \approx$ 0.89-1.66 depending on the parton distribution function and the choice of the renormalization and factorization scale at a center-of-mass energy of $\sqrt{s}$ = 7 TeV to $\frac{\mathrm{gg}}{\mathrm{q\bar{q}+\bar{q}q}} \approx$ 2.07-3.62 at a center-of-mass energy of $\sqrt{s}$ = 14 TeV. The reason of gluon fusion becoming the dominant production mechanism of the pp $\rightarrow$ t$\bar{\mathrm{t}}$H process at increasing center-of-mass energies $\sqrt{s}$ can be found in the higher probability to find a gluon in the parton distribution function of the colliding protons due to the increasing probability of gluon emission and parton splitting as predicted by the DGLAP evolution equations [Dok1977] [Gri1972] [Alt1977].
In this context, it is noteworthy that there should be no difference between the antiquark-quark annihilation cross section $\sigma_{\mathrm{t\bar{t}H}}(\mathrm{\bar{q}q})$ and the quark-antiquark annihilation cross section $\sigma_{\mathrm{t\bar{t}H}}(\mathrm{q\bar{q}})$ since both production processes can be described with the same s-channel matrix elements and are equal for a pp collision. However, it was observed that the cross sections of the antiquark-quark annihilation $\sigma_{\mathrm{t\bar{t}H}}(\mathrm{\bar{q}q})$ are always a little bit larger than the quark-antiquark annihilation cross sections $\sigma_{\mathrm{t\bar{t}H}}(\mathrm{q\bar{q}})$. Nonetheless, the cross sections of both quark-quark annihilation processes ($\bar{\mathrm{q}}$q $\rightarrow$ t$\bar{\mathrm{t}}$H and q$\bar{\mathrm{q}}$ $\rightarrow$ t$\bar{\mathrm{t}}$H) calculated by using the same parton distribution function and choice of the renormalization and factorization scale agree with each other if a 2σ uncertainty is taken into account.

6.4 Conclusion

As the comparison between the aMC@NLO cross section calculation results and the results of the LHC Higgs Working Group at a center-of-mass energy of $\sqrt{s}$ = 7 TeV shows, aMC@NLO delivers trustworthy results of the pp $\rightarrow$ t$\bar{\mathrm{t}}$H cross section which greatly depend on the perturbation order and the parton distribution function set used in the study. Furthermore, the results obtained with aMC@NLO at various center-of-mass energies $\sqrt{s}$ = 7, 8, 13, 14 TeV lead to the conclusion that it may be advantageous to

make use of a NLO perturbation theory approach and a NLO+PS event generator to generate the event samples needed for the analysis of the pp $\rightarrow$ t$\bar{\text{t}}$H process at least at higher center-of-mass energies of $\sqrt{s}$ = 13, 14 TeV due to the following reasons: The NLO K-factor increases with the center-of-mass energy $\sqrt{s}$, so that at higher center-of-mass energies like $\sqrt{s}$ = 13, 14 TeV the scaling of the LO cross section $\sigma_{\text{t}\bar{\text{t}}\text{H,LO}}$ of an LO pp $\rightarrow$ t$\bar{\text{t}}$H event sample to the value of a NLO cross section $\sigma_{\text{t}\bar{\text{t}}\text{H,NLO}}$ no longer appears to be justified as it leads to large uncertainties which should be avoided. Furthermore, the scale uncertainties of the NLO cross section calculations are significantly smaller (roughly by a factor of 8-10) than the scale uncertainties of the LO cross section calculations. Additionally, it is notable that the uncertainties due to the parton distribution function are the smallest when the NLO NNPDF30 parton distribution function set is applied to a NLO cross section calculation. Thus, it is comprehensible that the CMS Generator Group plans to use the NNPDF23 parton distribution function set in LO and the NNPDF30 parton distribution function set by default since both parton distribution functions have also the smallest scale uncertainties in comparison to the other two classes of parton distribution functions and integrate the most recent measurements.
As a conclusion, pp $\rightarrow$ t$\bar{\text{t}}$H event samples required for the comparison with the pp $\rightarrow$ t$\bar{\text{t}}$H measurement data obtained in the Run 2 of the LHC at a center-of-mass energy of either $\sqrt{s}$ = 13 TeV or $\sqrt{s}$ = 14 TeV should generally be generated with a NLO event generator and applying the NNPDF30 parton distribution function set in the NLO case. Therefore, the NNPDF23 parton distribution function set for additionally needed LO event samples is a good choice.
Finally, the study of the production cross sections of the pp $\rightarrow$ t$\bar{\text{t}}$H process has confirmed that at increasing center-of-mass energies of $\sqrt{s}$ = 7, 8, 13, 14 TeV gluon fusion is becoming more and more the dominant production mechanism of t$\bar{\text{t}}$H while the proportion of the quark-quark annihilation cross section ($\sigma_{\text{t}\bar{\text{t}}\text{H}}(\text{q}\bar{\text{q}}) + \sigma_{\text{t}\bar{\text{t}}\text{H}}(\text{q}\bar{\text{q}})$) on the increasing total cross section $\sigma_{\text{t}\bar{\text{t}}\text{H}}$ of the pp $\rightarrow$ t$\bar{\text{t}}$H process decreases.

Table 6.2: Total cross section and related uncertainties obtained with aMC@NLO for the $\mathrm{pp} \rightarrow \mathrm{t\bar{t}H}$ process and a center-of-mass energy $\sqrt{s} = 7$ TeV: The cross section $\sigma_{\mathrm{t\bar{t}H}}$ is given either in LO or NLO for a particular parton distribution function (PDF) and either a fixed or variable renormalization and factorization scale (Scale) together with a 4FS or 5FS was used. Additionally, the associated statistical uncertainties (Stat. unc.), the scale uncertainties (Scale unc.) and the uncertainties due to the applied parton distribution function (PDF unc.) are listed. Furthermore, the NLO K-factor $k_{\mathrm{NLO}} = \frac{\sigma_{\mathrm{t\bar{t}H}}(\mathrm{NLO})}{\sigma_{\mathrm{t\bar{t}H}}(\mathrm{LO})}$ of the corresponding LO and NLO cross section is stated.

$\sqrt{s}$	Order LO/NLO	PDF	Scale Var/Fix	FS 4FS/5FS	$\sigma_{\mathrm{t\bar{t}H}}$ [fb]	Stat. unc. [fb]	Scale unc. +	Scale unc. -	PDF unc. +	PDF unc. -	k_{NLO} $\frac{\sigma_{\mathrm{t\bar{t}H}}(\mathrm{NLO})}{\sigma_{\mathrm{t\bar{t}H}}(\mathrm{LO})}$
7 TeV	LO	MSTW2008lo68cl_nf4	Fix	4FS	86.67	2.0×10^{-1}	39.7%	−26.1%	2.6%	−2.7%	1.04
7 TeV	NLO	MSTW2008nlo68cl_nf4	Fix	4FS	90.40	5.6×10^{-1}	5.3%	−10.2%	3.1%	−3.4%	
7 TeV	LO	MSTW2008lo68cl_nf4	Var	4FS	75.07	1.7×10^{-1}	37.3%	−25.1%	2.5%	−2.6%	1.10
7 TeV	NLO	MSTW2008nlo68cl_nf4	Var	4FS	82.64	4.3×10^{-1}	5.8%	−10.1%	2.9%	−3.3%	
7 TeV	NLO	NNPDF30nlo_nf4	Fix	4FS	87.00	4.8×10^{-1}	5.0%	−10.0%	2.5%	−2.5%	0.91
7 TeV	NLO	NNPDF30nlo_nf4	Var	4FS	79.54	4.3×10^{-1}	5.9%	−10.0%	2.4%	−2.4%	
7 TeV	LO	CTEQ66	Fix	5FS	70.11	1.6×10^{-1}	35.2%	−24.1%	9.4%	−7.9%	1.19
7 TeV	NLO	CTEQ66	Fix	5FS	83.46	3.6×10^{-1}	3.6%	−9.1%	10.4%	−8.8%	
7 TeV	LO	CTEQ66	Var	5FS	61.62	1.4×10^{-1}	33.3%	−23.2%	9.2%	−7.7%	1.26
7 TeV	NLO	CTEQ66	Var	5FS	77.40	3.2×10^{-1}	4.8%	−9.3%	10.0%	−8.4%	
7 TeV	LO	MSTW2008lo68cl	Fix	5FS	87.50	2.0×10^{-1}	39.9%	−26.2%	2.5%	−2.5%	1.02
7 TeV	NLO	MSTW2008nlo68cl	Fix	5FS	89.63	5.6×10^{-1}	3.5%	−9.4%	3.0%	−3.4%	
7 TeV	LO	MSTW2008lo68cl	Var	5FS	76.12	1.7×10^{-1}	37.5%	−25.2%	2.4%	−2.5%	1.07
7 TeV	NLO	MSTW2008nlo68cl	Var	5FS	81.72	4.6×10^{-1}	4.3%	−9.4%	2.8%	−3.1%	
7 TeV	LO	NNPDF23lo	Fix	5FS	78.47	1.8×10^{-1}	34.8%	−23.8%	7.6%	−7.6%	1.12
7 TeV	NLO	NNPDF30nlo	Fix	5FS	88.19	5.3×10^{-1}	3.8%	−9.4%	2.7%	−2.7%	
7 TeV	LO	NNPDF23lo	Var	5FS	68.61	1.6×10^{-1}	32.7%	−22.9%	7.3%	−7.3%	1.17
7 TeV	NLO	NNPDF30nlo	Var	5FS	80.39	4.5×10^{-1}	4.8%	−9.5%	2.5%	−2.5%	

Table 6.3: Total cross section and related uncertainties obtained with aMC@NLO for the $pp \rightarrow t\bar{t}H$ process and a center-of-mass energy $\sqrt{s} = 8$ TeV: The cross section $\sigma_{t\bar{t}H}$ is given either in LO or NLO for a particular parton distribution function (PDF) and either a fixed or variable renormalization and factorization scale (Scale) together with a 5FS was used. Additionally, the associated statistical uncertainties (Stat. unc.), the scale uncertainties (Scale unc.) and the uncertainties due to the applied parton distribution function (PDF unc.) are listed. Furthermore, the NLO K-factor $k_{NLO} = \frac{\sigma_{t\bar{t}H}(NLO)}{\sigma_{t\bar{t}H}(LO)}$ of the corresponding LO and NLO cross section is stated.

$\sqrt{s}$	Order LO/NLO	PDF	Scale Var/Fix	FS 4FS/5FS	$\sigma_{t\bar{t}H}$ [fb]	Stat. unc. [fb]	Scale unc. +	Scale unc. -	PDF unc. +	PDF unc. -	k_{NLO} $\frac{\sigma_{t\bar{t}H}(NLO)}{\sigma_{t\bar{t}H}(LO)}$
8 TeV	LO	CTEQ66	Fix	5FS	103.8	2.3×10^{-1}	34.3%	−23.6%	8.5%	−7.3%	1.21
8 TeV	NLO	CTEQ66	Fix	5FS	125.5	5.6×10^{-1}	4.2%	−9.2%	9.4%	−8.1%	
8 TeV	LO	CTEQ66	Var	5FS	91.00	2.0×10^{-1}	32.4%	−22.7%	8.3%	−7.1%	1.26
8 TeV	NLO	CTEQ66	Var	5FS	114.8	5.0×10^{-1}	5.0%	−9.2%	9.0%	−7.7%	
8 TeV	LO	MSTW2008lo68cl	Fix	5FS	128.6	2.9×10^{-1}	38.9%	−25.7%	2.4%	−2.4%	1.05
8 TeV	NLO	MSTW2008nlo68cl	Fix	5FS	135.4	7.9×10^{-1}	4.5%	−9.6%	2.8%	−3.2%	
8 TeV	LO	MSTW2008lo68cl	Var	5FS	110.7	2.6×10^{-1}	36.6%	−24.7%	2.3%	−2.4%	1.11
8 TeV	NLO	MSTW2008nlo68cl	Var	5FS	123.3	7.0×10^{-1}	5.1%	−9.5%	2.6%	−3.0%	
8 TeV	LO	NNPDF23lo	Fix	5FS	115.2	2.7×10^{-1}	33.8%	−23.3%	7.0%	−7.0%	1.14
8 TeV	NLO	NNPDF30nlo	Fix	5FS	131.6	7.7×10^{-1}	3.8%	−9.1%	2.4%	−2.4%	
8 TeV	LO	NNPDF23lo	Var	5FS	101.1	2.4×10^{-1}	31.8%	−22.5%	6.7%	−6.7%	1.20
8 TeV	NLO	NNPDF30nlo	Var	5FS	121.0	6.8×10^{-1}	4.8%	−9.3%	2.3%	−2.3%	

Table 6.4: Total cross section and related uncertainties obtained with aMC@NLO for the $pp \rightarrow t\bar{t}H$ process and a center-of-mass energy $\sqrt{s} = 13$ TeV: The cross section $\sigma_{t\bar{t}H}$ is given either in LO or NLO for a particular parton distribution function (PDF) and either a fixed or variable renormalization and factorization scale (Scale) together with a 5FS was used. Additionally, the associated statistical uncertainties (Stat. unc.), the scale uncertainties (Scale unc.) and the uncertainties due to the applied parton distribution function (PDF unc.) are listed. Furthermore, the NLO K-factor $k_{NLO} = \frac{\sigma_{t\bar{t}H}(NLO)}{\sigma_{t\bar{t}H}(LO)}$ of the corresponding LO and NLO cross section is stated.

$\sqrt{s}$	Order LO/NLO	PDF	Scale Var/Fix	FS 4FS/5FS	$\sigma_{t\bar{t}H}$ [fb]	Stat. unc. [fb]	Scale unc. +	Scale unc. -	PDF unc. +	PDF unc. -	k_{NLO} $\frac{\sigma_{t\bar{t}H}(NLO)}{\sigma_{t\bar{t}H}(LO)}$
13 TeV	LO	CTEQ66	Fix	5FS	383.3	9.2×10^{-1}	30.9%	−21.9%	5.6%	−5.1%	1.26
13 TeV	NLO	CTEQ66	Fix	5FS	484.8	2.8	6.2%	−9.3%	6.0%	−5.5%	
13 TeV	LO	CTEQ66	Var	5FS	334.1	8.0×10^{-1}	29.1%	−21.0%	5.5%	−5.0%	1.30
13 TeV	NLO	CTEQ66	Var	5FS	436.0	2.2	6.0%	−9.0%	5.8%	−5.3%	
13 TeV	LO	MSTW2008lo68cl	Fix	5FS	463.2	1.1	35.4%	−24.2%	2.1%	−2.2%	1.11
13 TeV	NLO	MSTW2008nlo68cl	Fix	5FS	515.4	4.1	6.5%	−9.7%	2.2%	−2.7%	
13 TeV	LO	MSTW2008lo68cl	Var	5FS	398.8	9.7×10^{-1}	33.2%	−23.1%	2.0%	−2.1%	1.17
13 TeV	NLO	MSTW2008nlo68cl	Var	5FS	466.0	3.2	6.2%	−9.2%	2.0%	−2.5%	
13 TeV	LO	NNPDF23lo	Fix	5FS	420.9	1.1	30.3%	−21.6%	5.4%	−5.4%	1.22
13 TeV	NLO	NNPDF30nlo	Fix	5FS	512.7	3.5	5.7%	−9.2%	1.8%	−1.8%	
13 TeV	LO	NNPDF23lo	Var	5FS	368.4	9.9×10^{-1}	28.4%	−20.8%	5.1%	−5.1%	1.25
13 TeV	NLO	NNPDF30nlo	Var	5FS	460.3	3.1	5.7%	−8.9%	1.8%	−1.8%	

Table 6.5: Total cross section and related uncertainties obtained with aMC@NLO for the $pp \rightarrow t\bar{t}H$ process and a center-of-mass energy $\sqrt{s} = 14$ TeV: The cross section $\sigma_{t\bar{t}H}$ is given either in LO or NLO for a particular parton distribution function (PDF) and either a fixed or variable renormalization and factorization scale (Scale) together with a 5FS was used. Additionally, the associated statistical uncertainties (Stat. unc.), the scale uncertainties (Scale unc.) and the uncertainties due to the applied parton distribution function (PDF unc.) are listed. Furthermore, the NLO K-factor $k_{NLO} = \frac{\sigma_{t\bar{t}H}(NLO)}{\sigma_{t\bar{t}H}(LO)}$ of the corresponding LO and NLO cross section is stated.

$\sqrt{s}$	Order LO/NLO	PDF	Scale Var/Fix	FS 4FS/5FS	$\sigma_{t\bar{t}H}$ [fb]	Stat. unc. [fb]	Scale unc. +	Scale unc. -	PDF unc. +	PDF unc. -	k_{NLO} $\frac{\sigma_{t\bar{t}H}(NLO)}{\sigma_{t\bar{t}H}(LO)}$
14 TeV	LO	CTEQ66	Fix	5FS	461.7	1.1	30.4%	−21.7%	5.2%	−4.9%	1.27
14 TeV	NLO	CTEQ66	Fix	5FS	584.2	3.5	6.5%	−9.3%	5.6%	−5.2%	
14 TeV	LO	CTEQ66	Var	5FS	403.8	9.9×10^{-1}	28.6%	−20.8%	5.1%	−4.7%	1.30
14 TeV	NLO	CTEQ66	Var	5FS	523.5	2.4	6.0%	−8.8%	5.4%	−5.0%	
14 TeV	LO	MSTW2008lo68cl	Fix	5FS	559.8	1.4	34.9%	−23.9%	2.0%	−2.1%	1.12
14 TeV	NLO	MSTW2008nlo68cl	Fix	5FS	625.5	4.4	6.8%	−9.7%	2.1%	−2.6%	
14 TeV	LO	MSTW2008lo68cl	Var	5FS	481.5	1.2	32.7%	−22.9%	1.9%	−2.0%	1.15
14 TeV	NLO	MSTW2008nlo68cl	Var	5FS	555.5	3.7	5.5%	−8.8%	1.9%	−2.4%	
14 TeV	LO	NNPDF23lo	Fix	5FS	503.1	1.4	29.8%	−21.4%	5.2%	−5.2%	1.23
14 TeV	NLO	NNPDF30nlo	Fix	5FS	619.3	4.6	6.7%	−9.5%	1.8%	−1.8%	
14 TeV	LO	NNPDF23lo	Var	5FS	440.2	1.1	28.0%	−20.5%	5.0%	−5.0%	1.25
14 TeV	NLO	NNPDF30nlo	Var	5FS	549.7	3.7	5.6%	−8.8%	1.7%	−1.7%	

Table 6.6: Cross sections of the production mechanisms of the $pp \rightarrow t\bar{t}H$ process obtained with aMC@NLO for a center-of-mass energy $\sqrt{s} = 7$ TeV: The cross section of the gluon fusion $\sigma_{t\bar{t}H}(gg)$, the cross section of the antiquark-quark annihilation $\sigma_{t\bar{t}H}(\bar{q}q)$, and the cross section of the quark-antiquark annihilation $\sigma_{t\bar{t}H}(q\bar{q})$ and their statistical uncertainties (+/-) are given either in LO or NLO for a particular parton distribution function (PDF) and either a fixed or variable renormalization and factorization scale (Scale) together with a 4FS or 5FS was used. Additionally, the ratio $\frac{gg}{q\bar{q}+\bar{q}q}$ between the two main production mechanisms of gluon fusion and quark-quark annihilation is stated.

$\sqrt{s}$	Order LO/NLO	PDF	Scale Var/Fix	FS 4FS/5FS	$\sigma_{t\bar{t}H}(gg)$ [fb]	+/-	$\sigma_{t\bar{t}H}(\bar{q}q)$ [fb]	+/-	$\sigma_{t\bar{t}H}(q\bar{q})$ [fb]	+/-	$\frac{gg}{q\bar{q}+\bar{q}q}$
7 TeV	LO	MSTW2008lo68cl_nf4	Fix	4FS	44.18	1.3×10^{-1}	21.32	1.0×10^{-1}	21.16	1.0×10^{-1}	1.04
7 TeV	NLO	MSTW2008nlo68cl_nf4	Fix	4FS	55.26	5.2×10^{-1}	17.72	1.4×10^{-1}	17.40	1.5×10^{-1}	1.57
7 TeV	LO	MSTW2008lo68cl_nf4	Var	4FS	37.72	1.1×10^{-1}	18.69	9.0×10^{-2}	18.65	8.8×10^{-2}	1.01
7 TeV	NLO	MSTW2008nlo68cl_nf4	Var	4FS	49.19	3.7×10^{-1}	16.73	1.5×10^{-1}	16.70	1.3×10^{-1}	1.47
7 TeV	NLO	NNPDF30nlo_nf4	Fix	4FS	53.85	4.3×10^{-1}	16.60	1.4×10^{-1}	16.53	1.4×10^{-1}	1.63
7 TeV	NLO	NNPDF30nlo_nf4	Var	4FS	47.70	3.8×10^{-1}	15.97	1.2×10^{-1}	15.87	1.3×10^{-1}	1.50
7 TeV	LO	CTEQ66	Fix	5FS	36.91	1.1×10^{-1}	16.62	7.8×10^{-2}	16.57	7.6×10^{-2}	1.11
7 TeV	NLO	CTEQ66	Fix	5FS	52.03	2.9×10^{-1}	15.73	1.4×10^{-1}	15.69	1.4×10^{-1}	1.66
7 TeV	LO	CTEQ66	Var	5FS	31.89	9.5×10^{-2}	14.85	6.9×10^{-2}	14.85	6.9×10^{-2}	1.07
7 TeV	NLO	CTEQ66	Var	5FS	46.65	2.5×10^{-1}	15.45	1.4×10^{-1}	15.29	1.4×10^{-1}	1.52
7 TeV	LO	MSTW2008lo68cl	Fix	5FS	41.91	1.3×10^{-1}	22.84	1.0×10^{-1}	22.74	1.0×10^{-1}	0.92
7 TeV	NLO	MSTW2008nlo68cl	Fix	5FS	54.77	5.1×10^{-1}	17.55	1.5×10^{-1}	17.30	1.7×10^{-1}	1.57
7 TeV	LO	MSTW2008lo68cl	Var	5FS	35.85	1.1×10^{-1}	20.18	9.5×10^{-2}	20.07	9.3×10^{-2}	0.89
7 TeV	NLO	MSTW2008nlo68cl	Var	5FS	48.08	3.9×10^{-1}	16.89	1.6×10^{-1}	16.72	1.6×10^{-1}	1.43
7 TeV	LO	NNPDF23lo	Fix	5FS	47.91	1.5×10^{-1}	15.30	7.1×10^{-2}	15.24	7.2×10^{-2}	1.57
7 TeV	NLO	NNPDF30nlo	Fix	5FS	54.63	4.8×10^{-1}	16.81	1.5×10^{-1}	16.74	1.6×10^{-1}	1.63
7 TeV	LO	NNPDF23lo	Var	5FS	40.99	1.2×10^{-1}	13.81	6.4×10^{-2}	13.80	6.4×10^{-2}	1.48
7 TeV	NLO	NNPDF30nlo	Var	5FS	48.01	3.9×10^{-1}	16.19	1.4×10^{-1}	16.18	1.4×10^{-1}	1.48

Table 6.7: Cross sections of the production mechanisms of the $pp \rightarrow t\bar{t}H$ process obtained with aMC@NLO for a center-of-mass energy $\sqrt{s} = 8$ TeV: The cross section of the gluon fusion $\sigma_{t\bar{t}H}(gg)$, the cross section of the antiquark-quark annihilation $\sigma_{t\bar{t}H}(\bar{q}q)$, and the cross section of the quark-antiquark annihilation $\sigma_{t\bar{t}H}(q\bar{q})$ and their statistical uncertainties (+/-) are given either in LO or NLO for a particular parton distribution function (PDF) and either a fixed or variable renormalization and factorization scale (Scale) together with a 5FS was used. Additionally, the ratio $\frac{gg}{q\bar{q}+\bar{q}q}$ between the two main production mechanisms of gluon fusion and quark-quark annihilation is stated.

$\sqrt{s}$	Order LO/NLO	PDF	Scale Var/Fix	FS 4FS/5FS	$\sigma_{t\bar{t}H}(gg)$ [fb]	+/-	$\sigma_{t\bar{t}H}(\bar{q}q)$ [fb]	+/-	$\sigma_{t\bar{t}H}(q\bar{q})$ [fb]	+/-	$\frac{gg}{q\bar{q}+\bar{q}q}$
8 TeV	LO	CTEQ66	Fix	5FS	58.49	1.7×10^{-1}	22.67	1.0×10^{-1}	22.61	1.0×10^{-1}	1.29
8 TeV	NLO	CTEQ66	Fix	5FS	82.73	4.8×10^{-1}	21.46	1.9×10^{-1}	21.28	2.0×10^{-1}	1.94
8 TeV	LO	CTEQ66	Var	5FS	50.66	1.5×10^{-1}	20.34	9.6×10^{-2}	19.99	9.4×10^{-2}	1.26
8 TeV	NLO	CTEQ66	Var	5FS	73.18	4.2×10^{-1}	20.97	1.8×10^{-1}	20.65	1.9×10^{-1}	1.76
8 TeV	LO	MSTW2008lo68cl	Fix	5FS	67.10	2.0×10^{-1}	30.79	1.4×10^{-1}	30.68	1.4×10^{-1}	1.09
8 TeV	NLO	MSTW2008nlo68cl	Fix	5FS	87.83	7.2×10^{-1}	23.86	2.2×10^{-1}	23.72	2.2×10^{-1}	1.85
8 TeV	LO	MSTW2008lo68cl	Var	5FS	57.06	1.8×10^{-1}	26.99	1.2×10^{-1}	26.68	1.2×10^{-1}	1.06
8 TeV	NLO	MSTW2008nlo68cl	Var	5FS	77.53	6.2×10^{-1}	22.94	2.2×10^{-1}	22.80	2.2×10^{-1}	1.70
8 TeV	LO	NNPDF23lo	Fix	5FS	73.93	2.3×10^{-1}	20.67	9.6×10^{-2}	20.58	9.5×10^{-2}	1.79
8 TeV	NLO	NNPDF30nlo	Fix	5FS	86.29	6.9×10^{-1}	22.89	2.6×10^{-1}	22.45	2.0×10^{-1}	1.90
8 TeV	LO	NNPDF23lo	Var	5FS	63.78	1.9×10^{-1}	18.67	8.9×10^{-2}	18.66	8.7×10^{-2}	1.71
8 TeV	NLO	NNPDF30nlo	Var	5FS	77.20	6.1×10^{-1}	22.03	2.2×10^{-1}	21.72	2.0×10^{-1}	1.76

Table 6.8: Cross sections of the production mechanisms of the $pp \rightarrow t\bar{t}H$ process obtained with aMC@NLO for a center-of-mass energy $\sqrt{s} = 13$ TeV: The cross section of the gluon fusion $\sigma_{t\bar{t}H}(gg)$, the cross section of the antiquark-quark annihilation $\sigma_{t\bar{t}H}(\bar{q}q)$, and the cross section of the quark-antiquark annihilation $\sigma_{t\bar{t}H}(q\bar{q})$ and their statistical uncertainties (+/-) are given either in LO or NLO for a particular parton distribution function (PDF) and either a fixed or variable renormalization and factorization scale (Scale) together with a 5FS was used. Additionally, the ratio $\frac{gg}{q\bar{q}+\bar{q}q}$ between the two main production mechanisms of gluon fusion and quark-quark annihilation is stated.

$\sqrt{s}$	Order LO/NLO	PDF	Scale Var/Fix	FS 4FS/5FS	$\sigma_{t\bar{t}H}(gg)$ [fb]	+/-	$\sigma_{t\bar{t}H}(\bar{q}q)$ [fb]	+/-	$\sigma_{t\bar{t}H}(q\bar{q})$ [fb]	+/-	$\frac{gg}{q\bar{q}+\bar{q}q}$
13 TeV	LO	CTEQ66	Fix	5FS	262.5	8.2×10^{-1}	60.66	2.9×10^{-1}	60.15	2.8×10^{-1}	2.17
13 TeV	NLO	CTEQ66	Fix	5FS	369.1	2.6	58.08	5.7×10^{-1}	57.57	6.3×10^{-1}	3.19
13 TeV	LO	CTEQ66	Var	5FS	226.2	7.1×10^{-1}	54.02	2.5×10^{-1}	53.81	2.5×10^{-1}	2.10
13 TeV	NLO	CTEQ66	Var	5FS	326.8	2.0	54.71	5.2×10^{-1}	54.50	5.5×10^{-1}	2.99
13 TeV	LO	MSTW2008lo68cl	Fix	5FS	307.4	9.8×10^{-1}	77.97	3.6×10^{-1}	77.73	3.7×10^{-1}	1.97
13 TeV	NLO	MSTW2008nlo68cl	Fix	5FS	390.8	3.9	62.76	6.5×10^{-1}	61.76	6.9×10^{-1}	3.14
13 TeV	LO	MSTW2008lo68cl	Var	5FS	260.9	8.5×10^{-1}	69.15	3.2×10^{-1}	68.68	3.2×10^{-1}	1.89
13 TeV	NLO	MSTW2008nlo68cl	Var	5FS	346.8	3.0	59.68	6.0×10^{-1}	59.51	5.8×10^{-1}	2.91
13 TeV	LO	NNPDF23lo	Fix	5FS	311.4	1.0	54.80	2.5×10^{-1}	54.66	2.5×10^{-1}	2.84
13 TeV	NLO	NNPDF30nlo	Fix	5FS	395.8	3.3	58.51	6.0×10^{-1}	58.31	6.2×10^{-1}	3.39
13 TeV	LO	NNPDF23lo	Var	5FS	268.6	9.3×10^{-1}	50.19	2.3×10^{-1}	49.57	2.3×10^{-1}	2.69
13 TeV	NLO	NNPDF30nlo	Var	5FS	347.5	2.9	56.52	6.1×10^{-1}	56.23	6.4×10^{-1}	3.08

Table 6.9: Cross sections of the production mechanisms of the $pp \rightarrow t\bar{t}H$ process obtained with aMC@NLO for a center-of-mass energy $\sqrt{s} = 14$ TeV: The cross section of the gluon fusion $\sigma_{t\bar{t}H}(gg)$, the cross section of the antiquark-quark annihilation $\sigma_{t\bar{t}H}(\bar{q}q)$, and the cross section of the quark-antiquark annihilation $\sigma_{t\bar{t}H}(q\bar{q})$ and their statistical uncertainties (+/-) are given either in LO or NLO for a particular parton distribution function (PDF) and either a fixed or variable renormalization and factorization scale (Scale) together with a 5FS was used. Additionally, the ratio $\frac{gg}{q\bar{q}+\bar{q}q}$ between the two main production mechanisms of gluon fusion and quark-quark annihilation is stated.

$\sqrt{s}$	Order LO/NLO	PDF	Scale Var/Fix	FS 4FS/5FS	$\sigma_{t\bar{t}H}(gg)$ [fb]	+/-	$\sigma_{t\bar{t}H}(\bar{q}q)$ [fb]	+/-	$\sigma_{t\bar{t}H}(q\bar{q})$ [fb]	+/-	$\frac{gg}{q\bar{q}+\bar{q}q}$
14 TeV	LO	CTEQ66	Fix	5FS	324.0	1.0	69.00	3.3×10^{-1}	68.72	3.2×10^{-1}	2.35
14 TeV	NLO	CTEQ66	Fix	5FS	452.2	3.2	66.05	8.8×10^{-1}	65.90	7.0×10^{-1}	3.43
14 TeV	LO	CTEQ66	Var	5FS	280.3	9.0×10^{-1}	61.85	2.9×10^{-1}	61.58	2.9×10^{-1}	2.27
14 TeV	NLO	CTEQ66	Var	5FS	397.0	2.2	63.81	6.1×10^{-1}	62.67	5.7×10^{-1}	3.14
14 TeV	LO	MSTW2008lo68cl	Fix	5FS	382.5	1.2	89.20	4.2×10^{-1}	88.07	4.2×10^{-1}	2.16
14 TeV	NLO	MSTW2008nlo68cl	Fix	5FS	485.6	4.2	71.37	7.6×10^{-1}	68.47	7.4×10^{-1}	3.47
14 TeV	LO	MSTW2008lo68cl	Var	5FS	324.4	1.0	78.82	3.7×10^{-1}	78.17	3.6×10^{-1}	2.07
14 TeV	NLO	MSTW2008nlo68cl	Var	5FS	420.2	3.5	67.98	6.7×10^{-1}	67.24	7.0×10^{-1}	3.11
14 TeV	LO	NNPDF23lo	Fix	5FS	379.4	1.2	61.87	3.5×10^{-1}	61.70	2.9×10^{-1}	3.07
14 TeV	NLO	NNPDF30nlo	Fix	5FS	485.3	4.4	67.61	7.1×10^{-1}	66.31	7.1×10^{-1}	3.62
14 TeV	LO	NNPDF23lo	Var	5FS	327.4	1.0	56.84	2.6×10^{-1}	55.86	2.6×10^{-1}	2.91
14 TeV	NLO	NNPDF30nlo	Var	5FS	420.8	3.5	65.30	6.2×10^{-1}	63.58	6.3×10^{-1}	3.27

7. Comparison of LO and NLO event generation using aMC@NLO and Pythia8

In this chapter comparisons between inclusive leading-order (LO) and next-to-leading (NLO) event samples of the pp $\rightarrow$ $t\bar{t}$ process and the pp $\rightarrow$ $t\bar{t}H$ process will be made. After a motivation follows a section in which the production of the samples, the choice of the parameters used for the merging of the individual exclusive event samples to an inclusive sample of the particular process, and the event samples themselves are explained in more detail. This is followed by a description of the comparative studies carried out by using the aforementioned event samples and of the analysis tools developed for these studies.

7.1 Motivation

As already shown in chapter 6, using a NLO+PS event generator to generate the pp $\rightarrow$ $t\bar{t}H$ event samples would significantly reduce the scale uncertainties compared to a leading order (LO) event generator. The same should also be true for the generation of a next-to-leading order (NLO) pp $\rightarrow$ $t\bar{t}$ sample since both processes differ only in regard to the Higgs boson.

7.1.1 Current software status

With the first stable release of the MadGraph5_aMC@NLO [Alw2014] event generator in December 2013 there is an excellent and generally applicable tool to compare the LO and NLO event generation in a consistent manner. Furthermore, since spring 2014 it is possible to make use of the so-called FxFx merging technique (see section 4.5.3 for more information) in aMC@NLO, which allows to merge exclusive event samples with different jet multiplicities to an inclusive event sample of a particular process in NLO, while either the Herwig6 [Cor2002] or the Pythia8 [Sjö2014] general-purpose Monte-Carlo (GPMC) event generator is invoked afterwards. Until October 2014 each exclusive NLO sample had to be generated by the aMC@NLO matrix element event generator and fed into the GPMC event generator in a separate step. However, since the release of version 2.2.0 of the aMC@NLO matrix element event generator and the release of version 8.200

of the Pythia8 GPMC event generator in October/November 2014 it is also possible to use the so-called single-file FxFx merging technique in which the aMC@NLO matrix element event generator directly generates an inclusive NLO sample which then can be fed into the Pythia8 GPMC event generator in a second step. Based on this new single-file FxFx merging technique an aMC@NLO+ Pythia8 interface was implemented in the CMS software framework (CMSSW) [Inn2001] [Jon2008] which allows to create program packages usable to produce inclusive NLO event samples on the Worldwide LHC Computing Grid (WLCG) [Bir2005]. Due to the huge computing capacities available on the WLCG it is now also technically feasible to produce sizable $t\bar{t}$+0/1/2jets event samples with a combination of the aMC@NLO and Pythia8 event generator at reasonable expense while previously the jet multiplicity (number of additional jets) of the pp $\rightarrow t\bar{t}$ process and of the pp $\rightarrow t\bar{t}H$ had to be limited to one due to the large increase of computation time by considering higher jet multiplicities.

7.1.2 NLO for the pp $\rightarrow t\bar{t}$ and pp $\rightarrow t\bar{t}H$

For the production of the pp $\rightarrow t\bar{t}$ and the pp $\rightarrow t\bar{t}H$ event samples required for the Run 2 $t\bar{t}H$ analysis of the CMS measurement data the question arises if either an LO matrix element generator like MadGraph5 or a NLO matrix element generator like aMC@NLO should used together with the Pythia8 GPMC event generator by default. One major goal of this thesis therefore is to meet the urgent need to find out if the use of a NLO event generator would be beneficial for the $t\bar{t}H$ analysis of the CMS collaboration. For this reason, the comparison between a freshly produced NLO $t\bar{t}$+0/1/2jets event sample generated by using the single-file FxFx merging with an NLO $t\bar{t}$+0/1jets event sample, which was produced with the old FxFx merging technique, is motivated. Additionally, it is important to compare the NLO event generation with the LO event generation since one expects significantly reduced scale uncertainties due to the use of NLO perturbation theory as mentioned earlier. This topic is of interest since until now the differences between LO and NLO event samples of the pp $\rightarrow t\bar{t}$ process and the pp $\rightarrow t\bar{t}H$ with additional jets have not been sufficiently investigated in CMS. Furthermore, first studies showed that the generation of NLO pp $\rightarrow t\bar{t}$+jets and NLO pp $\rightarrow t\bar{t}H$+jets event samples has additional effects besides the decreased systematic uncertainties in a pp $\rightarrow t\bar{t}H$ analysis: The NLO event generation seems to increase the signal strength in the most sensitive analysis categories ($\geq$5 jets, $\geq$3 jets caused by a decaying bottom hadron) of the pp $\rightarrow t\bar{t}H$ analysis.

7.2 Production of event samples

All event samples in the subsequent comparisons were produced by using either the LO or NLO operation mode of aMC@NLO. Afterwards they were merged with the parton shower of the Pythia8 GPMC event generator by either applying MLM merging (see section 4.5.2) in the case of LO exclusive samples or FxFx merging (see section 4.5.3) in the case of NLO exclusive samples. For all event samples the Pythia8 GPMC event generator was invoked from within the CMS software framework (CMSSW), so that the event samples were stored in the event data model (EDM) defined by CMSSW which is based on the data format of the ROOT data analysis framework [Bru1997]. In this way, the event samples could later be analysed by making use of the CMS FrameworkLite (FWLite) [Jon2008] providing some additional software libraries and tools to handle the CMS EDM data format in ROOT.

Furthermore, in all cases a value of the matrix element minimum jet transverse momentum criterion of $p_{\mathrm{T,\,me}} = 10\,\mathrm{GeV}$, a value of the merging scale of $\mu_Q = 30\,\mathrm{GeV}$ (see the

subsequent subsection 7.2.1 for an explanation why this two parameter values were chosen), a value of the Higgs boson mass of $m_H = 125\,\text{GeV}$, and a value of the top quark mass of $m_t = 172.5\,\text{GeV}$ was chosen. If samples were produced in a five-flavour scheme (5FS) the mass of the bottom quark m_b was set to zero ($m_b = 0\,\text{GeV}$) by making use of the "loop_sm-no_b_mass" model instead of the commonly used "loop_sm" model in aMC@NLO. Moreover, a variable renormalization scale μ_R and a variable factorization scale μ_F were used since the authors of the FxFx merging [Alw2014] recommend to use variable scales instead of fixed scales. The individual samples are described in more detail in the subsequent sections.
The event samples were produced with miscellaneous versions of aMC@NLO, Pythia8, and CMSSW due to the short release cycles of these tools. However, the various versions of both event generators and of the CMS software framework used in this thesis should only differ in functionality, not in the description of the physics. So differences occuring later in the comparisons can be completely attributed to the variations of parameters of the corresponding event samples and should not be assigned to different release versions of the event generators or the CMS software framework.

7.2.1 Choice of the matrix element minimum jet transverse momentum selection criterion and merging scale

The merging scale μ_Q (see section 4.6.3) together with the matrix element minimum jet transverse momentum selection criterion $p_{\text{T, me}}$ (see section 4.6.4) are the two important parameters, when event samples of a ME+PS or a NLO+PS event generator are matched with the parton shower of a GPMC event generator. The authors of the FxFx merging algorithm [Alw2014] state that the FxFx merging procedure used to merge exclusive NLO event samples of various multiplicities to an inclusive NLO event samples exhibits a rather small, but non-zero dependence on the value of the merging scale μ_Q due to non-unitarity of the FxFx merging. However, they also note that in phase-space regions where matrix elements and parton shower will be vastly different the dependence on the merging scale μ_Q is bound to be large. They therefore came to the conclusion that the final choice of the merging scale μ_Q necessarily represents a non-perfect compromise between a matrix-element- and a parton-shower-dominated prediction and should be based on studies of the merging behaviour as a function of the merging scale μ_Q for processes in which the mass scale hierarchy is not overwhelming clear [Alw2014].

For the $\text{pp} \to \text{t}\bar{\text{t}}$ process as well as the $\text{pp} \to \text{t}\bar{\text{t}}\text{H}$ process the mass scale hierarchy is not well-defined since the masses of the final-state particles of the hard scattering process are large in comparison to the masses of the additional generated jets and the corresponding selection criteria of the transverse momenta of these additional jets $p_{\text{T, me}}$, compare e.g. the mass of the top quark $m_t = 172.5\,\text{GeV}$ to the mass of an additional jet with a transverse momentum of $p_T \gtrapprox 10\,\text{GeV}$. For this reason, elaborate studies were done in the context of a bachelor thesis [Sch2014a] to study the influence of various values of the merging scale μ_Q and the matrix element minimum jet transverse momentum selection criterion $p_{\text{T, me}}$. Based on theoretical considerations, the assumption was made that in the $\text{pp} \to \text{t}\bar{\text{t}}$ process and the $\text{pp} \to \text{t}\bar{\text{t}}\text{H}$ process the value of the merging scale μ_Q should be larger than the matrix element minimum jet transverse momentum selection criterion $p_{\text{T, me}}$ ($\mu_Q > p_{\text{T, me}}$) to achieve a reasonable merging [Ben2014]. The results of the aforementioned bachelor thesis [Sch2014a] verified this assumption and also lead to the conclusion that a value of the merging scale of $\mu_Q = 30\,\text{GeV}$ and a value of $p_{\text{T, me}} = 10\,\text{GeV}$ for the matrix element minimum jet transverse momentum selection criterion $p_{\text{T, me}}$ is a suitable choice for the FxFx merging of both the $\text{pp} \to \text{t}\bar{\text{t}}$ process and the $\text{pp} \to \text{t}\bar{\text{t}}\text{H}$ process. For this reason, these two values were also applied for the following comparison of LO and NLO event samples. Also in the LO case the same values were used to be comparable with the generation of the NLO events. Furthermore, the selection criterion for the transverse momenta p_T of the jets $p_{\mathrm{T,\,ana}}$, which is applied during the analysis of the event samples should be sufficiently larger than the merging scale μ_Q. Here a good choice in conjunction with the parameters suggested above is a value of $p_{\mathrm{T,\,ana}} = 50\,\mathrm{GeV}$, which was also later used during the analysis of the event samples (see section 7.3).

It is beyond the scope of this thesis to completely reflect the studies done for the determination of a good choice of the merging parameters. Nonetheless, in figure 7.1 a comparison of different merging scales ($10\,\mathrm{GeV} \leq \mu_Q \leq 100\,\mathrm{GeV}$) is presented for a matrix element minimum jet transverse momentum selection criterion of $p_{\mathrm{T,\,me}} = 10\,\mathrm{GeV}$ and an analysis level selection criterion for the transverse momentum of the jets occuring in the corresponding events of $p_{\mathrm{T,\,ana}} = 40\,\mathrm{GeV}$. For each value of μ_Q, the transverse momentum distribution of the hardest jet of an inclusive $\mathrm{t\bar{t}}$+0/1jets event sample is plotted. For this comparison, an inclusive 4FS $\mathrm{t\bar{t}}$+0/1jets event sample was used which was produced in NLO by using aMC@NLO version 2.1.1 and Pythia8 version 8.185 together with FxFx merging inside the CMS software framework version 7.1.0pre7 and which will be described in more detail later (see section 8.3.2). The comparison shows good agreement between all chosen merging scales except the merging scale with a value of $\mu_Q = 10\,\mathrm{GeV}$. The corresponding curve of the merging scale with a value of $\mu_Q = 10\,\mathrm{GeV}$ looks distorted. This is in line with the assumptation that the value of the merging scale μ_Q should be sufficiently larger than the value of the matrix element minimum jet transverse momentum selection criterion $p_{\mathrm{T,\,me}}$ which is not the case here. However, one can observe that all other merging scales μ_Q result in smooth distributions of various physics observables (for the sake of simplicity only the transverse momentum distribution of the hardest jet was shown) and that the merging is stable for different choices of the merging scale μ_Q. Consequently, it can be stated that the FxFx merging seems to be in accordance with the expectations and ready for use.

Additionally, in figure 7.2 a further result from the bachelor thesis [Sch2014a] using the same $\mathrm{t\bar{t}}$+0/1jets event sample is represented: In each subfigure the transverse momentum distribution of the jets originating from initial-state radiation (ISR) for three different merging scales ($\mu_Q = 20\,\mathrm{GeV}$ in green colour, $\mu_Q = 30\,\mathrm{GeV}$ in blue colour, and $\mu_Q = 60\,\mathrm{GeV}$ in red colour) is shown, where a matrix element minimum jet transverse momentum selection criterion of $p_{\mathrm{T,\,me}} = 10\,\mathrm{GeV}$ was applied. Different values of the analysis level selection criterion for the transverse momentum of the jets $p_{\mathrm{T,\,ana}}$ were used to obtain the subfigures. It can be seen that for an analysis level selection criterion of $p_{\mathrm{T,\,ana}} = 60\,\mathrm{GeV}$ and $p_{\mathrm{T,\,ana}} = 100\,\mathrm{GeV}$ there is a rather good agreement of the curves' shapes independent of the merging scale μ_Q , while for lower values of $p_{\mathrm{T,\,ana}}$ the curve of the merging scale with a value of $\mu_Q = 60\,\mathrm{GeV}$ significantly differs from the course of the other two curves. Furthermore, for $p_{\mathrm{T,\,ana}} \leq 30\,\mathrm{GeV}$ it can be observed that the shapes of all curves are different. All in all, these observations support the aforementioned argument that the analysis level selection criterion $p_{\mathrm{T,\,ana}}$ should be chosen in a way that it is sufficiently larger than the merging scale μ_Q and create confidence that an analysis selection criterion of $p_{\mathrm{T,\,ana}} = 50\,\mathrm{GeV}$ is a good choice in combination with the other two merging parameters of $\mu_Q = 30\,\mathrm{GeV}$ and $p_{\mathrm{T,\,me}} = 10\,\mathrm{GeV}$.

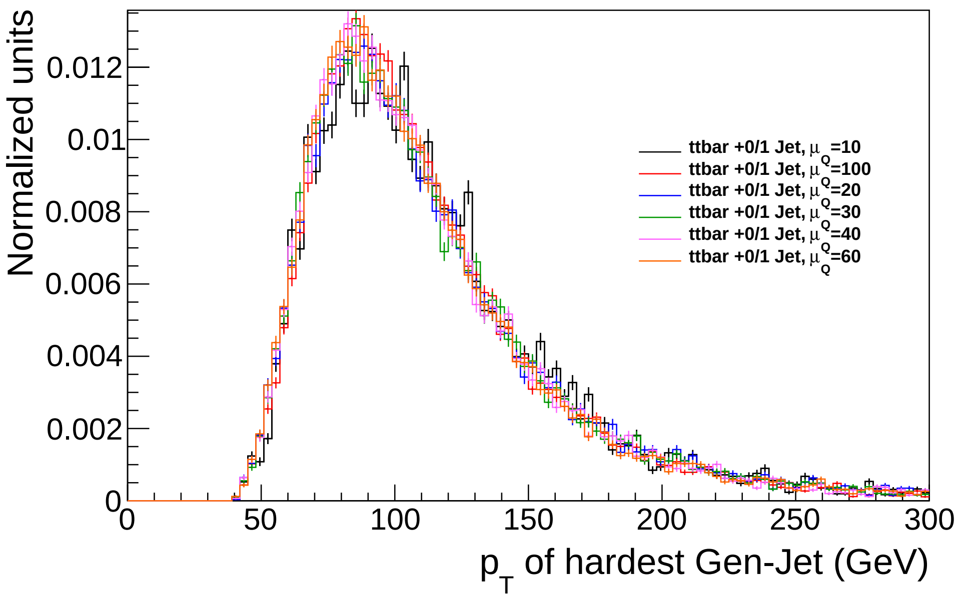

Figure 7.1: Comparison of different merging scales: For a matrix element minimum jet transverse momentum selection criterion of $p_{\mathrm{T,\ me}} = 10\,\mathrm{GeV}$ and an analysis level selection criterion of $p_{\mathrm{T,\ ana}} = 40\,\mathrm{GeV}$ the transverse momentum distribution of the hardest jet of a NLO $\mathrm{t\bar{t}}$+0/1jets event sample is shown in dependency of the merging scale ($10\,\mathrm{GeV} \leq \mu_Q \leq 100\,\mathrm{GeV}$) applied to the FxFx merging. Taken from [Sch2014b]

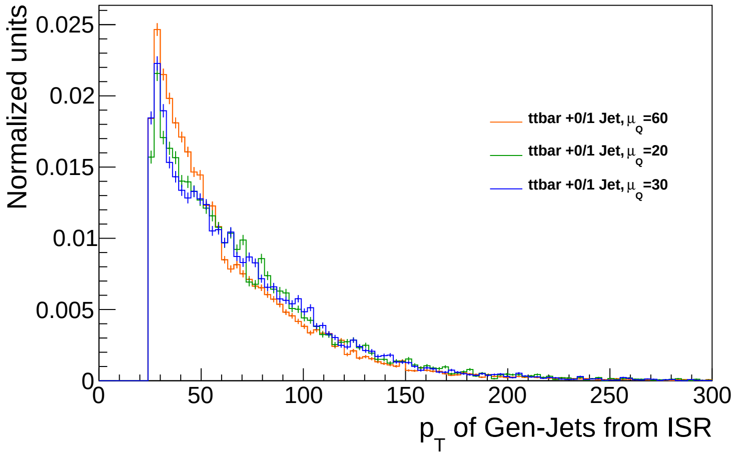

(a) $p_{\mathrm{T,\,ana}} = 25\,\mathrm{GeV}$

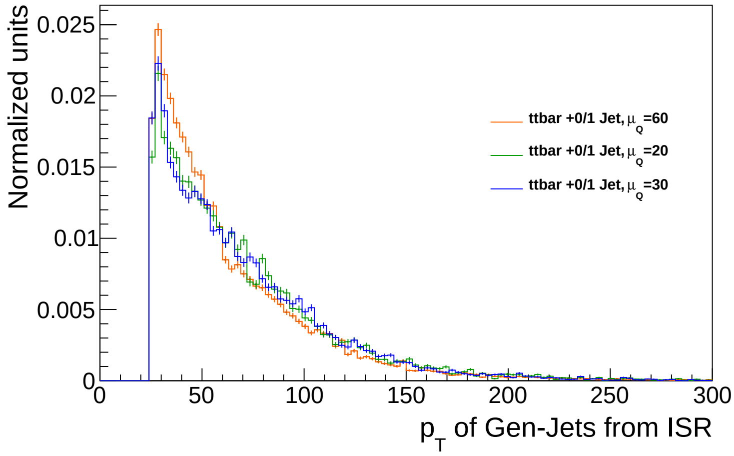

(b) $p_{\mathrm{T,\,ana}} = 30\,\mathrm{GeV}$

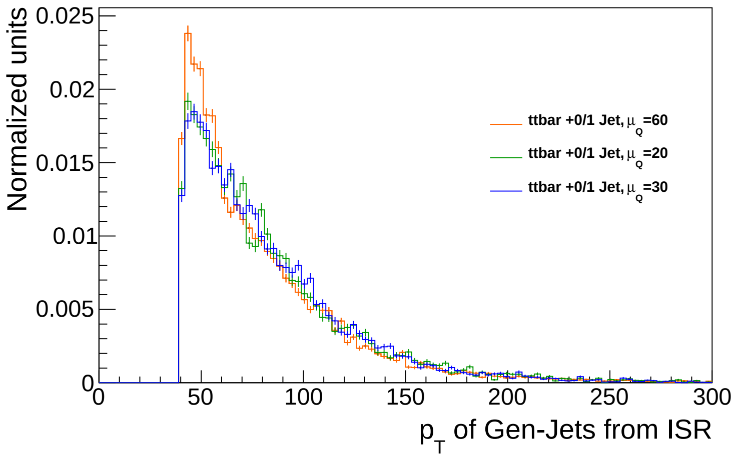

(c) $p_{\mathrm{T,\,ana}} = 40\,\mathrm{GeV}$

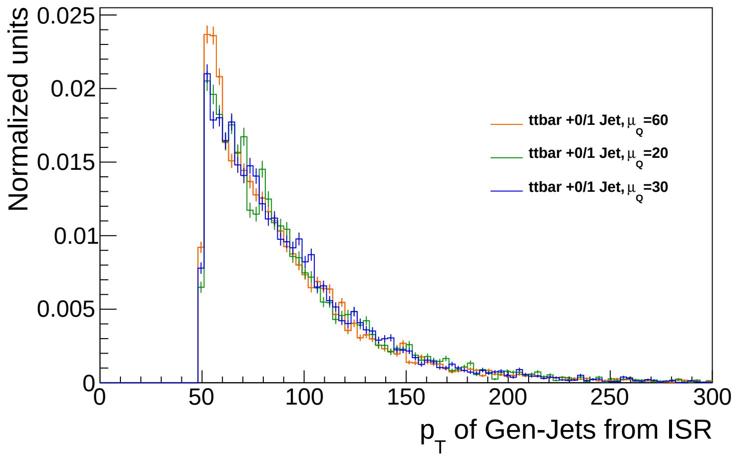

(d) $p_{\mathrm{T,\,ana}} = 50\,\mathrm{GeV}$

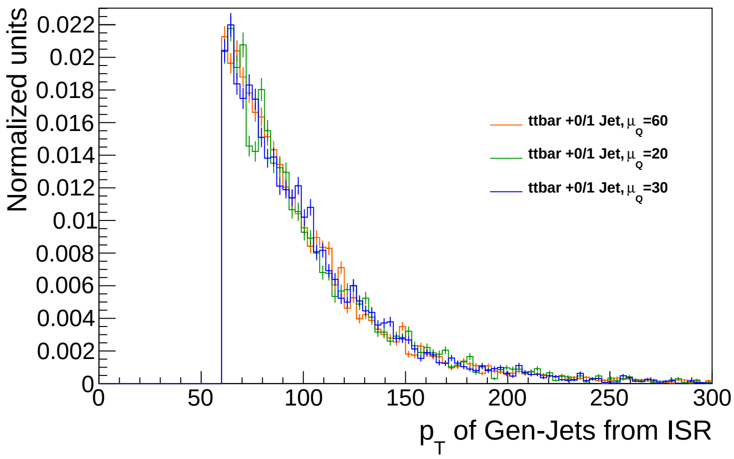

(e) $p_{\mathrm{T,\,ana}} = 60\,\mathrm{GeV}$

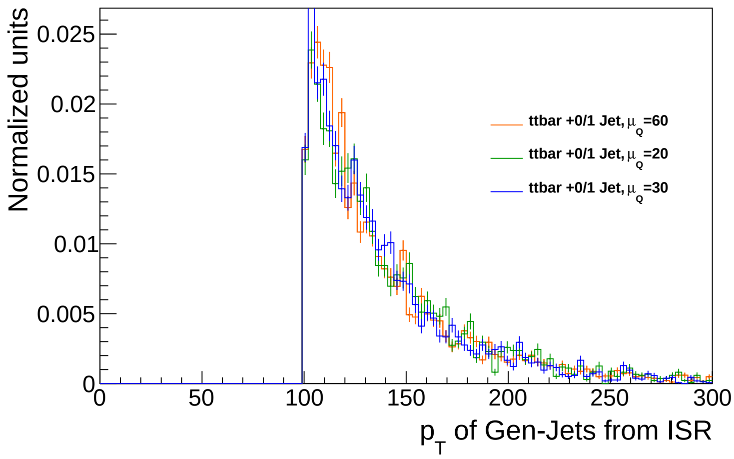

(f) $p_{\mathrm{T,\,ana}} = 100\,\mathrm{GeV}$

Figure 7.2: Comparison of different values of the analysis level selection criterion for the transverse momentum of the jets: In each subfigure the transverse momentum distribution of the jets originating from initial-state radiation (ISR) of a $t\bar{t}$+0/1jets event sample for three different merging scales ($\mu_Q = 20\,\mathrm{GeV}$ in green colour, $\mu_Q = 30\,\mathrm{GeV}$ in blue colour, and $\mu_Q = 60\,\mathrm{GeV}$ in red colour) is shown, where a matrix element minimum jet transverse momentum selection criterion of $p_{\mathrm{T,\,me}} = 10\,\mathrm{GeV}$ was applied. The subfigures differ in the value of the analysis level selection criterion $p_{\mathrm{T,\,ana}}$. The energy unit is GeV. Taken from [Sch2014b]

7.2.2 Sample $t\bar{t}$+0/1/2jets LO 4FS

The inclusive LO event sample of the pp → $t\bar{t}$+0/1/2jets process with a multiplicity of up to two additional jets was produced within the framework of a bachelor thesis [Sch2014a]. As a first step, an event sample of 100 000 events was generated by using the LO operation mode of version 2.1.1 of the aMC@NLO event generator together with a four-flavour scheme (4FS) and by applying MLM matching. Due to the unweighting of the event sample after this generation step the unweighted event sample consists of only 10 127 events. As a last step, version 8.185 of the Pythia8 GPMC event generator which is part of CMSSW version 7.1.0pre7 was used to process the parton-level event sample further and to obtain a particle-level event sample. Hereby the CTEQ6M [Pum2002] parton distribution function set was applied in both event generators.

7.2.3 Samples $t\bar{t}$+0/1jets NLO 4FS and $t\bar{t}$+0/1jets NLO 5FS

The first of the two inclusive NLO event sample of the pp → $t\bar{t}$+0/1jets process with a multiplicity of up to one additional jet was produced within the framework of a bachelor thesis [Sch2014a]: As a first step, exclusive event samples of the pp → $t\bar{t}$+0jet process and the pp → $t\bar{t}$+1jet process, each consisting of 100 000 events, were produced by using the NLO operation mode of the aMC@NLO version 2.1.1 together with a four-flavour scheme (4FS). Afterwards each of the two generated event samples with different multiplicity was further processed inside the CMSSW framework (CMSSW version 7.1.0pre7) with version 8.185 of the Pythia8 GPMC event generator. The two processed exclusive event samples at particle-level were combined together to a single inclusive, FxFx merged $t\bar{t}$+0/1jets event sample. Due to the use of the FxFx merging technique in the event generation the number of events in the inclusive event samples had been reduced to 79 466 events. The CTEQ6M [Pum2002] parton distribution function set was applied in both event generators.
The same procedures were executed to obtain the five-flavour scheme (5FS) event sample with a total number of events of 79 763.

7.2.4 Samples $t\bar{t}$+0/1/2jets NLO 4FS and $t\bar{t}$+0/1/2jets NLO 5FS

The first of the two inclusive NLO event sample of the pp → $t\bar{t}$+0/1/2jets process with a multiplicity of up to two additional jets was produced in the following way: An event sample consisting of 93 000 parton-level events of the pp → $t\bar{t}$+0/1/2jets was generated [Woo2014]. This parton-level event sample was generated by using the aMC@NLO+ Pythia8 interface inside the CMSSW framework (version 5.3.22) together with a four-flavour scheme (4FS), so that the event sample could be produced on the Worldwide LHC Computing Grid (WLCG) by using a predefined program package. In contrast to the other event samples the newest version of the aMC@NLO matrix element event generator version 2.2.2 was used, which allows to generate an inclusive event sample without having to generate each exclusive event sample before individually. Afterwards the parton-level event sample was further processed (by myself) inside the same version of the CMSSW framework 5.3.22 with the version 8.200 of the Pythia8 GPMC event generator. Due to making use of the FxFx merging technique the number of events in the inclusive event sample was reduced to 21 332 events. This newer version of the Pythia8 event generator is required when an inclusive FxFx merged event sample should be produced without having to generate and process exclusive event samples before combining them to an inclusive event sample. This procedure of directly producing an inclusive event sample is a new workflow for the FxFx merging technique and was available in the above-mentioned versions of both event generators for the first time. Nonetheless, the results of this way of FxFx merging should be identical to the previously used FxFx merging in which at first exclusive event samples had to be produced with the aMC@NLO matrix element event generator and further processed with the Pythia8 GPMC event generator before they could be combined to an inclusive event sample. It remains to note that the NNPDF30 [NNP2014] set of parton distribution functions was employed for the event generation. The same procedures were executed to obtain the five-flavour scheme (5FS) event sample with a total number of events of 22 420.

7.2.5 Sample $t\bar{t}$H+0/1/2jets LO 4FS

The inclusive LO event sample of the pp $\rightarrow$ $t\bar{t}$H+0/1/2jets process with a multiplicity of up to two additional jets was produced within the framework of a bachelor thesis [Sch2014a]. As a first step, an event sample of 100 000 events was generated by using the LO operation mode of the version 2.1.1 of the aMC@NLO event generator together with a four-flavour scheme (4FS) and by applying MLM matching. Due to the unweighting of the event sample after this generation step the unweighted event sample consists of only 10 477 events. As a last step, version 8.185 of the Pythia8 GPMC event generator, which is part of CMSSW version 7.1.0pre7 was used to process the parton-level event sample further and to obtain a particle-level event sample. Hereby the CTEQ6M [Pum2002] parton distribution function set was employed in both event generators.

7.2.6 Sample $t\bar{t}$H+0/1jets NLO 4FS

The inclusive NLO event sample of the pp $\rightarrow$ $t\bar{t}$H+0/1jets process with a multiplicity of up to one additional jet was produced within the framework of a bachelor thesis [Sch2014a]: As a first step, exclusive event samples of the pp $\rightarrow$ $t\bar{t}$H+0jets process and the pp $\rightarrow$ $t\bar{t}$H+1jet process, each consisting of 100 000 events, were produced by using the NLO operation mode of the aMC@NLO version 2.1.1 together with a four-flavour scheme (4FS). Afterwards each of the two generated event samples with different multiplicity was further processed inside the CMSSW framework (CMSSW version 7.1.0pre7) with version 8.185 of the Pythia8 GPMC event generator and the two processed exclusive event samples at particle-level were combined together to an inclusive, FxFx merged $t\bar{t}$+0/1jets event sample. Due to the use of the FxFx merging technique in the event generation the number of events in the finally obtained inclusive event samples had been reduced to 92 060 events. It remains to note that the CTEQ6M [Pum2002] parton distribution function set was employed in both event generators.

7.3 Comparative studies

For the comparative studies described in the subsequent sections an analysis selection criterion for the transverse momenta p_T of the jets occuring in the events of the corresponding event samples of $p_{\mathrm{T,\ ana}} = 50\,\mathrm{GeV}$ and an analysis selection criterion for the pseudo rapidity η of the jets occuring in the events of $|\eta|_{\mathrm{ana}} = 2.5$ was applied. In this thesis dedicated plotting and analysis scripts were used to analyze the event samples and to compare them with each other in a consistent way. In the following subsection 7.3.1 these scripts will be discussed in more detail.

7.3.1 Plotting and analysis scripts used for the comparative studies

The plotting and analysis scripts developed for this thesis are publicly available in a Github software repository (see [Har2014]). They are written in Python [Ros2003] and C++ [Str1995] and make use of the CMS FWLite [Jon2008] and the ROOT data analysis framework [Bru1997]. The first versions of the plotting and analysis scripts were developed with the aim to plot some basic distributions like the transverse momentum distribution of the hardest jet in a single event independently of the event generators which were used to generate the event samples. However, for a comprehensive comparative study between LO and NLO event generation, and especially an in-depth analysis of the FxFx merging technique used by the aMC@NLO and the Pythia8 event generator to obtain an inclusive NLO event sample an analyis of more difficult to determine observables like the number of gluons generated by the parton shower is necessary. For this reason, new versions of the plotting and analysis scripts, which interpret the complete event history of an event contained in the event samples and allow, among other things, to determine various physics observables, were developed based on my ideas and concepts in the context of a bachelor thesis [Sch2014c]. Nonetheless, there is one drawback: Expanding the functionality of the plotting and analysis scripts the general applicability of these scripts could not be maintained: Although all recent GPMC event generator use the HepMC Event Record [Dob2001] as a common data format to store the information about the events, it was necessary to take the specific event history and event description (e.g. the status codes of particles generated by the GPMC event generators which are different for each GPMC generator) into account to get access to the whole information of an event. In the context of the aforementioned dedicated bachelor thesis [Sch2014c] the plotting and analysis scripts were adopted to the event structure of the Pythia8 GPMC event generator. In this way, the full event history of single events can be plotted by using the Graphviz Visualization Software [Gan2000] which is useful to understand the event description used by the Pythia8 event generator. As an example, the complete event history of a pp → $t\bar{t}$H+1jet event is shown in figure 7.3. The event history consists of approximately 10^3 particles which are colour-coded according to their energy (high-energetic particles in red and orange, low-energetic particles in green and blue). In figure 7.4 another example of the broad range of functions of the plotting and analysis scripts is given, the same pp → $t\bar{t}$H+1jet event as before is shown. Jets originating from the Higgs boson are coloured in purple, jets originating from the $W^{\pm}$ bosons in red, and jets originating from the bottom quarks in orange.

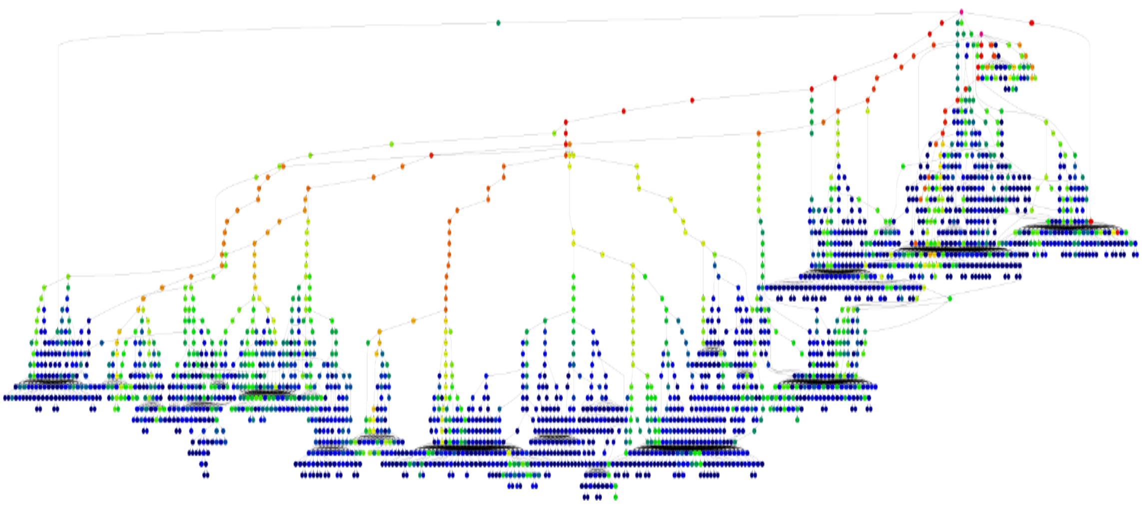

Figure 7.3: Graphical representation of the complete event history of a pp → $t\bar{t}$H+1jet event: The complete event history of a pp → $t\bar{t}$H+1jet event generated by the aMC@NLO and Pythia8 event generator and processed with the plotting and analysis scripts [Har2014] is drawn with the GraphViz Visualization Software [Gan2000]. The particles occuring are colour-coded according to their energy (high-energetic particles in red and orange, low-energetic particles in green and blue). Taken from [Sch2014d]

It is obvious that both graphical presentations are not very useful to study the event description by the Pythia8 event generator in more detail due to the huge amount of

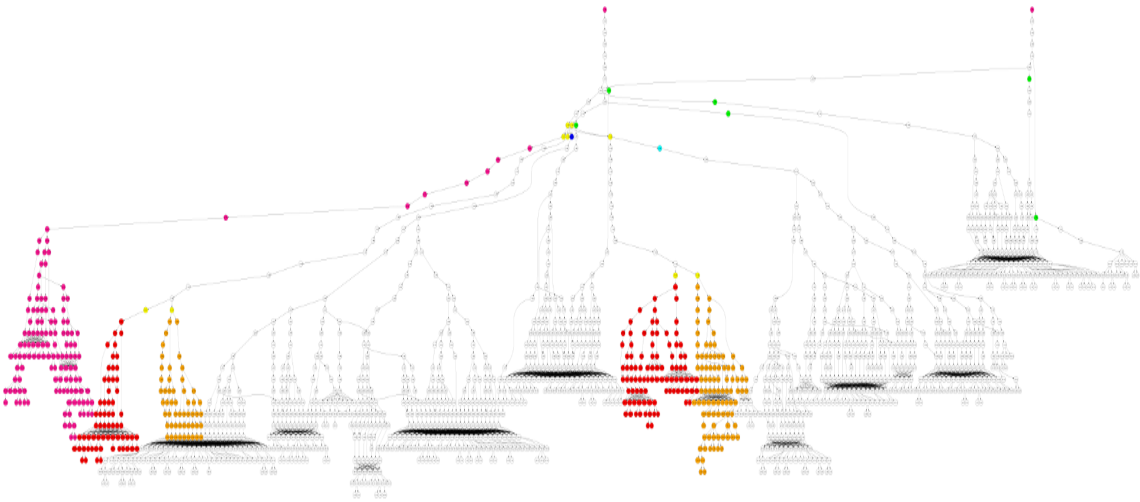

Figure 7.4: Colouring of jets occuring in the complete event history of a pp → $t\bar{t}$H+1jet event: The complete event history of a pp → $t\bar{t}$H+1jet event generated by the aMC@NLO and Pythia8 event generator and processed with the plotting and analysis scripts [Har2014] is drawn with the GraphViz Visualization Software [Gan2000]. Jets originating from the Higgs boson are coloured in purple, jets originating from the $W^{\pm}$ bosons in red, and jets originating from the bottom quarks in orange. Taken from [Sch2014d]

particles per event. Therefore the plotting and analysis scripts contain functions to discard the underlying event, to neglect particles below a given energy scale, and implement other selection criteria which cannot be completely described here (more information will be made available in [Sch2014c]). One of the major features of the scripts, the particle identification based on the particle itself and its production mechanism given by a status code (stated in the square brackets) used by the Pythia8 event generator, is displayed in figure 7.5 for the same pp → $t\bar{t}$H+1jet event. In this figure the hard scattering process generated by aMC@NLO is shown together with the major decay products of the pp → $t\bar{t}$H process and also initial-state radiation (ISR) and final-state radiation (FSR) generated by the parton shower of the Pythia8 GPMC event generator. Here, the status codes given in the event history by the Pythia8 GPMC event generator were used to identify the partons participating in the hard scattering process. By scanning the event history in a downward direction and by using the status codes the major decay products of the pp → $t\bar{t}$H process could be obtained in a second step. Afterwards all gluons with a particular status code, which were occuring in the event history between the hard scattering process and the decay of the major products, were considered together with their associated decay products as final-state radiation, while all gluons which were occuring in the event history between the initial proton-proton collision and the hard scattering process, were considered together with their decay products as initial-state radiation.
This particle identification feature of the plotting and analysis scripts demonstrated above was also applied to obtain the variables used in the subsequent comparative studies and to gather the information contained in each event in a histogram for the whole event sample. So far, the improved plotting and analysis scripts can only be used to analyse the output of the Pythia8 event generator. However, it is planned to implement the plotting and analysis scripts in the CMSSW framework and to extend their applicability to further GPMC event generators like the Herwig++ event generator, so that the comparative studies are not limited to one GPMC event generator.

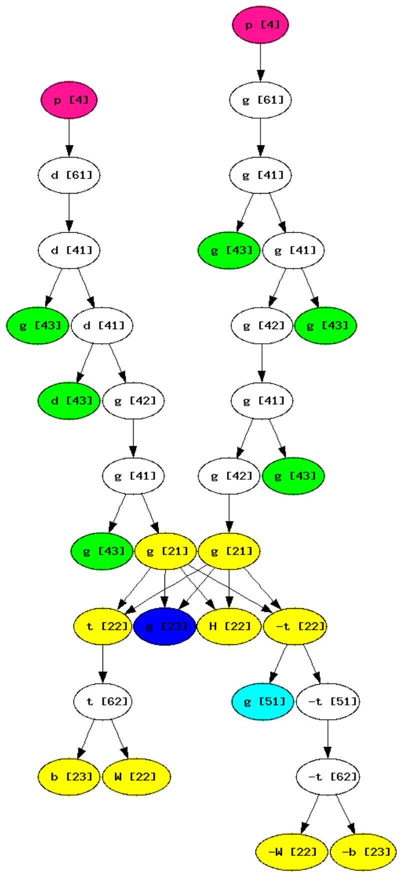

Figure 7.5: Graphical representation of the hard scattering process of a pp → $t\bar{t}$H+1jet event: The hard scattering process pp → $t\bar{t}$H+1jet generated by aMC@NLO is processed with the plotting and analysis scripts [Har2014] and drawn with the GraphViz Visualization Software [Gan2000]. Initial-state radiation, final-state radiation and the major decay products produced by the Pythia8 event generator and identified by the status codes given in square brackets are shown. The colliding protons are drawn in purple colour, the initial-state radiation (ISR) due to the emission of gluons by the parton shower of the Pythia8 event generator is drawn in green colour, the initial-state and final-state particles participating in the hard scattering process are drawn in yellow colour. The matrix element real emission, i.e. the emission of gluons which are described by a matrix element of the aMC@NLO event generator, is drawn in dark blue colour, the final-state radiation (FSR) generated by the parton shower is drawn in light blue colour, and the major decay products of the final-state particles, the $W^{\pm}$ bosons and the bottom quarks, are also drawn in yellow colour. Taken from [Sch2014d]

7.3.2 Comparison of 4FS LO and NLO event samples of the pp $\to$ t$\bar{\text{t}}$ process

The comparative study makes use of the event samples t$\bar{\text{t}}$+0/1/2jets LO 4FS, t$\bar{\text{t}}$+0/1jets NLO 4FS, and t$\bar{\text{t}}$+0/1/2jets NLO 4FS and the previously described plotting and analysis scripts to compare the LO MLM merging, the old version of the NLO FxFx merging and the new single-file FxFx merging for the pp $\to$ t$\bar{\text{t}}$ process. In figure 7.6 the number of jets n_{jets} occuring in the events of the corresponding event sample is shown. It is obvious from the histograms in the figure that the t$\bar{\text{t}}$+0/1/2jets NLO 4FS has a larger fraction of events with higher jet multiplicity and a higher arithmetic mean of the number of jets $\overline{n}_{\text{jets}} = 3.434 \pm 0.021$ than the other two event samples, the t$\bar{\text{t}}$+0/1jets NLO 4FS has on average the smallest number of jets $\overline{n}_{\text{jets}} = 2.749 \pm 0.009$ and the MLM merged t$\bar{\text{t}}$+0/1/2jets LO 4FS lies between the other two event samples with a mean value of the number of jets $\overline{n}_{\text{jets}} = 2.930 \pm 0.013$ (see also table 7.1 for further numbers). This is in line with the expectactions: Due to considering only up to one additional parton in the matrix element generator the t$\bar{\text{t}}$+0/1jets NLO 4FS event sample should have the smallest jet multiplicity and also the smallest mean number of jets $\overline{n}_{\text{jets}}$. Furthermore, the t$\bar{\text{t}}$+0/1/2jets NLO 4FS event sample should have more additional jets and, thus, also a larger number of jets than the t$\bar{\text{t}}$+0/1/2jets LO 4FS sample since in NLO additional real emission matrix elements are taken into account beside the Born matrix elements.

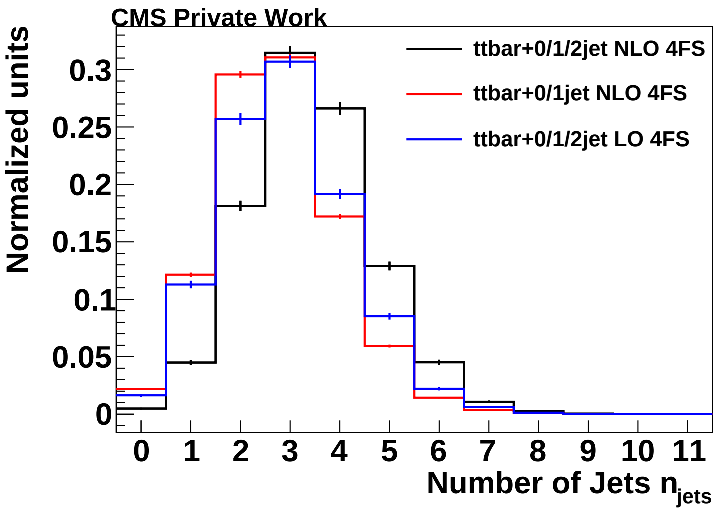

Figure 7.6: Comparison of the number of jets occuring in an event between various 4FS event samples of the pp $\to$ t$\bar{\text{t}}$ process: The distribution of the number of jets occuring in an event n_{jets} is shown for the corresponding event sample.

Figure 7.7 illustrates this difference in the number of additional matrix element emissions n_{MEE} by showing the number of additional partons generated by the matrix element generator. As expected, the aMC@NLO event generator produced only events with zero or one additional parton for the t$\bar{\text{t}}$+0/1jets NLO 4FS event sample and events with up to two additional partons for the t$\bar{\text{t}}$+0/1/2jets LO 4FS sample and the t$\bar{\text{t}}$+0/1/2jets NLO 4FS sample. In addition, it stands out that the NLO event samples have negative fractions of events with either $n_{\text{MEE}} = 2$ or $n_{\text{MEE}} = 3$ additional partons generated by the matrix element generator in the case of the t$\bar{\text{t}}$+0/1jets NLO 4FS event sample or the t$\bar{\text{t}}$+0/1/2jets NLO 4FS event sample, respectively. This can be attributed to the FxFx merging which considers the overlap between the emissions originating from the real emission matrix elements of the hard subprocesses with the highest multiplicity and the emissions of the parton shower, in particular the initial-state radiation (ISR) and the final-state

(FSR), which is following after the matrix element generator and part of a GPMC event generator, by introducing subtraction terms. Hereby, the value of the negative fraction of events depends on the probability that the parton shower overlaps with the real emission matrix element of the hard subprocess with the highest multiplicity which can be calculated for a particular parton shower by making use of Sudakov form factors. Moreover, it is to note that the probability for an overlap decreases with an increase in the highest multiplicity of the merged NLO event samples since the real emission matrix elements favour the emission of hard (high energy and/or large angle) additional partons. The parton shower, in contrast to that, uses collinear factorization to create additional partons. As a consequence the probability that additional partons generated by the parton shower are soft (low energy and/or small angle) increases with the number of additional partons. For this reason, the negative fraction of the $t\bar{t}$+0/1/2jets NLO 4FS event sample is much smaller than the negative fraction of the $t\bar{t}$+0/1jets NLO 4FS event sample. In this context, it should be noted that events with either $n_{\mathrm{MEE}} = 2$ or $n_{\mathrm{MEE}} = 3$ additional partons generated by the matrix element generator and with positive event weight as well as events with negative event weight occur, however, the fraction of events with negative event weight is larger in the case of either $n_{\mathrm{MEE}} = 2$ or $n_{\mathrm{MEE}} = 3$ additional partons generated by the matrix element generator.

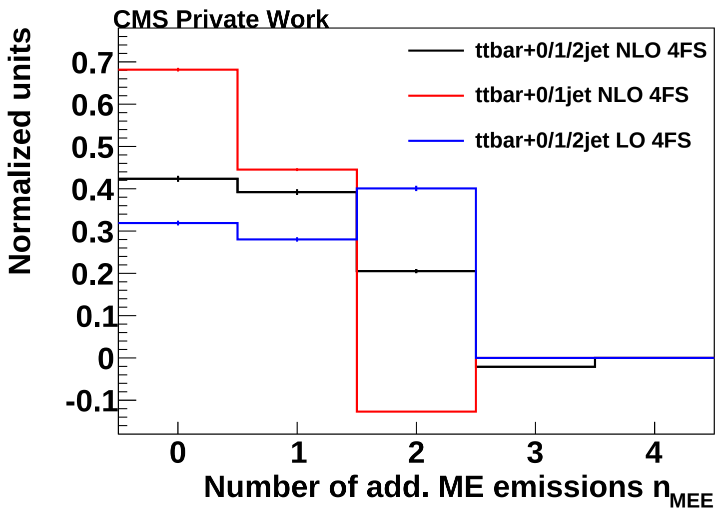

Figure 7.7: Comparison of the number of additional matrix element emissions between various 4FS event samples of the pp $\rightarrow t\bar{t}$ process: The distribution of the number of additional partons generated by the aMC@NLO matrix element generator n_{MEE} in an event is shown for the corresponding event sample.

Figure 7.8 shows the number of final-state partons produced by the parton shower n_{FSR} and demonstrates that the parton shower fills the parts of the phase-space which were taken account of by introducing the subtraction terms of the FxFx merging. It can be seen that all event samples have the same fraction of events with zero final-state partons ($n_{\mathrm{FSR}} = 0$) and also a similar fraction of events with one final-state parton ($n_{\mathrm{FSR}} = 1$). However, due to the FxFx merging and the consideration of events originating from the real emission matrix elements of the hard process with the highest multiplicity, the $t\bar{t}$+0/1jets NLO 4FS event sample contains a larger fraction of events with two or more final-state partons ($n_{\mathrm{FSR}} \geq 2$) than the other two event samples and the $t\bar{t}$+0/1/2jets NLO 4FS has the same fraction of events with three or more final-state partons ($n_{\mathrm{FSR}} \geq 3$) since for this sample events originating from real emission matrix elements of a hard process with a multiplicity of two are taken into account.
In this context, it is noteworthy that the probability for the emission of final-state radiation

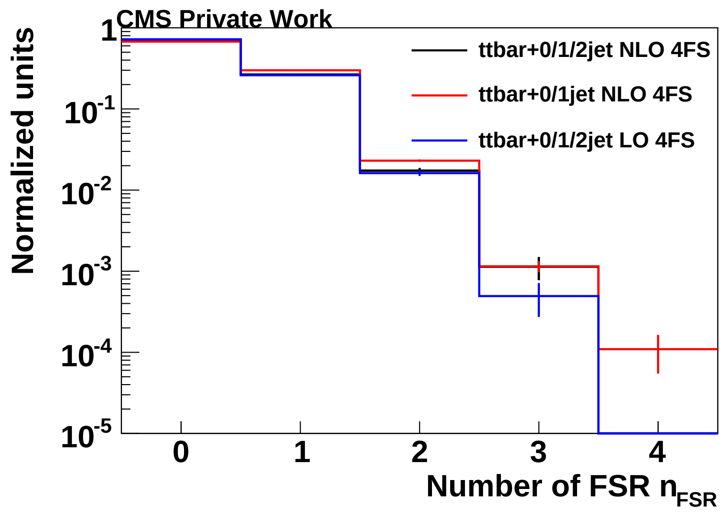

Figure 7.8: Comparison of the number of final-state radiation jets between various 4FS event samples of the pp $\rightarrow$ t$\bar{\text{t}}$ process: The distribution of the number of additional jets caused by final-state radiation n_{FSR} in an event is shown for the corresponding event sample.

depends mostly on the energy of the additional partons and only to a smaller extent on the number of additional partons (Final-state radiation from the top quark or top antiquark can be neglected due to the short lifetime of the top quark of only 5×10^{-25} s [Qua2006] and the fast decay into a $\text{W}^{\pm}$ boson and a down-type quark). This is the reason why both NLO event samples have a similar number of events with three or four final-state particles ($n_{\text{FSR}} = 3$ or $n_{\text{FSR}} = 4$). The fraction of such events is larger in comparison with the LO t$\bar{\text{t}}$+0/1/2jets sample because they have more additional partons originating from the matrix element computation with higher energy due to the additional real emission matrix elements in NLO, which is shown in figure 7.9. Here the energy of the additional partons generated by the matrix element generator E_{MEE} is displayed and it can be seen that the NLO event samples have a larger number of additional emissions with an energy above $E_{\text{MEE}} = 100$ GeV. The t$\bar{\text{t}}$+0/1jets NLO 4FS sample has the largest number of such high-energetic additional matrix element emissions, however, one should keep in mind that the t$\bar{\text{t}}$+0/1/2jets NLO 4FS event sample has only a smaller fraction of such high-energetic events since it also has a large probability to create two additional matrix element emissions instead of only zero or one emissions as the t$\bar{\text{t}}$+0/1jets NLO 4FS sample. In this way the energy is distributed among the two additional matrix element emissions.
Coming back to the original motivation of studying the difference between LO and NLO event samples, in figure 7.10a the energy distribution of all jets occuring in the single events of an event sample E_{jets} is displayed and in figure 7.10b the energy distribution of all jets caused by final-state radiation E_{FSR} is displayed. The difference in the energy distribution between the MLM merged LO event sample and the two FxFx merged NLO samples of the pp $\rightarrow$ t$\bar{\text{t}}$ process is rather small if all jets are considered. Nonetheless, especially for energies between $E_{\text{jets}} \approx 30$ GeV and $E_{\text{jets}} \approx 70$ GeV it can be seen that the LO t$\bar{\text{t}}$+0/1/2jets event sample and the NLO t$\bar{\text{t}}$+0/1jets event sample have a higher fraction of low-energetic jets than the NLO t$\bar{\text{t}}$+0/1/2jets event samples. This difference between the LO and NLO sample with up to a multiplicity of two becomes even more apparent if one takes only the energy of the jets caused by final-state radiation E_{FSR} into account. Figure 7.10b clearly shows that the LO event sample has a significantly larger fraction of low-energetic jets coming from final-state radiation below $E_{\text{FSR}} \approx 30$ GeV and that the two NLO event samples contain more jets caused by final-state radiation with an

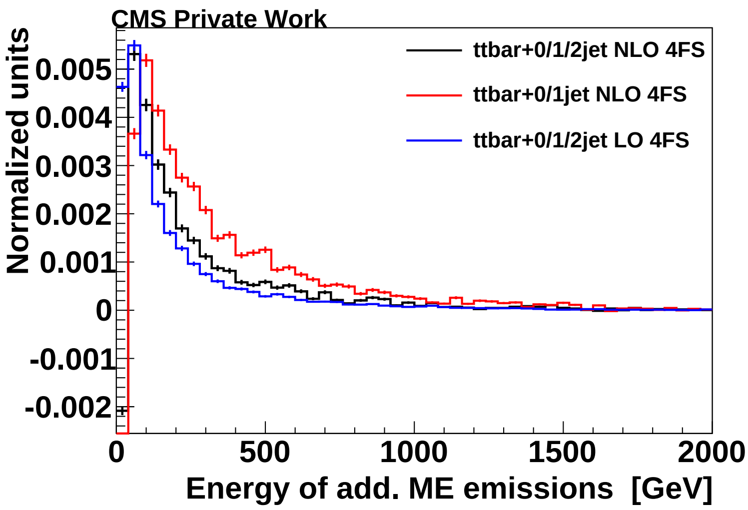

Figure 7.9: Comparison of the energy of additional matrix element emissions between various 4FS event samples of the pp $\to t\bar{t}$ process: The distribution of the energy of additional partons generated by the aMC@NLO matrix element generator is shown for the corresponding event sample.

energy above $E_{\mathrm{FSR}} \approx 30\,\mathrm{GeV}$. This larger fraction of high-energetic final-state radiation can be attributed to the consideration of real emission matrix elements by the matrix element generator and the application of the FxFx merging technique to merge the results of the NLO operation mode of the aMC@NLO event generator to the parton shower of the Pythia8 GPMC event generator.

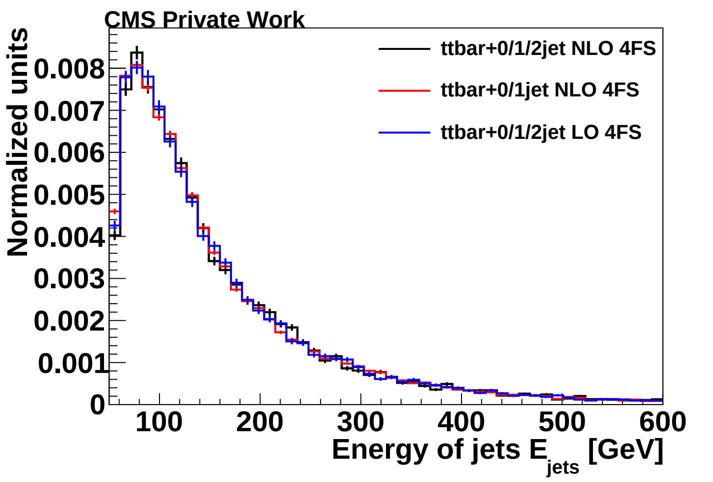

(a) Energy distribution of all jets occuring in an event E_{jets}

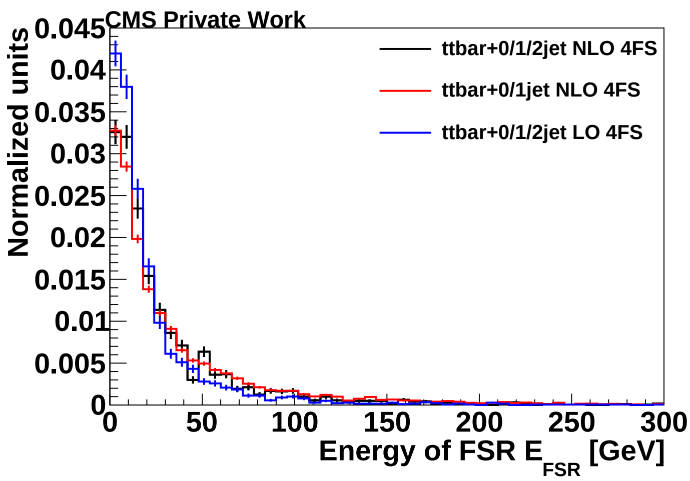

(b) Energy distribution of jets caused by final-state radiation E_{FSR}

Figure 7.10: Comparison of the energy of all jets and of jets caused by final-state radiation between various 4FS event samples of the pp $\to t\bar{t}$ process

For the number of occuring initial-state radiations n_{ISR} a similar behaviour as for the number of final-state radiations n_{FSR} can be shown. In figure 7.11 the energy distribution of the jets caused by initial-state radiation E_{ISR} is displayed. Generally the same comments as for the energy distribution of the final-state radiation E_{FSR} shown in figure 7.10b apply: The $t\bar{t}$+0/1/2jets LO 4FS event sample has a significantly larger fraction of low-energetic final-state radiation jets below $E_{\mathrm{ISR}} \approx 30\,\mathrm{GeV}$ than the two NLO event samples.

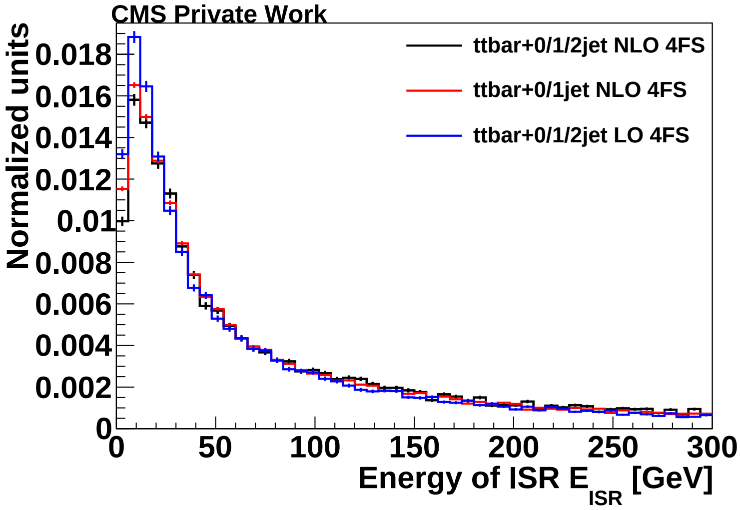

Figure 7.11: Comparison of the energy of initial-state radiation between various 4FS event samples of the pp → $t\bar{t}$ process: The distribution of the energy of additional jets caused by initial-state radiation n_{ISR} in an event is shown for the corresponding event sample.

In table 7.1 the average number of jets $\overline{n}_{\mathrm{jets}}$, the average energy of all jets $\overline{E}_{\mathrm{jets}}$, the average energy of the jets caused by initial-state radiation $\overline{E}_{\mathrm{ISR}}$, and the average energy of the jets originating from final-state radiation $\overline{E}_{\mathrm{FSR}}$ is given for each of the three samples and, additionally, also the values of the five-flavour scheme (5FS) event samples discussed in the next section are stated.

7.3.3 Comparison of 4FS LO and 5FS NLO event samples of the pp → $t\bar{t}$ process

The comparative study described above was repeated using two NLO five-flavour scheme (5FS) event samples, the $t\bar{t}$+0/1jets NLO 5FS event sample and the $t\bar{t}$+0/1/2jets NLO 5FS event sample. As before they were compared to the LO four-flavour scheme (4FS) event sample $t\bar{t}$+0/1/2jets LO 4FS with the help of the aforementioned plotting and analysis scripts. The comparison between these three event samples shows no significant differences to the comparative study done with the 4FS event samples if the uncertainties are taken into account. This also matches the expectations since the event generation and the FxFx merging technique should not depend on the use of either a four-flavour scheme or a five-flavour scheme. For the sake of completeness, however, the average number of jets $\overline{n}_{\mathrm{jets}}$, the average energy of all jets $\overline{E}_{\mathrm{jets}}$, the average energy of the jets caused by initial-state radiation $\overline{E}_{\mathrm{ISR}}$, and the average energy of the jets originating from final-state radiation $\overline{E}_{\mathrm{FSR}}$ is also given for the two NLO 5FS event samples in table 7.1 and a comparison between the $t\bar{t}$+0/1/2jets NLO 4FS event sample and the $t\bar{t}$+0/1/2jets NLO 5FS event sample in regard to the number of jets occuring in the events of the corresponding event sample n_{jets} is shown in figure 7.12. It can be seen from the ratio plot in figure 7.12 that the agreement between both samples is rather good if the uncertainties are considered. For the other variables which were graphically represented in the previously described comparison the agreement is comparable or even better. For this reason, figures containing the distributions of the other variables are not presented here.

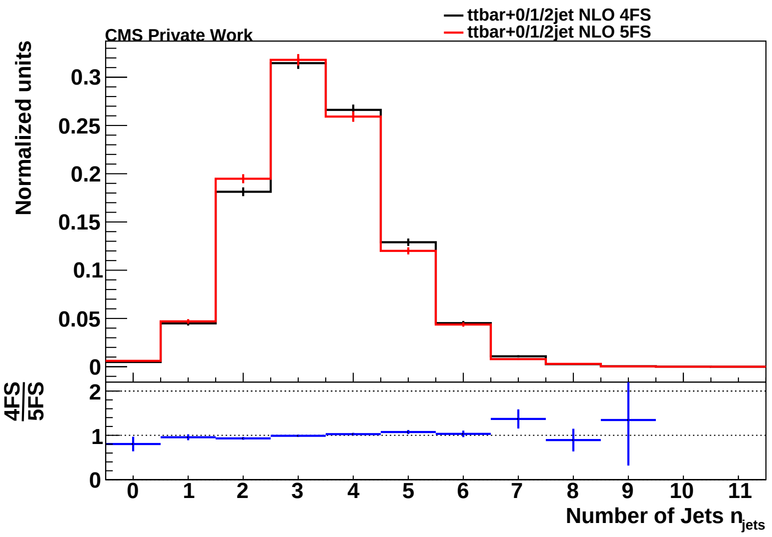

Figure 7.12: Comparison of the number of jets occuring in an event between a 4FS event sample and a 5FS event sample of the pp → $t\bar{t}$+0/1/2jets process: The distribution of the number of jets occuring in an event n_{jets} is shown for the corresponding event sample.

7.3.4 Comparison of 4FS LO and NLO event samples of the pp → $t\bar{t}$H process

In this comparative study a four-flavour scheme (4FS) LO event sample ($t\bar{t}$H+0/1/2jets LO 4FS) of the pp → $t\bar{t}$H+0/1/2jets process which was obtained by using the LO operation mode of the aMC@NLO event generator and MLM merging was compared to a four-flavour scheme NLO event sample ($t\bar{t}$H+0/1jets NLO 4FS) of the pp → $t\bar{t}$H+0/1jets process which was obtained by using the NLO operation mode of the aMC@NLO event generator and the old version of the FxFx merging technique. The results of this comparison are in essence comparable to the results of the comparative studies done for the pp → $t\bar{t}$ process: The difference in the average number of jets $\overline{n}_{\text{jets}}$ between the LO 4FS sample and the NLO 4FS sample is the same for both processes studied. As expected, the jets caused by initial-state radiation and the jets caused by final-state radiation also have a similar average energy of $\overline{E}_{\text{ISR}}$ and $\overline{E}_{\text{FSR}}$, respectively, for both processes since the initial-state radiation and final-state radiation produced by the parton shower should only depend on the energy scale of the hard subprocess, which is similar in both processes. Furthermore, like in the comparison of the pp → $t\bar{t}$ event samples, it can be observed that the additional partons generated by the matrix element on average have a higher energy in the NLO event sample compared to the LO event sample. Therefore in general it can be said that also in the case of the pp → $t\bar{t}$H process the use of a NLO matrix element event generator leads to the occurence of more harder (high energy and/or large angle) additional jets compared to when an LO matrix element is used. The graphical representations of the energy of the additional partons generated by the matrix element E_{MEE} and of the energy of the final-state radiation which are shown in figure 7.13a and accordingly figure 7.13b underline this statement. However, due to the additional Higgs boson the average number of jets in the events $\overline{n}_{\text{jets}}$ of the pp → $t\bar{t}$H event samples is indeed larger than the average number of jets $\overline{n}_{\text{jets}}$ of the corresponding pp → $t\bar{t}$ event samples. In this context it should be noted that the jets of the pp → $t\bar{t}$H event samples have also a larger energy $\overline{E}_{\text{jets}}$ on average (compare tables 7.1 and 7.2).

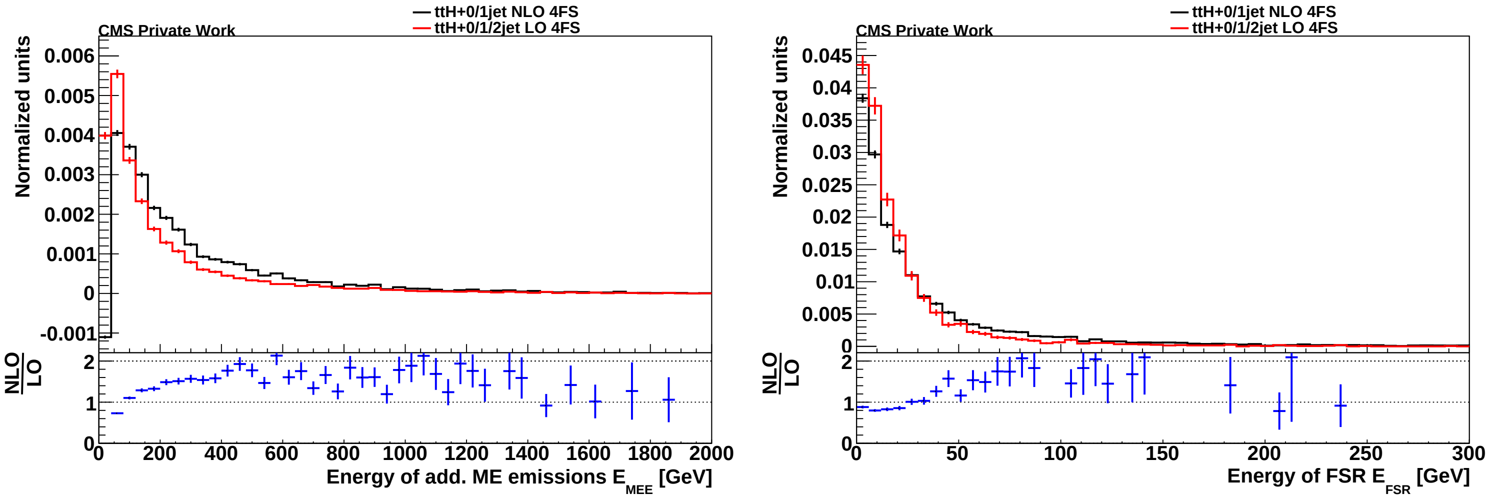

(a) Energy distribution of additional matrix element emissions E_{MEE}

(b) Energy distribution of jets caused by final-state radiation E_{FSR}

Figure 7.13: Comparison of the energy of jets originating from the aMC@NLO matrix element generator and of jets caused by final-state radiation between an LO and NLO 4FS event sample of the pp → $t\bar{t}$H+0/1jets process

7.4 Conclusion

The comparisons between LO and NLO samples discussed in this chapter clearly show that both the old version of the FxFx merging and the new single-file FxFx merging result in event samples according to the expectations and generate confidence in the application of the rather new NLO event generation and NLO merging techniques for the pp → $t\bar{t}$ process and the pp → $t\bar{t}$H process. Moreover, as can be seen in the comparative studies, the use of the NLO operation mode of the aMC@NLO matrix element event generator and merging the results of this matrix element generator with the parton shower of the Pythia8 GPMC event generator using the FxFx merging technique on average leads to a larger total number of jets n_{jets} in comparison with the event generation in LO, in which the LO operation mode of the aMC@NLO matrix element event generator and MLM merging for matching the matrix element computation with the Pythia8 GPMC event generator was used. This confirms previous unpublished results in the framework of this thesis and by other groups. Furthermore, it can be observed that the additional jets originating from the matrix element computation as well as from the parton shower have on average more energy in the case of NLO event generation than in LO event generation. Since events with larger jet multiplicity and harder additional jets are more likely to populate the more sensitive analysis categories of the $t\bar{t}$H analysis and NLO event generator promise a better description of the underlying physics, it seems sensible to use a NLO matrix element generator like aMC@NLO combined with a GPMC event generator like Pythia8 for the default event generation of the pp → $t\bar{t}$ event samples and the pp → $t\bar{t}$H event samples required for the Run 2 $t\bar{t}$H analysis of the CMS collaboration.

Table 7.1: Results from the comparison of LO and NLO event samples of the pp $\rightarrow$ t$\bar{\text{t}}$ process: The average number of jets $\overline{n}_{\text{jets}}$, the average energy of all jets $\overline{E}_{\text{jets}}$, the average energy of the jets caused by initial-state radiation $\overline{E}_{\text{ISR}}$, and the average energy of the jets originating from final-state radiation $\overline{E}_{\text{FSR}}$ is given for all pp $\rightarrow$ t$\bar{\text{t}}$ event samples used in the comparative studies.

Event sample	$\overline{n}_{\text{jets}}$	$\overline{E}_{\text{jets}}$ [GeV]	$\overline{E}_{\text{ISR}}$ [GeV]	$\overline{E}_{\text{FSR}}$ [GeV]
t$\bar{\text{t}}$+0/1/2jets LO 4FS	2.930 ± 0.013	156.6 ± 0.5	67.43 ± 0.35	22.68 ± 0.57
t$\bar{\text{t}}$+0/1jets NLO 4FS	2.749 ± 0.009	156.2 ± 0.4	71.45 ± 0.28	36.19 ± 0.51
t$\bar{\text{t}}$+0/1/2jets NLO 4FS	3.434 ± 0.021	157.4 ± 0.8	74.66 ± 0.62	30.70 ± 1.09
t$\bar{\text{t}}$+0/1jets NLO 5FS	2.749 ± 0.009	156.8 ± 0.4	70.98 ± 0.27	35.14 ± 0.63
t$\bar{\text{t}}$+0/1/2jets NLO 5FS	3.372 ± 0.021	157.5 ± 0.9	73.51 ± 0.63	32.29 ± 1.22

Table 7.2: Results from the comparison of LO and NLO event samples of the pp $\rightarrow$ t$\bar{\text{t}}$H process: The average number of jets $\overline{n}_{\text{jets}}$, the average energy of all jets $\overline{E}_{\text{jets}}$, the average energy of the jets caused by initial-state radiation $\overline{E}_{\text{ISR}}$, and the average energy of the jets originating from final-state radiation $\overline{E}_{\text{FSR}}$ is given for all pp $\rightarrow$ t$\bar{\text{t}}$ event samples used in the comparative studies.

Event sample	$\overline{n}_{\text{jets}}$	$\overline{E}_{\text{jets}}$ [GeV]	$\overline{E}_{\text{ISR}}$ [GeV]	$\overline{E}_{\text{FSR}}$ [GeV]
t$\bar{\text{t}}$H+0/1/2jets LO 4FS	4.241 ± 0.014	166.9 ± 0.4	68.81 ± 0.36	22.55 ± 0.51
t$\bar{\text{t}}$H+0/1jets NLO 4FS	4.091 ± 0.010	167.3 ± 0.3	71.52 ± 0.26	33.42 ± 0.52

8. Comparison between simulated and measurement data

8.1 Introduction

In this chapter next-to-leading order (NLO) simulated event samples of the pp $\rightarrow t\bar{t}$ process from NLO+PS event generators will be compared to event samples of the same process originating from leading order (LO) matrix element generators and to data of the pp $\rightarrow t\bar{t}$ process measured by the CMS detector. After a motivation the production of the samples and the measurement of the pp $\rightarrow t\bar{t}$ data will be explained. This is followed by an overview about the Rivet analysis used for the subsequent comparison of the simulated event samples with the measurement data, before finally a conclusion will be drawn.

8.2 Motivation

All the studies described in the previous chapters of this thesis were comparisons between simulation data obtained in leading order (LO) and next-to-leading order (NLO) by using the aMC@NLO matrix element event generator and merging it with the parton shower of the Pythia8 general-purpose Monte Carlo (GPMC) event generator. The studies done before showed that the NLO+PS event generator consisting of the NLO operation mode of the aMC@NLO event generator and the Pythia8 GPMC event generator provides plausible results with favourable characteristics like a larger number of high-energetic jets in an event sample in comparison to the LO event generation with a ME+PS event generator due to the contribution of the additional real emission matrix elements. However, the ultimate test for any event generator is whether it can accurately predict measurement data and is in close agreement with the measured data samples. For this reason, a Rivet [Buc2010] analysis was applied to compare the measurement data obtained at a center-of-mass energy of $\sqrt{s} = 8$ TeV and an LO event sample produced by the MadGraph5+Pythia6 event generators with pp $\rightarrow t\bar{t}$ event samples generated by the rather new NLO event generators. This Rivet analysis is a rather simple version of the analysis routine described in the publication "Measurement of jet multiplicity distributions in $t\bar{t}$ production in pp collisions at $\sqrt{s} = 7$ TeV" [CMS2014] which was not using the Rivet framework. It is planned that a more advanced version of the present Rivet analysis will be used in the forthcoming publication using the $\sqrt{s} = 8$ TeV measurement data taken in 2012. Thus, by applying the preliminary Rivet analysis to novel NLO Monte Carlo event generators a contribution to this new publication can be made.

In the context of the NLO event samples used for this study, it is notable that since the 7th December 2014 an official $\mathrm{t\bar{t}}$+0/1/2jets event sample exists which was produced by the CMS collaboration on the Worlwide LHC Computing Grid (WLCG) [Bir2005] using the aforementioned aMC@NLO+ Pythia8 interface together with single-file FxFx merging and which was considered in the subsequent comparison between NLO event samples and measurement data. This sample is part of a validating campaign of the CMS collaboration in which the above-mentioned new single-file FxFx merging, the rather new NLO operation mode of the aMC@NLO matrix element generator and the Pythia8 GPMC event generator are tested. Here, the aim is to make sure that aMC@NLO+Pythia8 could be applied for the Monte Carlo production of the event samples required for the Run 2 analyses starting in 2015. This thesis is one of the first publications which will make use of this $\mathrm{t\bar{t}}$+0/1/2jets NLO sample and supports the validation campaign in this way.
In addition to the NLO+PS combination of aMC@NLO matrix element event generator and the Pythia8 GPMC event generator employed previously, also the most recent version 2.1.1 of the Sherpa [Gle2008] GPMC event generator was used, which allows to generate $\mathrm{pp} \to \mathrm{t\bar{t}}$ event samples in NLO, too. Sherpa was not yet applied in the CMS collaboration to generate official NLO $\mathrm{pp} \to \mathrm{t\bar{t}}$ event samples because the OpenLoops [Cas2011] matrix element generator required for the computation of one-loop matrix elements was not included in the CMS software framework (CMSSW) [Inn2001] [Jon2008] until the 10th December 2014. Nonetheless, it is planned to make use of the Sherpa GPMC event generator to validate the NLO event samples produces by the combination of the aMC@NLO matrix element generator and the Pythia8 GPMC event generator. So the generation of NLO $\mathrm{pp} \to \mathrm{t\bar{t}}$+jets event samples, already now, is a proof of concept and an initial step in this direction.

8.3 Production of the samples

In the following subsections the event samples at particle-level produced at a center-of-mass energy of $\sqrt{s} = 8$ TeV and used for the comparison with the measurement data are described. In all cases a five-flavour scheme (5FS), a variable renormalization scale μ_R, and a variable factorization scale μ_F was used to obtain the event samples.

8.3.1 Samples $\mathrm{t\bar{t}}$+0/1/2/3jets LO , $\mathrm{t\bar{t}}$+0/1/2/3jets LO ScaleUp, $\mathrm{t\bar{t}}$+0/1/2/3jets LO ScaleDown, $\mathrm{t\bar{t}}$+0/1/2/3jets LO MergUp, and $\mathrm{t\bar{t}}$+0/1/2/3jets LO MergDown

The inclusive LO event sample of the $\mathrm{pp} \to \mathrm{t\bar{t}}$+0/1/2/3jets with a multiplicity of up to three additional jets was produced by the CMS collaboration and has the official name “TTJets MSDecays central TuneZ2star 8TeV-madgraph-tauola”. For the generation of the sample the MadGraph5 matrix element generator was combined with the parton shower of the Pythia6 GPMC event generator by applying MLM merging with a merging scale of $\mu_Q = 20\,\mathrm{GeV}$ and a matrix element mininum jet transverse momentum selection criterion of $p_{\mathrm{T,\,me}} = 20\,\mathrm{GeV}$. Furthermore, the CTEQ6L1 [Nad2008] parton distribution function set was chosen. Additionally, the official event samples “TTJets MSDecays scaleup TuneZ2star 8TeV-madgraph-tauola” and “TTJets MSDecays scaledown TuneZ2star 8TeV-madgraph-tauola” were considered in the subsequent comparison in which the renormalization scale μ_R and the factorization scale μ_F were varied by a factor of 4 (Sample $\mathrm{t\bar{t}}$+0/1/2/3jets LO ScaleUp) and 0.25 (Sample $\mathrm{t\bar{t}}$+0/1/2/3jets LO ScaleDown), respectively, to give an estimate of the theoretical uncertainties due to scale variations. Besides considering the scale variations the effects of the MLM merging were taken into account by varying the corresponding merging scale μ_Q and by applying the “TTJets MSDecays matchingup TuneZ2star 8TeV-madgraph-tauola” and “TTJets MSDecays matchingdown

TuneZ2star 8TeV-madgraph-tauola" event samples. For the $t\bar{t}$+0/1/2/3jets LO MergUp and the $t\bar{t}$+0/1/2/3jets LO MergDown event sample a merging scale of $\mu_Q = 40$ GeV and $\mu_Q = 10$ GeV was chosen. One million events of each event sample were used for the subsequent comparison with the measurement data (see section 8.6).

8.3.2 Sample $t\bar{t}$+0/1/2jets NLO

The inclusive NLO event sample of the pp $\rightarrow$ $t\bar{t}$+0/1/2jets process with a multiplicity of up to two additional jets was produced by the CMS collaboration and has the official name "TTJets TuneCUETP8M1 8TeV-amcatnloFXFX-pythia8". This event sample and its production does not differ significantly from the $t\bar{t}$+0/1/2jets NLO 5FS sample described in section 7.2.4. It consists of 5 023 923 events instead of only 22 420 events. Additionally, the MadSpin [Art2012] program package implemented in the MadGraph5_aMC@NLO event generator was used to decay the final-state particles and to take into account $t\bar{t}$ spin correlations. The sample was generated by using the aMC@NLO+Pythia8 interface inside version 5.3.22 of the CMS software framework (CMSSW) [Inn2001] [Jon2008]. The events at parton-level were generated by version 2.2.1 of the aMC@NLO matrix element event generator and then further processed with version 8.200 of the Pythia8 GPMC event generator, while the single-file FxFx merging technique with a merging scale of $\mu_Q = 30$ GeV and a matrix element mininum jet transverse momentum selection criterion of $p_{\mathrm{T,\ me}} = 10$ GeV was applied. Furthermore, the NNPDF30 [NNP2014] parton distribution function set was chosen. In appendix B.1 more technical details about the production of this event sample are given. 1.2 million events of this sample were used for the subsequent comparison with the measurement data (see section 8.6).

8.3.3 Samples $t\bar{t}$+0(NLO)/1/2/3jets and $t\bar{t}$+0(NLO)/1(NLO)/2/3jets

The inclusive samples of the pp $\rightarrow$ $t\bar{t}$+jets process with a multiplicity of up to three additional jets were produced by using version 2.1.1 of the Sherpa [Gle2008] GPMC event generator and by making use of the configuration of the top quark pair production given as an example by the Sherpa authors [She2014]. The Born matrix elements were computed with the Amegic++ [Kra2001] matrix element generator and the real emission matrix elements with the Comix [Gle2008b] matrix element generator, which are both implemented in Sherpa, whereas the OpenLoops [Cas2011] program was used to compute the virtual corrections. The matrix element computation was matched with the parton shower by using the MC@NLO technique for massive particles [Hoe2012] together with a merging scale of $\mu_Q = 30$ GeV and the MEPS@NLO [Hoe2013] [Hoe2014] method was applied to merge the single exclusive event samples to an inclusive event sample. The inclusive event sample $t\bar{t}$+0(NLO)/1/2/3jets is the result of merging an exclusive NLO event sample of the pp $\rightarrow$ $t\bar{t}$+0jet process with the exclusive LO event samples of the pp $\rightarrow$ $t\bar{t}$+1jet, pp $\rightarrow$ $t\bar{t}$+2jets, and the pp $\rightarrow$ $t\bar{t}$+3jets process. In contrast to that, the inclusive event sample $t\bar{t}$+0(NLO)/1(NLO)/2/3jets is the result of merging the two exclusive NLO event samples of the pp $\rightarrow$ $t\bar{t}$+0jet and the pp $\rightarrow$ $t\bar{t}$+1jet process with the exclusive LO event samples of the pp $\rightarrow$ $t\bar{t}$+2jets and the pp $\rightarrow$ $t\bar{t}$+3jets process. For the generation of the two event samples which each consists of one million events, the CTEQ6L1 [Nad2008] parton distribution function set was used. In appendix B.2 more technical details about the production of these event samples are given.

8.4 Measurement data

The measurement data of the CMS detector used in this comparison have been taken from the full single muon and single electron data sets measured at a center-of-mass energy of $\sqrt{s} = 8$ TeV which was delivered by the LHC in 2012 and corresponds to an integrated

luminosity of 19.7 fb^{-1}. By applying dedicated triggers μ+jets and e+jets events were collected from the data sets. Furthermore, event cleaning techniques were applied to veto beam scrapping events and events with anomalous noise of the hadron calorimeter. Moreover, the presence of at least one well reconstructed primary vertex was required so that the number of useable events was reduced further. Subsequently, more event reconstruction and selection steps were done to obtain a data sample at reconstruction level which contains mainly $\mathrm{t\bar{t}}$ events from either the μ+jets or the e+jets decay channel. The background is composed of other $\mathrm{t\bar{t}}$ events and several other process and was estimated via Monte Carlo and data-driven methods, before a background subtraction was applied. Afterwards effects from trigger and detector efficiencies and acceptances were corrected by using a regularised unfolding method [Höc1995] [Blo2002] [CMS2012b]. For the unfolding a response matrix that accounts for migrations of events across the bin boundaries of the binned data sample and for efficiencies of the detector was calculated from simulated $\mathrm{t\bar{t}}$ events using the above-mentioned MadGraph5+Pythia6 event sample. The unfolded data was subsequently corrected to consider the acceptance in the particle-level phase space, before the normalised differential $\mathrm{t\bar{t}}$ production cross section as a function of the number of jets n_{jets} (so-called jet multiplicity) $\frac{1}{\sigma_{\mathrm{t\bar{t}}}}\frac{d\sigma_{\mathrm{t\bar{t}}}}{dn_{\mathrm{jets}}}$ could be measured by using the obtained signal sample at particle-level (see section 8.5 for a definition of the used phase space).
The technical details described above cannot be covered by this work extensively and reference is therefore made to the publication of the associated analysis at a center-of-mass energy of $\sqrt{s} = 7$ TeV [CMS2014] and [Des2014].

8.5 Determination of the normalised differential $\mathrm{t\bar{t}}$ production cross section as a function of the number of jets using a Rivet analysis

For the determination of the normalised differential $\mathrm{t\bar{t}}$ production cross section as a function of the number of jets $\frac{1}{\sigma_{\mathrm{t\bar{t}}}}\frac{d\sigma_{\mathrm{t\bar{t}}}}{dn_{\mathrm{jets}}}$ are Rivet [Buc2010] analysis was used. Rivet is a toolkit for validation of Monte Carlo event generators and for the comparison between Monte Carlo event samples and measurement data obtained in experimental analyses. Rivet's design emphasizes to be independent of the origin of measurement data and event samples used for the comparisons. Therefore, it provides generator- and measurement-independent definitions of particles objects and based on these definitions tags particle objects.
This Rivet analysis is in general based on analysis strategy used in the publication [CMS2014] and has been developed in the context of two bachelor theses [Mar2014] [Sch2014d] to allow the determination of the normalised differential $\mathrm{t\bar{t}}$ production cross section as a function of the jet multiplicity (number of jets) $\frac{1}{\sigma_{\mathrm{t\bar{t}}}}\frac{d\sigma_{\mathrm{t\bar{t}}}}{dn_{\mathrm{jets}}}$ in the upcoming analysis of the CMS measurement data at a center-of-mass energy of $\sqrt{s} = 8$ TeV. The analysis requires for the determination of the differential cross section $\frac{1}{\sigma_{\mathrm{t\bar{t}}}}\frac{d\sigma_{\mathrm{t\bar{t}}}}{dn_{\mathrm{jets}}}$ that an event consists of at least four jets, two of which must contain the decay products of a bottom hadron, and that exactly one muon or one electron fulfills the requirements of a lepton reconstructed with high quality ("good muon" or "good electron"). Furthermore, jets in an event are rejected if the selected leptons and jets are not well-separated to avoid counting leptons misidentified as jets. Additionally, in order to remove Z^0+jets and dileptonic top background events, events are rejected if they contain extra muons or electrons which could be reconstructed by using loose selection criteria ("loose muon" or "loose electron"). The kinematics restrictions applied to the jets, the muons and the electrons are given in table 8.1: All jets including jets from bottom quarks must have a minimum transverse momentum of $p_T(\mathrm{jet}) > 30\,\mathrm{GeV}$, moreover it is required that the jets have a maximum value of the pseudorapidity of $|\eta|(\mathrm{jet}) < 2.5$ and a minimum distance to the selected leptons defined by a cone radius of $\Delta R(\mathrm{jet} \leftrightarrow \mathrm{lepton}) > 0.4$. The muons must have a minimum trans-

verse momentum of p_T(good μ) $> 30\,\text{GeV}$ and a pseudorapidity of $|\eta|$(good μ) < 2.4 to fall into the category of a good muon or at least a minimum transverse momentum of p_T(loose μ) $> 15\,\text{GeV}$ and a pseudorapidity of $|\eta|$(loose μ) < 2.5 to fall into the category of a loose muon. The same selection criteria apply for the electrons. Good electrons must have a minimum transverse momentum of p_T(good e) $> 30\,\text{GeV}$ and a pseudorapidity of $|\eta|$(good e) < 2.4 while for loose electrons a minimum transverse momentum of p_T(loose e) $> 15\,\text{GeV}$ and a pseudorapidity of $|\eta|$(loose e) < 2.5.
is required. For all events which pass the selection criteria described above the Rivet analysis routine determines the number of jets n_{jets} in the corresponding event together with the event weight and fills then a histogram of the number of jets n_{jets} with the event weight. The differential $t\bar{t}$ cross section as a function of the number of jets $\frac{d\sigma_{t\bar{t}}}{dn_{\text{jets}}}$ is then derived by counting the sum of the event weights stored in each histogram bin (In appendix B.3 the complete software code of the preliminary Rivet analysis is given). In an additional step the differential $t\bar{t}$ cross section was normalised to unity by summing up all histogram bins to obtain the total event weight and by dividing each bin by the total event weight. Moreover, the statistical uncertainty is calculated for each bin by considering a binomial distribution which takes the event weights in the bins into account.

Table 8.1: Kinematic requirements of jets, muons and electrons in the analysis: The particle objects in an event are characterised by their tag and must fulfill a transverse momentum p_T selection criterion, a pseudorapidity $|\eta|$ selection criterion and in the case of jets additionally a cone radius selection criterion to fall into one of the categories.

Category	Tag	p_T [GeV]	$\|\eta\|$	ΔR(jet$\leftrightarrow$lepton)
Jet	Jet	> 30	< 2.5	> 0.4
Good Muon	Muon	> 30	< 2.4	–
Loose Muon	Muon	> 15	< 2.5	–
Good Electron	Electron	> 30	< 2.4	–
Loose Electron	Electron	> 15	< 2.5	–

8.6 Comparison of the normalised differential $t\bar{t}$ production cross section as a function of the number of jets

The normalised differential $t\bar{t}$ production cross section as a function of the number of jets $\frac{1}{\sigma_{t\bar{t}}}\frac{d\sigma_{t\bar{t}}}{dn_{\text{jets}}}$ of each event sample and of the measurement data described above was obtained by applying the aforementioned Rivet analysis. The normalised differential $t\bar{t}$ production cross sections as a function of the number of jets $\frac{1}{\sigma_{t\bar{t}}}\frac{d\sigma_{t\bar{t}}}{dn_{\text{jets}}}$ were then compared by making use of the ROOT [Bru1997] data analysis framework. Figure 8.1a shows a comparison of the normalised differential cross section of the measurement data with the simulated event samples and in table 8.2 the corresponding numbers are given. Additionally, in figure 8.1b a comparison of the normalised differential cross section $\frac{1}{\sigma_{t\bar{t}}}\frac{d\sigma_{t\bar{t}}}{dn_{\text{jets}}}$ of the measurement data, of the LO event sample $t\bar{t}$+0/1/2/3jets LO generated by using the MadGraph5 and the Pythia6 event generator together with the event samples $t\bar{t}$+0/1/2/3jets LO ScaleUp, $t\bar{t}$+0/1/2/3jets LO ScaleDown, $t\bar{t}$+0/1/2/3jets LO MergUp, and $t\bar{t}$+0/1/2/3jets LO MergDown, which were used to determine the uncertainties due to variations of the renormalization scale μ_R and the factorization scale μ_F as well of the merging scale μ_Q is represented. The associated numerical results are stated in table 8.3.

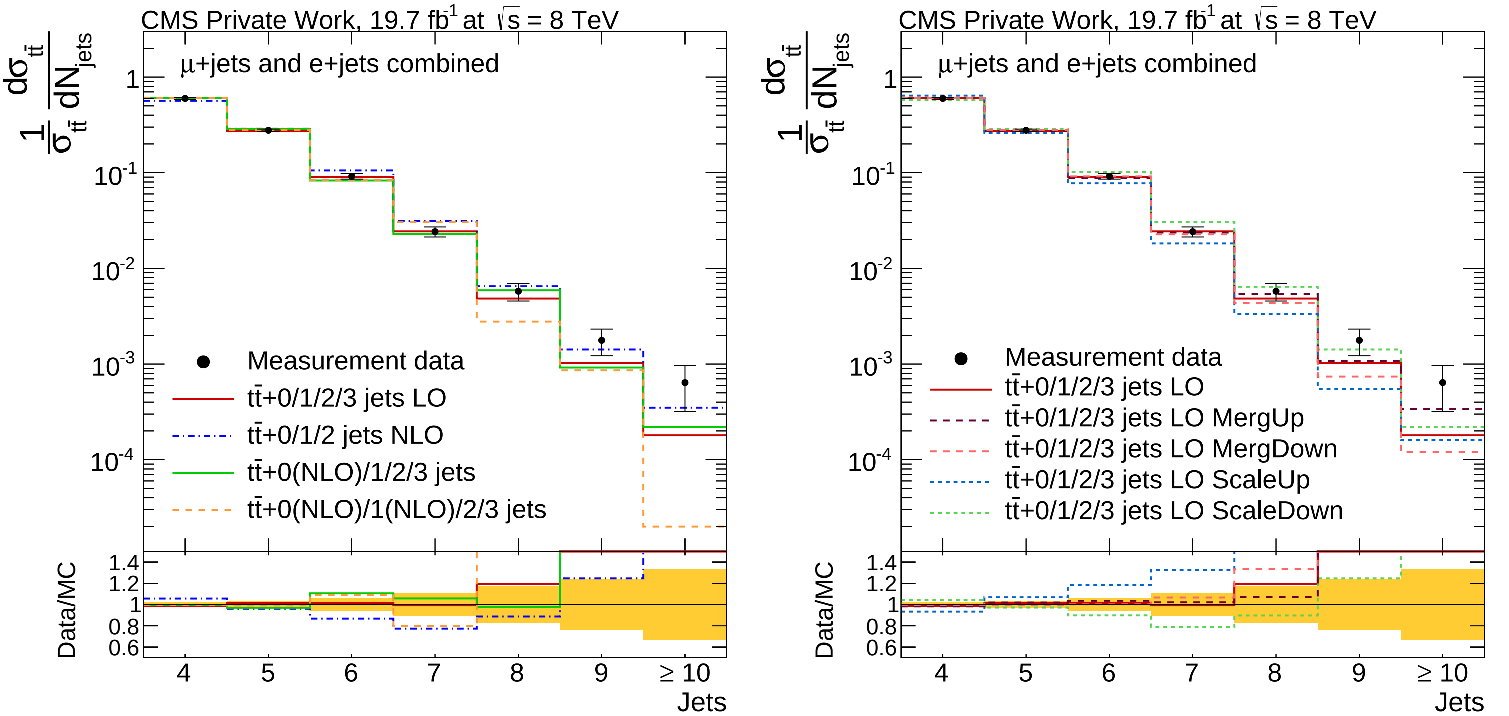

(a) Comparison of measurement data, LO event sample, and NLO event samples

(b) Comparison of measurement data and varied LO event samples

Figure 8.1: The normalised differential $t\bar{t}$ production cross section as a function of the number of jets: The measurement data is compared to predictions from MadGraph5+Pythia6 ($t\bar{t}$+0/1/2/3jets LO), aMC@NLO+Pythia8 ($t\bar{t}$+0/1/2jets NLO), and Sherpa ($t\bar{t}$+0(NLO)/1/2/3jets and $t\bar{t}$+0(NLO)/1(NLO)/2/3jets) (left plot), as well as from MadGraph5+Pythia6 with varied renormalisation and factorization scales ($t\bar{t}$+0/1/2/3jets LO ScaleUp and $t\bar{t}$+0/1/2/3jets LO ScaleDown), and merging scales ($t\bar{t}$+0/1/2/3jets LO MergUp and $t\bar{t}$+0/1/2/3jets LO MergDown) (right plot). The inner (outer) error bars indicate the statistical (combined statistical und systematic) uncertainty. The shaded band corresponds to the combined statistical and systematic uncertainty. The plots were created by using the ROOT [Bru1997] data analysis framework.

As can be seen in figure 8.1a, it is rather difficult to make general statements about the difference between the normalised differential $t\bar{t}$ production cross section as a function of the number of jets $\frac{1}{\sigma_{t\bar{t}}}\frac{d\sigma_{t\bar{t}}}{dn_{\text{jets}}}$ obtained from the event generators and the differential cross section of the measurement data. However, it can be said that the description of the measurement data with 10 and more jets ($n_{\text{jets}} \geq 10$) by all event generators is fairly poor. This is to be expected since very large jet multiplicities (number of jets) are always a consequence of the parton shower. The only exception is the aMC@NLO+Pythia8 event generator which shows a rather different distribution. Nonetheless, the description of the measurement data is quite good for smaller numbers of jet n_{jets}:
The Sherpa event generator, considering the $t\bar{t}$+0(NLO)/1/2/3jets event sample, shows the best agreement with data for smaller numbers of jets n_{jets} and performs rather well in the region of $n_{\text{jets}} = 4$ to $n_{\text{jets}} = 8$ jets. The second Sherpa sample ($t\bar{t}$+0(NLO)/1(NLO)/2/3jets) shows only a good agreement with the measurement data for $n_{\text{jets}} = 4$ to $n_{\text{jets}} = 6$ jets. Furthermore, it is to note that the Sherpa $t\bar{t}$+0(NLO)/1(NLO)/2/3jets event sample overestimates the differential cross section $\frac{1}{\sigma_{t\bar{t}}}\frac{d\sigma_{t\bar{t}}}{dn_{\text{jets}}}$ for a jet multiplicity of $n_{\text{jets}} = 7$ and significantly underestimates it for a jet multiplicity of $n_{\text{jets}} = 8$. In contrast to that, the Sherpa $t\bar{t}$+0(NLO)/1/2/3jets event sample shows a smoother decrease with increasing numbers of jets n_{jets}. These differences between the two Sherpa samples could not be clarified in this thesis and will be subject of further study. Nevertheless, it should be noted that the good agreement of the Sherpa $t\bar{t}$+0(NLO)/1/2/3jets event sample with the measurement data, which is also reflected in the similar average jet numbers in an event $\overline{n}_{\text{jets}}$ (compare table 8.2), is remarkable since only the default configuration of Sherpa was used and no further tuning was applied.
The $t\bar{t}$+0/1/2/3jets LO event sample generated with the MadGraph5+ Pythia6 event generator also shows good agreement with the measurement data for smaller number of jets $n_{\text{jets}} \leq 7$. This can be attributed to taking into account up to three additional partons in the matrix element of the $t\bar{t}$+0/1/2/3jets process. Consequently, it would be only logical that for larger numbers of jets $n_{\text{jets}} \geq 8$ in which the parton shower must provide at least one additional jet the normalised differential $t\bar{t}$ production cross section as a function of the number of jets $\frac{1}{\sigma_{t\bar{t}}}\frac{d\sigma_{t\bar{t}}}{dn_{\text{jets}}}$ in comparison to the measurement data is underestimated. However, further studies are needed to confirm this assumption. Nevertheless, in this context it is also notable that even when variations of the renormalization scale μ_R and factorization scale μ_F as well as of the merging scale μ_Q are considered for the LO event sample as shown in figure 8.1b the agreement with the measurement data is still fairly poor for higher jet multiplicities of $n_{\text{jets}} \geq 9$. In the case of a number of jets of $n_{\text{jets}} = 9$ only a downward variation of the renormalization scale μ_R and the factorization scale μ_F by a factor of 0.25 can explain the measurement data while in the case of a jet multiplicity of $n_{\text{jets}} = 10$ an upward variation of the merging scale ($\mu_Q = 40\,\text{GeV}$ instead of $\mu_Q = 20\,\text{GeV}$) is needed to be consistent with the measurement data. In this regard it must be noted that the statistics of the event samples for higher numbers of jets are rather limited.
The $t\bar{t}$+0/1/2jets NLO event sample obtained from the aMC@NLO+Pythia8 event generator shows a different distribution of the normalised differential $t\bar{t}$ production cross section as a function of the number of jets $\frac{1}{\sigma_{t\bar{t}}}\frac{d\sigma_{t\bar{t}}}{dn_{\text{jets}}}$ than the other event samples: It has a larger differential cross section $\frac{1}{\sigma_{t\bar{t}}}\frac{d\sigma_{t\bar{t}}}{dn_{\text{jets}}}$ for a number of jets from $n_{\text{jets}} = 6$ onwards and describes the measurement data quite well for a jet multiplicity larger than $n_{\text{jets}} \geq 8$, but cannot describe the measurement data well for smaller jet multiplicities of $n_{\text{jets}} \leq 6$.
Unfortunately, a direct comparison between the $t\bar{t}$+0/1/2/3jets LO event sample and the $t\bar{t}$+0/1/2jets NLO event sample is not possible due to the significant differences of the Pythia6 GPMC event generator, used to obtain the LO event sample, and the Pythia8 GPMC event generator, used to generate the NLO sample: The Pythia6 event generator makes use of a p_T-ordered parton shower while the Pythia8 event generator applies an

dipole shower. Furthermore, different tunes of the parton shower were used. Therefore it cannot be decided, whether the observed differences between the two samples are a result of the different order of perturbation theory which is used by the matrix element generator or whether the different parton shower is the cause. An official $\mathrm{t\bar{t}}$+0/1/2/3jets LO event sample with the Pythia8 GPMC event generator which is produced on the Worlwide LHC Computing Grid (WLCG) at the moment and which will have comparable settings to the $\mathrm{t\bar{t}}$+0/1/2jets NLO event sample will provide more clarification in this regard.
Moreover, it is noteworthy that at the moment only the scale uncertainties of the LO event sample, which are quite large, could be studied since NLO samples with varied scales are also not yet available. However, this will be the topic of a further study because it is expected that the uncertainties due to the renormalization scale μ_R and the factorization scale μ_F are significantly smaller in NLO than in LO while the uncertainties of the FxFx merging due to the used merging scale μ_Q are not yet fully studied.
As a last point, it must be mentioned that also for the POWHEG Box and the MC@NLO event generator the normalised differential $\mathrm{t\bar{t}}$ production cross section as a function of the number of jets $\frac{1}{\sigma_{\mathrm{t\bar{t}}}}\frac{d\sigma_{\mathrm{t\bar{t}}}}{dn_{\mathrm{jets}}}$ at a center-of-mass energy of $\sqrt{s} = 7$ TeV and $\sqrt{s} = 8$ TeV was determined. In the figure 2.2a which is taken from [CMS2014] the results of these event generators are shown together with the result from the LO MadGraph5+ Pythia6 event generator for a center-of-mass-energy of $\sqrt{s} = 7$ TeV.

8.7 Conclusion

It is to early to draw specific conclusions in regard to the comparison of NLO event generators and NLO merging techniques with measurement data and LO event generators since further studies have to be done first. However, it seems fair to say that the combination of the MadGraph5 matrix element generator and the Pythia6 GPMC event generator, which describes the normalised differential $\mathrm{t\bar{t}}$ production cross section as a function of the number of jets $\frac{1}{\sigma_{\mathrm{t\bar{t}}}}\frac{d\sigma_{\mathrm{t\bar{t}}}}{dn_{\mathrm{jets}}}$ quite well for smaller numbers of jets $n_{\mathrm{jets}} \leq 7$, was a good choice to be used by default to generate the pp $\rightarrow \mathrm{t\bar{t}}$+jets event samples up to now. Moreover, one can state that the first results obtained with the NLO event generators for inclusive NLO event samples of the pp $\rightarrow \mathrm{t\bar{t}}$+jets process, especially the result of the Sherpa $\mathrm{t\bar{t}}$+0(NLO)/1/2/3jets event sample, are promising. Nonetheless, further studies seem necessary to fully comprehend the NLO event generation when additional merging techniques are used to obtain NLO inclusive pp $\rightarrow \mathrm{t\bar{t}}$+jets event samples.

Table 8.2: The normalised differential $t\bar{t}$ production cross section as a function of the number of jets given for the measurement data and the event samples: In addition to the normalised differential cross section as a function of the number of jets $\frac{1}{\sigma t\bar{t}} \frac{d\sigma_{t\bar{t}}}{dn_{\text{jets}}}$, the statistical uncertainties obtained by considering a binomial distribution and the average number of jets in the selected events of an event sample $\overline{n}_{\text{jets}}$ are given. For the measurement data the combined stastical and systematic uncertainties are stated.

Number of jets	Measurement data		$t\bar{t}$+0/1/2/3jets LO		$t\bar{t}$+0/1/2jets NLO		$t\bar{t}$+0(NLO)/1/2/3jets		$t\bar{t}$+0(NLO)/1(NLO)/2/3jets	
n_{jets}	$\frac{1}{\sigma t\bar{t}} \frac{d\sigma_{t\bar{t}}}{dn_{\text{jets}}}$	+/-	$\frac{1}{\sigma t\bar{t}} \frac{d\sigma_{t\bar{t}}}{dn_{\text{jets}}}$	+/-	$\frac{1}{\sigma t\bar{t}} \frac{d\sigma_{t\bar{t}}}{dn_{\text{jets}}}$	+/-	$\frac{1}{\sigma t\bar{t}} \frac{d\sigma_{t\bar{t}}}{dn_{\text{jets}}}$	+/-	$\frac{1}{\sigma t\bar{t}} \frac{d\sigma_{t\bar{t}}}{dn_{\text{jets}}}$	+/-
4	0.59808	2.6%	0.60519	0.3%	0.56598	0.8%	0.60102	1.6%	0.60186	3.1%
5	0.27761	3.0%	0.27393	0.6%	0.28879	1.4%	0.28609	3.3%	0.27996	6.4%
6	0.09172	6.5%	0.09045	1.2%	0.10567	2.5%	0.08295	7.4%	0.08416	12.7%
7	0.02421	12.0%	0.02438	2.4%	0.03129	4.3%	0.02289	10.1%	0.03035	36.8%
8	0.00577	21.0%	0.00484	5.5%	0.00650	9.8%	0.00590	17.4%	0.00278	24.0%
9	0.00177	31.0%	0.00103	12.0%	0.00142	22.2%	0.00092	33.5%	0.00086	45.8%
≥10	0.00064	49.0%	0.00018	28.8%	0.00035	40.8%	0.00022	28.6%	0.00002	336.4%
$\overline{n}_{\text{jets}}$	4.570 ± 0.022		4.554 ± 0.003		4.629 ± 0.007		4.550 ± 0.014		4.555 ± 0.028	

Table 8.3: The normalised differential $t\bar{t}$ production cross section as a function of the number of jets given for the measurement data and the event samples used for the scale and merging variations: In addition to the normalised differential cross section as a function of the number of jets $\frac{1}{\sigma t\bar{t}} \frac{d\sigma_{t\bar{t}}}{dn_{jets}}$, the statistical uncertainties obtained by considering a binomial distribution and the average number of jets in the selected events of an event sample $\overline{n}_{jets}$ are given. For the measurement data the combined stastical and systematic uncertainties are stated.

Number of jets	Measurement data		$t\bar{t}$+0/1/2/3jets LO		$t\bar{t}$+0/1/2/3jets LO ScaleUp		$t\bar{t}$+0/1/2/3jets LO ScaleDown		$t\bar{t}$+0/1/2/3jets LO MergUp		$t\bar{t}$+0/1/2/3jets LO MergUp	
n_{jets}	$\frac{1}{\sigma t\bar{t}} \frac{d\sigma_{t\bar{t}}}{dn_{jets}}$	+/-	$\frac{1}{\sigma t\bar{t}} \frac{d\sigma_{t\bar{t}}}{dn_{jets}}$	+/-	$\frac{1}{\sigma t\bar{t}} \frac{d\sigma_{t\bar{t}}}{dn_{jets}}$	+/-	$\frac{1}{\sigma t\bar{t}} \frac{d\sigma_{t\bar{t}}}{dn_{jets}}$	+/-	$\frac{1}{\sigma t\bar{t}} \frac{d\sigma_{t\bar{t}}}{dn_{jets}}$	+/-	$\frac{1}{\sigma t\bar{t}} \frac{d\sigma_{t\bar{t}}}{dn_{jets}}$	+/-
4	0.59808	2.6%	0.60519	0.3%	0.64040	0.3%	0.57355	0.3%	0.60858	0.3%	0.60108	0.3%
5	0.27761	3.0%	0.27393	0.6%	0.25979	0.7%	0.28563	0.6%	0.27238	0.6%	0.27948	0.6%
6	0.09172	6.5%	0.09045	1.2%	0.07751	1.4%	0.10210	1.1%	0.08852	1.2%	0.09154	1.2%
7	0.02421	12.0%	0.02438	2.4%	0.01824	2.9%	0.03065	2.1%	0.02371	2.5%	0.02270	2.5%
8	0.00577	21.0%	0.00484	5.5%	0.00334	6.9%	0.00643	4.6%	0.00538	5.2%	0.00433	5.8%
9	0.00177	31.0%	0.00103	12.0%	0.00055	16.9%	0.00142	9.8%	0.00108	11.7%	0.00074	14.0%
≥10	0.00064	49.0%	0.00018	28.8%	0.00016	31.6%	0.00022	25.0%	0.00034	20.8%	0.00012	35.4%
$\overline{n}_{jets}$	4.570 ± 0.022		4.554 ± 0.003		4.487 ± 0.003		4.616 ± 0.003		4.467 ± 0.003		4.552 ± 0.003	

9. Summary and Outlook

As it can be seen throughout this whole thesis, Monte Carlo (MC) event generators are versatile tools for validating theoretical models of particle physics. The reduction of uncertainties related to their usage becomes more and more important due to improvements in experimental data acquisition with particle detectors. This can be achieved by applying the most advanced techniques in event generation and by using merging techniques to combine next-to-leading order (NLO) matrix element generators and parton showers (PS) of general-purpose event generators (GPMC) instead of using leading order (LO) event generators. Here, the newly available NLO merging techniques like FxFx merging and MEPS@NLO together with the most recent NLO+PS event generators like aMC@NLO+Pythia8 and Sherpa promise a better description of the physics by providing the possibility to generate inclusive event samples at NLO accuracy.

The CMS collaboration has mostly used LO event generators in the past, but plans to make use of (such) NLO+PS event generators in the future, e.g. to generate the $\mathrm{pp} \rightarrow \mathrm{t\bar{t}}$+jets and the $\mathrm{pp} \rightarrow \mathrm{t\bar{t}H}$+jets event samples required for the analysis of the measurement data obtained in the Run 2 (starting 2015) of the Large Hadron Collider (LHC). For this reason, a comprehensive testing and validation campaign of the event generation in NLO was started, in which the work presented in this thesis is embedded.

One example of this work can be found in chapter 6 in which studies of the cross section calculations of the $\mathrm{pp} \rightarrow \mathrm{t\bar{t}H}$ process with the event generator aMC@NLO were performed: For the $\mathrm{pp} \rightarrow \mathrm{t\bar{t}H}$ analysis the use of NLO event samples appears particularly promising since the NLO K-factor k_{NLO}, which is applied to scale the cross section $\sigma_{\mathrm{t\bar{t}H,LO}}$ of a LO $\mathrm{pp} \rightarrow \mathrm{t\bar{t}H}$+jets event sample to the NLO cross section $\sigma_{\mathrm{t\bar{t}H,NLO}}$, introduces rather large scale uncertainties. It could be shown by comparing LO and NLO cross sections of the $\mathrm{pp} \rightarrow \mathrm{t\bar{t}H}$ process obtained with the aMC@NLO matrix element generator that these scale uncertainties would be significantly reduced if NLO event samples would be used for the $\mathrm{pp} \rightarrow \mathrm{t\bar{t}H}$ analysis. Furthermore, a comparison between results obtained with the aMC@NLO matrix element generator and results of the LHC Higgs Working Group leads to the conclusion that the aMC@NLO matrix element generator delivers trustworthy results for the $\mathrm{pp} \rightarrow \mathrm{t\bar{t}H}$ process.

The comparative studies of LO and NLO event generation were continued in chapter 7 with a comparison between LO and NLO event samples of the $\mathrm{pp} \rightarrow \mathrm{t\bar{t}}$+jets process and the $\mathrm{pp} \rightarrow \mathrm{t\bar{t}H}$+jets process. A major focus of these comparisons was to study the LO MLM and the NLO FxFx merging techniques which are used to merge events generated with the matrix element generator with events from the parton shower. First, a parameter study was carried out to find a good choice of parameters required for the FxFx merging. A comparison between the old version of the FxFx merging technique and the new single-file FxFx merging technique has also been performed. The comparisons show that the NLO event generation together with the FxFx merging technique leads – independent of the version used and as expected – on average to a larger number of jets and to a larger amount of high-energetic additional jets observed in a subsequent analysis in comparison to the LO event generation. For the analysis of the event samples self-developed plotting and analysis scripts were applied. These plotting and analysis scripts were improved in a dedicated bachelor thesis and could successfully be used to derive various important but poorly accessible physics observables. Moreover, the plotting scripts supported an improvement of the comparative studies done because they provide a graphical representation of the history of an event and in this way lead to a better understanding of the $\mathrm{pp} \to \mathrm{t\bar{t}}$ process and the $\mathrm{pp} \to \mathrm{t\bar{t}H}$ process. For this reason, it is most likely that some features of the plotting and analysis scripts like the particle identification algorithm will be implemented in the CMS software framework in the future.

The most decisive criterion for each new event generator and merging technique is the comparison with measurement data such as the one performed and documented in chapter 8: The normalised differential $\mathrm{t\bar{t}}$ production cross section as a function of the number of jets of NLO event samples generated with aMC@NLO+Pythia8 and Sherpa, of LO event samples obtained from MadGraph5+Pythia6, and of measurement data was determined and compared with each other at a center-of-mass energy of $\sqrt{s} = 8$ TeV by using a Rivet analysis. Further studies are necessary before conclusions on the benefits of NLO event generation and NLO merging techniques compared to LO event generation can be drawn, however, one can say that the previously applied LO MadGraph5+Pythia6 event generator was a good choice for the generation of $\mathrm{pp} \to \mathrm{t\bar{t}}$+jets event samples. Moreover, the first comparisons between the inclusive NLO event samples and the measurement data seem promising. Especially the Sherpa event generator must be mentioned which showed an impressive agreement with the measurement despite the fact that only the default settings were used. It remains to note that a more advanced version of the Rivet analysis will be used in a forthcoming publication and, thus, a contribution to this publication by applying the Rivet analysis could be made.

A complete validation of the event generators planned to be used in Run 2 of the LHC and a decision on the event generators used by default for the production of the default $\mathrm{pp} \to \mathrm{t\bar{t}}$ and $\mathrm{pp} \to \mathrm{t\bar{t}H}$ event samples is still outstanding in the CMS collaboration. Nonetheless, many elaborate studies were already done and many encouraging results were obtained with regard to NLO event generation. For this reason, it seems most likely that the NLO aMC@NLO+Pythia8 event generator will be used by default instead of the LO MadGraph5+Pythia8 event generator for the production of these samples.

Bibliography

[Aba1995] S. Abachi et al. (DØ Collaboration): Observation of the Top Quark, in: Phys. Rev. Lett. 74 (1995) 14, pp. 2632–2637, s.l., 1995, URL: http://journals.aps.org/prl/abstract/10.1103/PhysRevLett.74.2632, Date viewed: 08.12.2014

[Abe1995] F. Abe et al. (CDF Collaboration): Observation of Top Quark Production in $\overline{p}$p Collisions with the Collider Detector at Fermilab, in Phys. Rev. Lett. 74 (1995) 14, pp. 2626–2631, s.l., 1995, URL: http://journals.aps.org/prl/abstract/10.1103/PhysRevLett.74.2626, Date viewed: 26.11.2014

[Ali2010] S. Alioli et al.: A general framework for implementing NLO calculations in shower Monte Carlo programs: the POWHEG BOX, in: JHEP 06 (2010) 043, arXiv:hep-ph/1002.2581, Version from 12th February 2010, s.l., 2010, URL: http://arxiv.org/abs/arXiv:1002.2581, Date viewed: 23.11.2014

[Ali2014] S. Alioli et al.: Homepage of the POWHEG BOX, s.l., 2014, URL: http://powhegbox.mib.infn.it/, Date viewed: 24.11.2014

[Alt1977] G. Altarelli and G. Parisi: Asymptotic freedom in parton language, in: Nucl. Phys. B126 (1977), pp. 298–318, s.l., 1977, URL: http://npac2013.lal.in2p3.fr/2010-2011/Cours/Exam-IF/Altarelli-Parisi.pdf, Date viewed: 20.11.2014

[Alt2009] G. Altarelli: QCD evolution equations for parton densities, in: Scholarpedia 4(1):7124, Revision #91681 from 13th January 2009, s.l., 2009, URL: http://www.scholarpedia.org/article/QCD_evolution_equations_for_parton_densities, Date viewed: 20.11.2014

[Alw2006] J. Alwall et al.: A standard format for Les Houches Event Files, in: Comput. Phys. Commun. 176 (2007), pp. 300–304, arXiv:hep-ph/0609017, Version from 3rd September 2006, s.l. 2007, URL: http://arxiv.org/abs/hep-ph/0609017, Date viewed: 24.11.2014

[Alw2014] J. Alwall et al.: The automated computation of tree-level and next-to-leading order differential cross sections, and their matching to parton shower simulations, in: JHEP 07 (2014) 079, arXiv:hep-ph/1405.0301, Version from 21th July 2014, s.l., 2014, URL: http://arxiv.org/abs/1405.0301, Date viewed: 20.10.2014

[And2002] B. Andersson et al.: Recent Developments in the Lund Model, arXiv:hep-ph/0212122, Version from 9th December 2002, s.l, 2002, URL: http://arxiv.org/abs/hep-ph/0212122, Date viewed: 09.11.2014

[Arn1983] G. Arnison et al. (The UA1 Collaboration): Experimental observation of isolated large transverse energy electrons with associated missing energy at $\sqrt{s}$ = 540 GeV, in: Phys. Lett. B 122 (1983) 1, pp. 103–116, s.l., 1983, URL: http://www.sciencedirect.com/science/article/pii/0370269383911772, Date viewed: 26.11.2014

[Arn1983b] G. Arnison et al. (The UA1 Collaboration): Experimental observation of lepton pairs of invariant mass around 95 GeV/c^2 at the CERN SPS collider, in: Phys. Lett. B 126 (1983) 5, pp. 398–410, s.l., 1983, URL: http://www.sciencedirect.com/science/article/pii/0370269383901880, Date viewed: 08.12.2014

[Art2012] P. Artoisenet et al.: Automatic spin-entangled decays of heavy resonances in Monte Carlo simulations, in: JHEP 03 (2013) 015, arXiv:hep-ph/1212.3460, Version from 11th March 2013, s.l., 2012, URL: http://arxiv.org/abs/arXiv:1212.3460, Date viewed: 24.11.2014

[ATL2012] The ATLAS Collaboration: Observation of a new particle in the search for the Standard Model Higgs boson with the ATLAS detector at the LHC, in: Phys. Lett. B 716 (2012) 1, pp. 1–29, arXiv:hep-ex/1207.7214, Version from 31th August 2012, s.l., 2012, URL: http://arxiv.org/abs/1207.7214, Date viewed: 27.11.2014

[Aub1974] J.J. Aubert et al.: Experimental Observation of a Heavy Particle J, in: Phys. Rev. Lett. 33 (1974) 23, pp. 1404–1406, s.l., 1974, URL: http://link.aps.org/doi/10.1103/PhysRevLett.33.1404, Date viewed: 26.11.2014

[Aug1974] J.E. Augustin et al.: Discovery of a Narrow Resonance in e^+e^- Annihilation, in: Phys. Rev. Lett. 33 (1974) 23, pp. 1406–1408, s.l., 1974, URL: http://link.aps.org/doi/10.1103/PhysRevLett.33.1406, Date viewed: 26.11.2014

[Bag1983] P. Bagnaia et al. (The UA2 Collaboration): Evidence for $Z^0 \rightarrow e^+e^-$ at the CERN $\bar{p}$p collider, in: Phys. Lett. B 129 (1983) 1–2, pp. 130–140, s.l., 1983, URL: http://www.sciencedirect.com/science/article/pii/037026938390744X, Date viewed: 26.11.2014

[Bah2008] M. Bahr et al.: Herwig++ Physics and Manual, in: Eur. Phys. J. C58 (2008), pp. 639–707, arXiv:hep-ph/0803.0883, Version from 2nd December 2008, s.l., 2008, URL: http://arxiv.org/abs/0803.0883, Date viewed: 21.11.2014

[Bal2010] R.D. Ball et al.: A first unbiased global NLO determination of parton distributions and their uncertainties, in: Nucl. Phys. B 838 (2010) 1–2, pp. 136–206, arXiv:hep-ph/1002.4407, Version from 19th May 2010, s.l., 2010, URL: http://arxiv.org/abs/1002.4407, Date viewed: 30.11.2014

[Ban1983] M. Banner et al. (The UA2 Collaboration): Observation of single isolated electrons of high transverse momentum in events with missing transverse energy at the CERN $\bar{p}$p collider, in: Phys. Lett. B 122 (1983) 5–6, pp.476-485, s.l., 1983, URL: http://www.sciencedirect.com/science/article/pii/0370269383916052, Date viewed: 26.11.2014

[Bar2011] D. Barney: CMS slice raw illustrator files, CMS Document 5581-v1, Version from 04th October 2011, s.l., 2011, URL: https://cms-docdb.cern.ch/cgi-bin/PublicDocDB/ShowDocument?docid=5581, Date viewed: 25.10.2014

[Bee2001] W. Beenakker et al.: Higgs Radiation off Top Quarks at the Tevatron and the LHC, in. Phys. Rev. Lett. 87 (2001) 20, pp. 201805, arXiv:hep-ph/0107081, Version from 9th July 2001, s.l., 2001, URL: http://arxiv.org/abs/hep-ph/0107081, Date viewed: 29.11.2014

[Bee2002] W. Beenakker et al.: NLO QCD corrections to t anti-t H production in hadron collisions, in: Nucl. Phys. B 653 (2003) 1–2, pp. 151–203, arXiv:hep-ph/0211352, Version from 22th November 2002, s.l., 2002, URL: http://arxiv.org/abs/hep-ph/0211352, Date viewed: 29.11.2014

[Ben1987] M. Bengtsson and T. Sjöstrand: Coherent parton showers versus matrix elements - implications of PETRA/PEP data, in: Phys. Let. B 185 (1987) 3–4, pp. 435–440, s.l., 1987, URL: http://www.sciencedirect.com/science/article/pii/0370269387910318, Date viewed: 23.11.2014

[Ben2014] J. Bendavid and V. Ciulli: Private Communication “Choosing the right merging scale for FxFx merging”, in: CMS Generator Meeting, Geneva, 26.05.2014

[Ber2013] Z. Bern et al.: The BlackHat Library for One-Loop Amplitudes, arXiv:hep-ph/1310.2808, Version from 16th October 2013, s.l., 2013, URL: http://arxiv.org/abs/1310.2808, Date viewed: 22.11.2014

[Bil1982] S.M. Bilenky and J. Hosek: Glashow-Weinberg-Salam theory of electroweak interactions and the neutral currents, in: Phys. Rep. 90 (1982) 2, pp. 73–157, s.l., 1982, URL: http://www.sciencedirect.com/science/article/pii/0370157382900163, Date viewed: 26.11.2014

[Bin2004] D. Binosi and L. Theußl: JaxoDraw: A graphical user interface for drawing Feynman diagrams, in: Comp. Phys. Comm. 161 (2004) 1–2, pp. 76–86, s.l., 2004

[Bir2005] I. Bird et al. (The LCG TDR Editorial Board): LHC Computing Grid – Technical design report, Geneva, 2005, URL: http://cdsweb.cern.ch/record/840543/files/lhcc-2005-024.pdf, Date viewed: 09.12.2014

[Blo2002] V. Blobel: An Unfolding Method for High Energy Physics Experiments, arXiv:hep-ex/0208022, Version from 16th August 2002, s.l., 2002, URL: http://arxiv.org/abs/hep-ex/0208022, Date viewed: 11.12.2014

[Boo2001] E. Boos et al.: Generic User Process Interface for Event Generators, arXiv:hep-ph/0109068, Version from 9th September 2001, s.l., 2001, URL: http://arxiv.org/abs/hep-ph/0109068, Date viewed: 24.11.2014

[Bot2011] M. Botje et al.: The PDF4LHC Working Group Interim Recommendations, arXiv:hep-ph/1101.0538, Version from 3rd January 2011, s.l., 2011, URL: http://arxiv.org/abs/1101.0538, Date viewed: 30.11.2014

[Bru1997] R. Brun and F. Rademakers: ROOT – An object oriented data analysis framework, in: Nucl. Inst. & Meth. in Phys. Res. A 389 (1997) 1–2, pp. 81–86, s.l., 1997, URL: http://www.sciencedirect.com/science/article/pii/S016890029700048X, Date viewed: 03.12.2014

[Brü2012] Brücke-Osteuropa: Luftbild vom CERN, in: Wikimedia Commons, Version from 4th November 2012 12:17, URL: http://commons.wikimedia.org/wiki/File:CERN-aerial_1.jpg, Date viewed: 24.10.2014

[Buc2010] A. Buckley et al.: Rivet user manual, arXiv:hep-ph/1003.0694, Version from 28th February 2013, s.l., 2010, URL: http://arxiv.org/abs/1003.0694, Date viewed: 10.12.2014

[Buc2011] A. Buckley et al.: General-purpose event generators for LHC physics, arXiv:hep-ph/1101.2599, Version from 13th January 2011, s.l., 2011, URL: http://arxiv.org/abs/1101.2599, Date viewed: 21.11.2014

[Buc2013] A. Buckley: New access to PDF data via LHAPDF6, in: Les Houches 2013: Physics at TeV Colliders: Standard Model Working Group Report, arXiv:hep-ph/1405.1067, Version from 5th May 2014, s.l., 2013, URL: http://arxiv.org/abs/1405.1067, Date viewed: 29.11.2014

[Buf1733] G.–L. Leclerc Comte de Buffon: Editor’s note concerning a lecture given 1733 by Mr. Leclerc Buffon to the Royal Academy of Sciences in Paris, in: Histoire de l’Acad. Roy. des Sci., pp. 43–45, s.l., 1733

[But1996] J.M. Butterworth et al.: Multiparton Interactions in Photoproduction at HERA, in: Z. Phys. C72 (1996), pp. 637–646, arXiv:hep-ph/9601371, Version from 30th January 1996, s.l., 1996, URL: http://arxiv.org/abs/hep-ph/9601371, Date viewed: 21.11.2014

[Cac2011] M. Cacciari et al.: FastJet user manual, arXiv:hep-ph/1111.6097, Version from 25 November 2011, s.l., 2011, URL: http://arxiv.org/abs/1111.6097, Date viewed: 24.11.2014

[Cas2011] F. Cascioli et al.: Scattering Amplitudes with Open Loops, arXiv:hep-ph/1111.5206, Version from 5 March 2012, s.l., 2011, URL: http://arxiv.org/abs/1111.5206, Date viewed: 22.11.2014

[Cat1993] S. Catani et al.: Longitudinally-invariant k_T-clustering algorithms for hadron-hadron collisions, in: Nucl. Phys. B 406 (1993) 1–2, pp.187–224, s.l., 1993

[Cat2001] S. Catani et al.: QCD Matrix Elements + Parton Showers, in: JHEP 0111 (2001) 063, arXiv:hep-ph/0109231, Version from 25th September 2005, s.l., 2001, URL: http://arxiv.org/abs/hep-ph/0109231, Date viewed: 22.11.2014

[Cer2001] CERN – European Organization for Nuclear Research: The Z Particle Branching Ratios and the Number of Families, in: Particle Physics Education CD-ROM, Geneva, 2001, URL: http://physicsmasterclasses.org/exercises/keyhole/en/projects/number_of_families.html, Date viewed: 15.10.2014

[Cer2009] CERN – European Organization for Nuclear Research: LHC – the guide, CERN-Brochure-2009-003-Eng, Geneva, 2009, URL: http://cds.cern.ch/record/1165534, Date viewed: 24.10.2014

[Cer2013] CERN – European Organization for Nuclear Research: The CERN accelerator complex, OPEN-PHO-ACCEL-2013-056, Geneva, 2013, URL: http://cds.cern.ch/record/1621894, Date viewed: 24.10.2014

[Cer2014a] CERN – European Organization for Nuclear Research: About CERN, s.l, 2014, URL: http://home.web.cern.ch/about, Date viewed: 24.10.2014

[Cer2014b] CERN – European Organization for Nuclear Research: Annual Report of the European Organization for Nuclear Research, Geneva, 2014

[Cer2014c] CERN – European Organization for Nuclear Research: The Large Hadron Collidier, s.l., 2014, URL: http://home.web.cern.ch/topics/large-hadron-collider, Date viewed: 24.10.2014

[CMS1996] The CMS Collaboration: CMS – The Compact Muon Solenoid, Version from 1st May 2014, s.l., 1996, URL: http://cds.cern.ch/record/1140134/, Date viewed: 25.11.2014

[CMS2012a] The CMS Collaboration: Observation of a new boson at a mass of 125 GeV with the CMS experiment at the LHC, in: Phys. Lett. B 716 (2012) 1, pp. 30-61, arXiv:hep-ex/1207.7235, Version from 28th January 2013, s.l., 2012, URL: http://arxiv.org/abs/1207.7235, Date viewed: 27.11.2014

[CMS2012b] The CMS Collaboration: Measurement of differential top-quark pair production cross sections in pp collisions at $\sqrt{s} = 7$ TeV, in: Eur. Phys. J. C. 73 (2013) 3, pp. 2339, arXiv:hep-ex/1211.2220, Version from 29th April 2013, s.l., 2013, URL: http://arxiv.org/abs/1211.2220, Date viewed: 11.12.2014

[CMS2013] The CMS Collaboration: CMS Factsheet, CMS Document 4030-v4, Version from 08th November 2013, s.l., 2013, URL: https://cms-docdb.cern.ch/cgi-bin/PublicDocDB/ShowDocument?docid=4030, Date viewed: 25.10.2014

[CMS2014] The CMS Collaboration: Measurement of jet multiplicity distributions in $t\bar{t}$ production in pp collisions at $\sqrt{s} = 7$ TeV, in: Eur. Phys. J. C 74 (2014) 8, pp. 3014, Heidelberg, 2014, URL: `http://dx.doi.org/10.1140/epjc/s10052-014-3014-0`, Date viewed: 10.11.2014

[Col2004] J. Collins et al.: Factorization of Hard Processes in QCD, arXiv:hep-ph/0409313, Version from 27th September 2004, s.l., 2004, URL: `http://arxiv.org/abs/hep-ph/0409313v1`, Date viewed: 04.11.2014

[Col2011] J.C. Collins: Foundations of perturbative QCD, Cambridge, 2011

[Cor2002] G. Corcella et al.: Herwig6.5: an event generator for Hadron Emission Reactions With Interfering Gluons (including supersymmetric processes), in: JHEPH 0101:010 (2001), arXiv:hep-ph/0011363, Version from 22th October 2002, s.l., 2002, URL: `http://arxiv.org/abs/hep-ph/0011363`, Date viewed: 21.11.2014

[Daw2002] S. Dawson et al.: Associated Top Quark-Higgs Boson Production at the LHC, in: Phys. Rev. D 67 (2003) 7, pp. 071503, arXiv:hep-ph/0211438, Version from 28th November 2002, s.l., 2002, URL: `http://arxiv.org/abs/hep-ph/0211438`, Date viewed: 29.11.2014

[Des2014] A. Descroix: PhD thesis in preparation, Karlsruhe, To be published

[Dob2001] The HepMC C++ Monte Carlo event record for high energy physics, in: Comp. Phys. Comm. 134 (2001) 1, pp. 41–46, s.l., 2001, URL: `http://www.sciencedirect.com/science/article/pii/S0010465500001892`, Date viewed: 08.12.2014

[Dok1977] Y.L. Dokshitser: Calculation of structure functions of deep-inelastic scattering and e^+e^- annihilation by perturbation theory in quantum chromodynamics, in: Sov. Phys. JETP 46 (1977) 4, pp. 641–653, s.l., 1977, URL: `http://www.jetp.ac.ru/cgi-bin/dn/e_046_04_0641.pdf`, Date viewed: 20.11.2014

[DON2000] DONUT Collaboration: Observation of Tau Neutrino Interactions, in: Phys. Lett. B 504 (2001), pp. 218–224, arXiv:hep-ex/0012035, s.l., 2000, URL: `http://arxiv.org/abs/hep-ex/0012035`, Date viewed: 26.11.2014

[Ell1993] S.D. Ellis and D.E. Soper: Successive Combination Jet Algorithm For Hadron Collisions, in: Phys. Rev. D (1993), pp. 3160–3166, arXiv:hep-ph/9305266, Version from 14th May 1993, s.l., 1993, URL: `http://arxiv.org/abs/hep-ph/9305266`, Date viewed: 24.11.2014

[Eng1964] F. Englert and R. Brout: Broken Symmetry and the Mass of Gauge Vector Mesons, in: Phys. Rev. Lett. 13 (1964) 9, pp. 321-323, s.l., 1964, URL: `http://link.aps.org/doi/10.1103/PhysRevLett.13.321`, Date viewed: 26.11.2014

[Fel2010] J. Feltesse: Introduction to Parton Distribution Functions, in: Scholarpedia 5(11):10160, Revision #91386 from 6th November 2010, s.l., 2010, URL: `http://www.scholarpedia.org/article/Introduction_to_Parton_Distribution_Functions`, Date viewed: 20.11.2014

[Fey1949a] R.P. Feynman: The Theory of Positrons, in: Phys. Rev. 76 (1949) 6, pp. 749–759, s.l., 1949, URL: `http://link.aps.org/doi/10.1103/PhysRev.76.749`, Date viewed: 27.11.2014

[Fey1949b] R.P. Feynman: Space-Time Approach to Quantum Electrodynamics, Phys. Rev. 76 (1949) 6, pp. 769–789, 1949, s.l., 1949, URL: `http://link.aps.org/doi/10.1103/PhysRev.76.769`, Date viewed: 28.10.2014

[For2012] J.R. Forshaw et al.: On the breaking of collinear factorization in QCD, arXiv:hep-ph/1206.6363, Version from 12th November 2012, s.l., 2012, URL: http://arxiv.org/abs/1206.6363, Date viewed: 15.12.2014

[Fre2011] R. Frederix et al.: Scalar and pseudoscalar Higgs production in association with a top-antitop pair, in: Phys. Lett. B 701 (2001) 4, pp. 427–433, arXiv:hep-ph/1104.5613, Version from 17th June 2011, s.l., 2011, URL: http://arxiv.org/abs/1104.5613, Date viewed: 29.11.2014

[Fre2012] R. Frederix and S. Frixione: Merging meets matching in MC@NLO, arXiv:hep-ph/1209.6215, Version from 27th September 2012, s.l., 2012, URL: http://arxiv.org/abs/1209.6215, Date viewed: 24.11.2014

[Fre2013] R. Frederix: NLO and aMC@NLO, in: 2nd Taipei School on FeynRules – MadGraph for LHC Physics, Taipei, 2013

[Fri1977] H. Fritzsch: Quantum Flavourdynamics, in: Deeper Pathways in High-Energy Physics 12, pp. 275-322, s.l., 1977, URL: http://dx.doi.org/10.1007/978-1-4757-1565-1_14, Date viewed: 27.11.2014

[Fri2002] S. Frixione and B.R. Webber: Matching NLO QCD computations and parton shower simulations, in: JHEP 0206 (2002) 029, arXiv:hep-ph/0204244, Version from 12th July 2002, s.l., 2002, URL: http://arxiv.org/abs/hep-ph/0204244, Date viewed: 23.11.2014

[Fri2007] S. Frixione et al.: Matching NLO QCD computations with Parton Shower simulations: the POWHEG method, arXiv:hep-ph/0709.2092, Version from 13 September 2007, s.l., 2007, URL: http://arxiv.org/abs/arXiv:0709.2092, Date viewed: 23.11.2014

[Fri2010] S. Frixione et al.: NLO QCD corrections in Herwig++ with MC@NLO, in: JHEP 1101 (2011) 053, arXiv:hep-ph/1010.0568, Version from 4th October 2010, s.l., 2010, URL: http://arxiv.org/abs/1010.0568, Date viewed: 24.11.2014

[Gan2000] E.R. Gansner and S.C. North: An open graph visualization system and its applications to software engineering, in: Softw. Pract. Exper. 30 (2000) 11, pp. 1203-1233, s.l, 2000, URL: http://www.graphviz.org/Documentation/GN99.pdf, Date viewed: 03.12.2014

[Geh1999] T. Gehrmann et al.: A compilation of structure functions in deep inelastic scattering, in: J. Phys. G: Nucl. Part. Phys. 25 (1999) 12A, pp. A1, s.l., 1999, URL: http://stacks.iop.org/0954-3899/25/i=12A/a=301, Date viewed: 20.11.2014

[Geh2012] T. Gehrmann et al.: NLO QCD matrix elements + parton showers in e+e- -> hadrons, in: JHEP 1301 (2013) 144, arXiv:hep-ph/1207.5031, Version from 13th February 2013, s.l., 2012, URL: http://arxiv.org/abs/arXiv:1207.5031, Date viewed: 22.11.2014

[Geh2013] A. Gehrmann-De Ridder: Perturbative QCD (1/3), in: CERN Academic Training Lecture Regular Programme, Geneva, 2013, URL: https://indico.cern.ch/event/230448/, Date viewed: 05.11.2014

[Gie2012a] S. Gieseke: Monte Carlos – Lecture 1, in: DESY MC school 2012, Hamburg, 2012, URL: https://indico.desy.de/getFile.py/access?sessionId=1&resId=0&materialId=0&confId=5064, Date viewed: 22.10.2014

[Gie2012b] S. Gieseke: Monte Carlos – Lecture 2, in: DESY MC school 2012, Hamburg, 2012, URL: https://indico.desy.de/getFile.py/access?sessionId=1&resId=1&materialId=0&confId=5064, Date viewed: 22.10.2014

[Gie2012d] S. Gieseke: Monte Carlos – Lecture 3, in: DESY MC school 2012, Hamburg, 2012, URL: `https://indico.desy.de/getFile.py/access?sessionId=1&resId=2&materialId=0&confId=5064`, Date viewed: 22.10.2014

[Gie2012d] S. Gieseke: Monte Carlos – Lecture 4, in: DESY MC school 2012, Hamburg, 2012, URL: `https://indico.desy.de/getFile.py/access?sessionId=3&resId=1&materialId=0&confId=5064`, Date viewed: 22.10.2014

[Gle2008] T. Gleisberg et al.: Event generation with SHERPA 1.1, in: JHEP 0902 (2009) 007, arXiv:hep-ph/0811.4622, s.l., 2008, URL: `http://arxiv.org/abs/0811.4622`, Date viewed: 21.11.2014

[Gle2008b] T. Gleisberg and S. Hoeche: Comix a new matrix element generator, in: JHEP 2008 (2008) 12, pp. 039, arXiv:hep-ph/0808.3674, Version from 24th November 2008, s.l., 2008, URL: `http://arxiv.org/abs/0808.3674`, Date viewed: 10.12.2014

[Gri1972] V.N. Gribov and L.N. Lipatov: e^+e^--pair annihilation and deep inelastic ep-scattering in perturbation theory , in: Sov. J. Nucl. Phys. 15, pp. 438–450, s.l., 1972

[Gro2006] R.C. Group: Measurement of the Inclusive Jet Cross Section Using the Midpoint Algorithm in Run II at the Collider Detector at Fermilab (CDF), s.l. 2006, URL: `http://www-cdf.fnal.gov/~group/WORK/DISS_PAGE/thesis_final.pdf`, Date viewed: 28.11.2014

[Gun1991] J.F. Gunion: Associated top-anti-top-Higgs production as a large source of WH events: implications for Higgs detection in the $l\nu\gamma\gamma$ final state, in: Phys. Lett. B 261 (1991) 4, pp. 510–517, s.l., 1991, URL: `http://www.sciencedirect.com/science/article/pii/0370269391904653`, Date viewed: 29.11.2014

[Gur1964] G.S. Guralnik et al.: Global Conservation Laws and Massless Particles, in: Phys. Rev. Lett. 135 (1964) 20, pp. 585-587, s.l., 1964, URL: `http://link.aps.org/doi/10.1103/PhysRevLett.13.585`, Date viewed: 26.11.2014

[Har2011] R. Harlander et al.: Bottom-quark associated Higgs-boson production: reconciling the four- and five-flavour scheme approach, arXiv:hep-ph/1112.3478, Version from 15th December 2011, s.l., 2011, URL: `http://arxiv.org/abs/1112.3478`, Date viewed: 14.12.2014

[Har2014] M.A. Harrendorf et al.: Plotting scripts for FxFx-Merging, s.l., 2014, URL: `https://github.com/mharrend/plotscripts`, Date viewed: 08.12.2014

[Has1973a] F.J. Hasert et al.: Search for elastic muon-neutrino electron scattering, in: Phys. Lett. B 46 (1973) 1, pp. 121–124, s.l., 1973, URL: `http://www.sciencedirect.com/science/article/pii/0370269373904942`, Date viewed: 26.11.2014

[Has1973b] F.J. Hasert et al.: Observation of neutrino-like interactions without muon or electron in the gargamelle neutrino experiment, in: Phys. Lett. B 46 (1973) 1, pp. 138–140, s.l., 1973, URL: `http://www.sciencedirect.com/science/article/pii/0370269373904991`, Date viewed: 26.11.2014

[Has1974] F.J. Hasert et al.: Observation of neutrino-like interactions without muon or electron in the Gargamelle neutrino experiment, in: Nucl. Phys. B 73 (1974) 1, pp. 1–22, s.l., 1974, URL: `http://www.sciencedirect.com/science/article/pii/0550321374900388`, Date viewed: 26.11.2014

[Hig1964a] P.W. Higgs: Broken symmetries, massless particles and gauge fields, in: Phys. Lett. 12 (1964) 2, pp. 132–133, s.l., 1964, URL: `http://www.sciencedirect.com/science/article/pii/0031916364911369`, Date viewed: 26.11.2014

[Hig1964b] P.W. Higgs: Broken Symmetries and the Masses of Gauge Bosons, in: Phys. Rev. Lett. 13 (1964) 16, pp. 508–509, s.l., 1964, URL: http://link.aps.org/doi/10.1103/PhysRevLett.13.508, Date viewed: 26.11.2014

[Hla1961] E. Hlawka: Funktionen von beschränkter Variation in der Theorie der Gleichverteilung, in: Ann. Mat. Pura Appl. 54 (1961) 1, pp. 325–333, s.l., 1961

[Hla1971] E. Hlawka: Discrepancy and Riemann integration, in: Studies in Pure Mathematics 3 (1971), New York, 1971

[Höc1995] A. Höcker and V. Kartvelishvili: SVD approach to data unfolding, in: Nucl. Instrum. Meth. A 372 (1996) 3, pp. 469–481, arXiv:hep-ph/9509307, Version from 19th September 1995, s.l., 1995, URL: http://arxiv.org/abs/hep-ph/9509307, Date viewed: 11.12.2014

[Hoe2012] S. Hoeche et al.: QCD matrix elements + parton showers: The NLO case, in: JHEP 1304 (2013) 027, arXiv:hep-ph/1207.5030, Version from 20 July 2012, s.l., 2012, URL: http://arxiv.org/abs/arXiv:1207.5030, Date viewed: 22.11.2014

[Hoe2013] S. Hoeche et al.: Zero and one jet combined NLO analysis of the top quark forward-backward asymmetry, in: Phys. Rev. D 88 (2013) 1, pp. 014040, arXiv:hep-ph/1306.2703, Version from 17th July 2013, s.l., 2013, URL: http://arxiv.org/abs/1306.2703, Date viewed: 10.12.2014

[Hoe2014] S. Hoeche et al.: Next-to-leading order QCD predictions for top-quark pair production with up to two jets merged with a parton shower, arXiv:hep-ph/1402.6293, Version from 25th February 2014, s.l., 2014, URL: http://arxiv.org/abs/arXiv:1402.6293, Date viewed: 03.12.2014

[Hus2011] U. Husemann: 6. QCD, in: Master course "Teilchenphysik für Fortgeschrittene (2202031)", lecture no. 12, Karlsruhe, 2011, URL: http://www-ekp.physik.uni-karlsruhe.de/~husemann/teaching/2011_ws/teilchenphysik/docs/Vorlesung_12.pdf, Date viewed: 28.11.2014, Note: Restricted access, Username: Students, Password: only

[Inn2001] V. Innocente et al.: CMS software architecture: Software framework, services and persistency in high level trigger, reconstruction and analysis, in: Comp. Phys. Comm. 140 (2001) 1–2, pp. 31–44, s.l., 2001, URL: http://www.sciencedirect.com/science/article/pii/S0010465501002533, Date viewed: 05.12.2014

[Jon2008] C.D. Jones et al.: Analysis environments for CMS, in: J. Phys.: Conf. Ser. 119 (2008) 3, pp. 032027, s.l., 2008, URL: http://stacks.iop.org/1742-6596/119/i=3/a=032027, Date viewed: 05.12.2014

[Kla2012] P. Klabbers: Operation and Performance of the CMS Level-1 Trigger during 7 TeV Collisions, in: Phys. Proc. 37 (2012) 0, pp. 1908–1916, s.l., 2012, URL: http://www.sciencedirect.com/science/article/pii/S1875389212019074, Date viewed: 25.11.2014

[Kob1973] CP-Violation in the Renormalizable Theory of Weak Interaction, in: Prog. Theor. Phys. 49 (1973) 2, pp. 652–657, s.l., 1973, URL: http://ptp.oxfordjournals.org/content/49/2/652.full.pdf+html, Date viewed: 26.11.2014

[Kok1942] J.F. Koksma: Ein allgemeiner Satz der Theorie der Gleichverteilung mod 1., in: Mathematica Zutphen B 11 (1942) 7–11, pp. 49–52, s.l., 1942

[Kra2001] F. Krauss et al.: AMEGIC++ 1.0, A Matrix Element Generator in C++, in: JHEP 2002 (2002) 02, pp. 044 , arXiv:hep-ph/0109036, Version from 5th September 2001, s.l., 2001, URL: `http://arxiv.org/abs/hep-ph/0109036`, Date viewed: 10.12.2014

[Kra2002] F. Krauss: Matrix Elements and Parton Showers in Hadronic Interactions, in: JHEP 0208 (2002) 015, arXiv:hep-ph/0205283, Version from 24th May 2002, s.l., 2002, URL: `http://arxiv.org/abs/hep-ph/0205283`, Date viewed: 22.11.2014

[Kun1984] Z. Kunszt: Associated production of heavy Higgs boson with top quarks, in: Nucl. Phys. B 247 (1984) 2, pp. 339–359, s.l., 1984, URL: `http://www.sciencedirect.com/science/article/pii/0550321384905534`, Date viewed: 29.11.2014

[Lav2005] N. Lavesson and L. Lönnblad: W+jets Matrix Elements and the Dipole Cascade, in: JHEP 0507 (2005) 054, arXiv:hep-ph/0503293, Version from 5th April 2005, s.l., 2005, URL: `http://arxiv.org/abs/hep-ph/0503293`, Date viewed: 22.11.2014

[Lav2008] N. Lavesson and L. Lönnblad: Merging parton showers and matrix elements – back to basics, in: JHEP 0804 (2008) 085, arXiv:hep-ph/0712.2966, Version from 23th April 2008, s.l., 2008, URL: `http://arxiv.org/abs/0712.2966v2`, Date viewed: 24.11.2014

[LHC2011] LHC Higgs Cross Section Working Group: Handbook of LHC Higgs Cross Sections: 1. Inclusive Observables, arXiv:hep-ph/arXiv:1101.0593, Version from 20th May 2011, s.l., 2011, URL: `http://arxiv.org/abs/1101.0593`, Date viewed: 28.11.2014

[LHC2012] LHC Higgs Cross Section Working Group: Handbook of LHC Higgs Cross Sections: 2. Differential Distributions, arXiv:hep-ph/arXiv:1201.3084, Version from 15th January 2012, s.l., 2012, URL: `http://arxiv.org/abs/1201.3084`, Date viewed: 28.11.2014

[LHC2013] LHC Higgs Cross Section Working Group: Handbook of LHC Higgs Cross Sections: 3. Higgs Properties, arXiv:hep-ph/arXiv:1307.1347, Version from 29th November 2013, s.l., 2013, URL: `http://arxiv.org/abs/1307.2347`, Date viewed: 28.11.2014

[Lön2001] L. Lönnblad: Correcting the Colour-Dipole Cascade Model with Fixed Order Matrix Elements, in: JHEP 0205 (2002) 046, arXiv:hep-ph/0112284, Version from 26 May 2002, s.l, 2001, URL: `http://arxiv.org/abs/hep-ph/0112284`, Date viewed: 22.11.2014

[Lön2014] L. Lönnblad: ThePEG – Toolkit for High Energy Physics Event Generation, s.l., 2014, URL: `http://home.thep.lu.se/ThePEG/`, Date viewed: 21.11.2014

[Mal2007] F. Maltoni et al.: Choosing the Factorization Scale in Perturbative QCD, arXiv:hep-ph/0703156, Version from 14th March 2007, s.l., 2007, URL: `http://arxiv.org/abs/hep-ph/0703156`, Date viewed: 26.11.2014

[Mal2012] F. Maltoni: Predictive Monte Carlo tools for the LHC. Lecture II, in: CERN Academic Training Lectures – May 2012, Geneva, 2012

[Man2001] M. Mangano et al.: Multijet matrix elements and shower evolution in hadronic collisions: W b bbar + n jets as a case study, in: Nucl. Phys. B (2002) 632, pp. 343–362, arXiv:hep-ph/0108069, Version from 7th August 2001, s.l., 2001, URL: `http://arxiv.org/abs/hep-ph/0108069`, Date viewed: 22.11.2014

[Mar1991] W.J. Marciana and F.E. Paige: Associated production of Higgs bosons with $t\bar{t}$ pairs, in: Phys. Rev. Lett. 66 (1991) 19, pp. 2433–2435, s.l., 1991, URL: http://link.aps.org/doi/10.1103/PhysRevLett.66.2433, Date viewed: 29.11.2014

[Mar2009] A.D. Martin et al.: Parton distributions for the LHC, in: Eur. Phys. J. C 63 (2009) 2, pp. 189–285, arXiv:hep-ph/0901.0002, Version from 7th July 200, s.l., 2009, URL: http://arxiv.org/abs/0901.0002, Date viewed: 29.11.2014

[Mar2014] A. Marek: Rivet-Implementierung einer ttbar+Jets-Analyse am CMS-Experiment, Karlsruhe, 2014

[Met1949] N. Metropolis and S. Ulam: The Monte Carlo method, in: J. Amer. statistical Assoc. 44 (1949), pp. 335–341, s.l., 1949

[Mis2014] MissMJ and Nasfarley88: Standard Model of Elementary Particles, in: Wikimedia Commons, Version from 1st October 2014 08:55, URL: http://commons.wikimedia.org/wiki/File:Standard_Model_of_Elementary_Particles.svg, Date viewed: 22.10.2014

[Nad2008] P.M. Nadolsky et al.: Implications of CTEQ global analysis for collider observables, in: Phys. Rev. D 78 (2008) 1, pp. 013004, arXiv:hep-ph/0802.0007, Version from 17th March 2008, s.l., 2008, URL: http://arxiv.org/abs/0802.0007, Date viewed: 30.11.2014

[Nas2004] P. Nason: A New Method for Combining NLO QCD with Shower Monte Carlo Algorithms, in: JHEP 0411 (2004) 040, arXiv:hep-ph/0409146, Version from 13th September 2004, s.l., 2004, URL: http://arxiv.org/abs/hep-ph/0409146, Date viewed: 23.11.2014

[Ng1984] J.N. NG and P. Zakarauskas: QCD-parton calculation of conjoined production of Higgs bosons and heavy flavors in p $\overline{p}$ collisions, in: Phys. Rev. D 29 (1984) 5, pp. 876–886, s.l., 1984, URL: http://link.aps.org/doi/10.1103/PhysRevD.29.876, Date viewed: 29.11.2014

[NNP2013] The NNPDF Collaboration: Parton distributions with QED corrections, arXiv:hep-ph/1308.0598, Version from 4th November 2013, s.l., 2013, URL: http://arxiv.org/abs/1308.0598, Date viewed: 20.11.2014

[NNP2014] The NNPDF Collaboration: Parton distributions for the LHC Run II, arXiv:hep-ph/1410.8849, Version from 6th November 2014, s.l., 2014, URL: http://arxiv.org/abs/1410.8849, Date viewed: 30.11.2014

[Oli2014] K.A. Olive et al. (Particle Data Group): 2014 Review of Particle Physics, in: Chin. Phys. C 38 (2014) 090001, s.l., 2014, URL: http://pdg.lbl.gov/2014/reviews/contents_sports.html, Date viewed: 21.14.2014

[Oss2007a] G. Ossola et al.: CutTools: a program implementing the OPP reduction method to compute one-loop amplitudes, arXiv:hep-ph/0711.3596, s.l., 2007, URL: http://arxiv.org/abs/0711.3596, Date viewed: 08.11.2014

[Oss2007b] G. Ossola: A new method for the numerical evaluation of one-loop amplitudes, arXiv:hep-ph/0709.2332, Version from 14th September 2007, Napoli, 2007, URL: http://arxiv.org/abs/0709.2332, Date viewed: 23.11.2014

[Per1975] Evidence for Anomalous Lepton Prediction in e^+e^- Annihilation, in: Phys. Rev. Lett. 35 (1975) 22, pp. 1489–1492, s.l., 1975, URL: http://link.aps.org/doi/10.1103/PhysRevLett.35.1489, Date viewed: 26.11.2014

[Ple2008] T. Plehn: LHC Phenomology for Physics Hunters, arXiv:hep-ph/0810.2281, Version from 7th February 2009, s.l., 2008, URL: `http://arxiv.org/abs/0810.2281`, Date viewed: 26.11.2014

[Pre2014] S. Prestel: Lectures on combining parton showers and matrix elements – Lecture I, in: MCnet school 20014, Ambleside, 2014, URL: `https://indico.hep.manchester.ac.uk/getFile.py/access?contribId=6&resId=0&materialId=slides&confId=4413`, Date viewed: 15.10.2014

[Pum2002] J. Pumplin et al.: New Generation of Parton Distributions with Uncertainties from Global QCD Analysis, arXiv:hep-ph/0201195, Version from 3rd February 2002, s.l., 2002, URL: `http://arxiv.org/abs/hep-ph/0201195`, Date viewed: 20.11.2014

[Qua2006] A. Quadt: Top quark physics at hadron colliders, in: Europ. Phys. J. C 48 (2006) 3, pp. 835-1000, s.l., 2006, URL: `http://dx.doi.org/10.1140/epjc/s2006-02631-6`, Date viewed: 09.12.2014

[Qua2013a] G. Quast and A. Raspereza: Higg-Physik – Motivation and overview, in: Master course 2013 "Higgs Physics", lecture no. 1, Karlsruhe, 2013, URL: `http://www-ekp.physik.uni-karlsruhe.de/~quast/vorlesung/TP2HiggsSS13/V04_Calculation-ofPhysicsProcesses.pdf`, Date viewed: 20.10.2014

[Qua2013b] G. Quast and A. Raspereza: Computation of Physics Processes, in: Master course 2013 "Higgs Physics", lecture no. 5, Karlsruhe, 2013, URL: `http://www-ekp.physik.uni-karlsruhe.de/~quast/vorlesung/TP2HiggsSS13/V04_Calculation-ofPhysicsProcesses.pdf`, Date viewed: 20.10.2014

[Qua2013c] G. Quast and A. Raspereza: Components of Analysis Chain, in: Master course 2013 "Higgs Physics", lecture no. 7, Karlsruhe, 2013, URL: `http://www-ekp.physik.uni-karlsruhe.de/~quast/vorlesung/TP2HiggsSS13/V07_AnalysisChain.pdf`, Date viewed: 20.10.2014

[Rai1979] R. Raitio and W.W. Wada: Higgs-boson production at large transverse momentum in quantum chromodynamics, in: Phys. Rev. D 19 (1979) 3, pp. 941–944, s.l., 1979, URL: `http://link.aps.org/doi/10.1103/PhysRevD.19.941`, Date viewed: 29.11.2014

[Rei2001] L. Reina and S. Dawson: Next-to-Leading Order Results for t-tbar-h Production at the Tevatron, in: Phys. Rev. Lett. 87 (2001) 20, pp. 201804, arXiv:hep-ph/0107101, Version from 9th July 2001, s.l., 2001, URL: `http://arxiv.org/abs/hep-ph/0107101`, Date viewed: 29.11.2014

[Ric1947] R.D. Richtmyer and J. v. Neumann: Statistical methods in neutron diffusion, Los Alamos Scientific Laboratory report LAMS–551, Los Alamos, 1947, URL: `http://library.lanl.gov/cgi-bin/getfile?00329286.pdf`, Date viewed: 05.11.2014

[Ros2003] G.v. Rossum and F.L. Drake: Python Language Reference Manual – Release 2.3, Bristol, 2003, URL: `homepages.ipact.nl/~wichizaya/work/ref.pdf`, Date viewed: 08.12.2014

[Sch1948] J. Schwinger: Quantum Electrodynamics. I. A Covariant Formulation, in: Phys. Rev. 74 (1948) 10, pp. 1439–1461, s.l., 1948, URL: `http://link.aps.org/doi/10.1103/PhysRev.74.1439`, Date viewed: 27.11.2014

[Sch2014a] K. Schweiger: Neue Jet-Merging-Algorithmen für Monte-Carlo-Generatoren in nächstführender Ordnung für die $t\bar{t}$+Jets-Produktion, Karlsruhe, 2014, URL: `https://ekp-invenio.physik.uni-karlsruhe.de/record/48594?ln=en`, Date viewed: 25.11.2014

[Sch2014b] K. Schweiger: Private Communication “Results of the study of the merging scale and matrix element minimum jet transverse momentum selection criterion”, September 2014

[Sch2014c] F. Schaaf: Verbesserung der computergestützen Analyse, Karlsruhe, To be published

[Sch2014d] F. Schaaf: Private Communication “Plots used for the Pythia8 event study & visualization talk in the CMS Generator Meeting”, 20th October 2014

[Sey1994] M.H. Seymour: Matrix-Element Corrections to Parton Shower Algorithms, in: Comp. Phys. Commun. 90 (1995), pp. 95–101, arXiv:hep-ph/9410414, Version from 31th October 1994, s.l., 1994, URL: `http://arxiv.org/abs/hep-ph/9410414`, Date viewed: 24.11.2014

[She2014] The Sherpa Team: Sherpa Manual Version 2.1.1, s.l., 2014, URL: `https://sherpa.hepforge.org/doc/SHERPA-MC-2.1.1.html`, Date viewed: 10.12.2014

[Sjö2006] T. Sjöstrand et al.: PYTHIA 6.4 Physics and Manual, in: JHEP 0605 (2006) 026, arXiv:hep-ph/0603175, s.l., 2006, URL: `http://arxiv.org/abs/hep-ph/0603175`, Date viewed: 21.11.2014

[Sjö2012] T. Sjöstrand: The Monte Carlos, Version from 15 February 2012, s.l., 2012, URL: `http://home.thep.lu.se/~torbjorn/preprints/th92susy.pdf`, Date viewed: 23.11.2014

[Sjö2014] T. Sjöstrand et al.: An Introduction to PYTHIA 8.2, arXiv:hep-ph/arXiv:1410.3012, Version from 11th October 2014, s.l., 2014, URL: `http://arxiv.org/abs/1410.3012`, Date viewed: 21.11.2014

[Sob1991] I.M. Sobol: Die Monte-Carlo-Methode, Berlin, 1991

[Str1995] B. Stroustrup: The C++ programming language, s.l., 1995

[Tay2011] L. Taylor: CMS detector design, Version from 23th November 2011, s.l., 2011, URL: `http://cms.web.cern.ch/news/cms-detector-design`, Date viewed: 01.11.2014

[Tom1946] S. Tomonaga: On a Relativistically Invariant Formulation of the Quantum Theory of Wave Fields, in: Prog. Theor. Phys. 1 (1946) 2, pp. 27–42, s.l, 1946, URL: `http://ptp.oxfordjournals.org/content/1/2/27.full.pdf+html`, Date viewed: 27.11.2014

[Wal2010] D. Waldram: Renormalization in QED, Version from 5th June 2010, s.l., 2010, URL: `http://www.imperial.ac.uk/workspace/theoreticalphysics/public/MSc/QED/renorm-new-print.pdf`, Date viewed: 25.11.2014

[Web1984] B.R. Webber: A QCD Model for Jet Fragmentation Including Soft Gluon Interference, in: Nucl. Phys. B 238 (1984) 492, s.l., 1984

[Web2011] B.R. Webber: Parton shower Monte Carlo event generators, in: Scholarpedia 6(12):10662, Revision #128236 from 1st December 2011, s.l., 2011, URL: `http://www.scholarpedia.org/article/Parton_shower_Monte_Carlo_event_generators`, Date viewed: 07.11.2014

[Wei1964] S. Weinberg: Feynman Rules for Any Spin. II. Massless Particles, in: Phys. Rev. 134 (1964) 4B, pp. B882–B896, s.l., 1964, URL: `http://link.aps.org/doi/10.1103/PhysRev.134.B882`, Date viewed: 04.11.2014

[Woo2014] J. Wood: Private Communication “Single-File FXFX Merging for 8TeV production”, 18th September 2014

Appendix

A Cross section calculations with aMC@NLO in LO and NLO for the $t\bar{t}H$ analysis

In the subsequent subsections is either for the 4FS or the 5FS a generic parameter card, proc card, and a run card shown which was used for the cross section calculation with aMC@NLO in LO and NLO for the $t\bar{t}H$ analysis. The following parameters in the run card were adjusted to obtain the various results with aMC@NLO published in chapter 6 of this thesis:

- ebeam1 and ebeam2: Defines the energy of the particle beams. The values were set in a way to obtain a center-of-mass energy $\sqrt{s}$ of either ($\sqrt{s}\ =\ 7,\ 8,\ 14$ TeV
- lhaid: The number of the parton distribution function to use. Additionally, the PDF_set_min and PDF_set_max parameter was set to the corresponding number of the error set of the particular parton distribution function which should be used.
- fixed_ren_scale, fixed_fac_scale, fixed_QES_scale: Defines if a fixed or variable renormalization scale μ_R and factorization scale $\mu_F$is used. In case of fixed scales the values of muR_ref_fixed, muF1_ref_fixed, muF2_ref_fixed, and QES_ref_fixed were set to $\mu_R = \mu_F = m_t + \frac{m_H}{2} = 235\,\text{GeV}$.
- maxjetflavour: Defines if either a 4FS or a 5FS is used. The proc card and parameter card have to be adjusted accordingly.

A.1 Parameter card for the 4FS

```
######################################################################
## PARAM_CARD AUTOMATICALY GENERATED BY MG5 FOLLOWING UFO MODEL   ####
######################################################################
##                                                                  ##
##  Width set on Auto will be computed following the information    ##
##        present in the decay.py files of the model.               ##
##        See  arXiv:1402.1178 for more details.                    ##
##                                                                  ##
######################################################################

###################################
## INFORMATION FOR LOOP
###################################
Block loop
    1 9.118800e+01 # MU_R

###################################
## INFORMATION FOR MASS
###################################
Block mass
    5 4.750000e+00 # MB
    6 1.725000e+02 # MT
```

```
   15 1.777000e+00 # MTA
   23 9.118800e+01 # MZ
   25 1.250000e+02 # MH
## Dependent parameters, given by model restrictions.
## Those values should be edited following the
## analytical expression. MG5 ignores those values
## but they are important for interfacing the output of MG5
## to external program such as Pythia.
  1 0.000000 # d : 0.0
  2 0.000000 # u : 0.0
  3 0.000000 # s : 0.0
  4 0.000000 # c : 0.0
  11 0.000000 # e- : 0.0
  12 0.000000 # ve : 0.0
  13 0.000000 # mu- : 0.0
  14 0.000000 # vm : 0.0
  16 0.000000 # vt : 0.0
  21 0.000000 # g : 0.0
  22 0.000000 # a : 0.0
  24 80.419002 # w+ : cmath.sqrt(MZ__exp__2/2. + cmath.sqrt(MZ__exp__4/4. - (
    aEW*cmath.pi*MZ__exp__2)/(Gf*sqrt__2)))

###################################
## INFORMATION FOR SMINPUTS
###################################
Block sminputs
    1 1.325070e+02 # aEWM1
    2 1.166390e-05 # Gf
    3 1.180000e-01 # aS

###################################
## INFORMATION FOR YUKAWA
###################################
Block yukawa
    5 4.750000e+00 # ymb
    6 1.725000e+02 # ymt
   15 1.777000e+00 # ymtau

###################################
## INFORMATION FOR DECAY
###################################
DECAY   6 1.491500e+00 # WT
DECAY  23 2.441404e+00 # WZ
DECAY  24 2.047600e+00 # WW
DECAY  25 6.382339e-03 # WH
## Dependent parameters, given by model restrictions.
## Those values should be edited following the
## analytical expression. MG5 ignores those values
## but they are important for interfacing the output of MG5
## to external program such as Pythia.
DECAY  1 0.000000 # d : 0.0
DECAY  2 0.000000 # u : 0.0
DECAY  3 0.000000 # s : 0.0
DECAY  4 0.000000 # c : 0.0
DECAY  5 0.000000 # b : 0.0
DECAY  11 0.000000 # e- : 0.0
DECAY  12 0.000000 # ve : 0.0
DECAY  13 0.000000 # mu- : 0.0
DECAY  14 0.000000 # vm : 0.0
DECAY  15 0.000000 # ta- : 0.0
DECAY  16 0.000000 # vt : 0.0
DECAY  21 0.000000 # g : 0.0
DECAY  22 0.000000 # a : 0.0
```

A.2 Proc card for the 4FS

```
#************************************************************
#*                    MadGraph5_aMC@NLO                     *
#*                                                          *
#*                *                       *                 *
#*                  *        * *        *                   *
#*                    * * * * 5 * * * *                     *
#*                  *        * *        *                   *
#*                *                       *                 *
#*                                                          *
#*                                                          *
#*         VERSION 2.2.2                2014-11-06          *
#*                                                          *
#*    The MadGraph5_aMC@NLO Development Team - Find us at   *
#*    https://server06.fynu.ucl.ac.be/projects/madgraph     *
#*                                                          *
#************************************************************
#*                                                          *
#*              Command File for MadGraph5_aMC@NLO          *
#*                                                          *
#*     run as ./bin/mg5_aMC  filename                       *
#*                                                          *
#************************************************************
set group_subprocesses Auto
set ignore_six_quark_processes False
set loop_optimized_output True
set gauge unitary
set complex_mass_scheme False
import model sm
define p = g u c d s u~ c~ d~ s~
define j = g u c d s u~ c~ d~ s~
define l+ = e+ mu+
define l- = e- mu-
define vl = ve vm vt
define vl~ = ve~ vm~ vt~
import model loop_sm
generate p p > t t~ h [QCD]
output crosssection_ttH_4F
```

A.3 Run card for the 4FS

```
#*********************************************************************
#                       MadGraph5_aMC@NLO                            *
#                                                                    *
#                     run_card.dat aMC@NLO                           *
#                                                                    *
#  This file is used to set the parameters of the run.               *
#                                                                    *
#  Some notation/conventions:                                        *
#                                                                    *
#   Lines starting with a hash (#) are info or comments              *
#                                                                    *
#   mind the format:   value    = variable     ! comment             *
#*********************************************************************
#
#******************
# Running parameters
#******************
#
#*********************************************************************
# Tag name for the run (one word)                                    *
#*********************************************************************
  tag_2     = run_tag ! name of the run
```

```
#*********************************************************************
# Number of LHE events (and their normalization) and the required      *
# (relative) accuracy on the Xsec.                                     *
# These values are ignored for fixed order runs                        *
#*********************************************************************
 10000 = nevents ! Number of unweighted events requested
    -1 = req_acc ! Required accuracy (-1=auto determined from nevents)
    -1 = nevt_job! Max number of events per job in event generation.
                 !  (-1= no split).
#*********************************************************************
# Normalize the weights of LHE events such that they sum or average to *
# the total cross section                                              *
#*********************************************************************
 average = event_norm       ! average or sum
#*********************************************************************
# Number of points per itegration channel (ignored for aMC@NLO runs)   *
#*********************************************************************
 0.01    = req_acc_FO       ! Required accuracy (-1=ignored, and use the
                        ! number of points and iter. below)
# These numbers are ignored except if req_acc_FO is equal to -1
 5000    = npoints_FO_grid  ! number of points to setup grids
 4       = niters_FO_grid   ! number of iter. to setup grids
 10000   = npoints_FO       ! number of points to compute Xsec
 6       = niters_FO        ! number of iter. to compute Xsec
#*********************************************************************
# Random number seed                                                   *
#*********************************************************************
     0    = iseed       ! rnd seed (0=assigned automatically=default))
#*********************************************************************
# Collider type and energy                                             *
#*********************************************************************
    1    = lpp1     ! beam 1 type (0 = no PDF)
    1    = lpp2     ! beam 2 type (0 = no PDF)
 3500    = ebeam1   ! beam 1 energy in GeV
 3500    = ebeam2   ! beam 2 energy in GeV
#*********************************************************************
# PDF choice: this automatically fixes also alpha_s(MZ) and its evol.  *
#*********************************************************************
 lhapdf     = pdlabel    ! PDF set
 10550      = lhaid      ! if pdlabel=lhapdf, this is the lhapdf number
#*********************************************************************
# Include the NLO Monte Carlo subtr. terms for the following parton    *
# shower (HERWIG6 | HERWIGPP | PYTHIA6Q | PYTHIA6PT | PYTHIA8)         *
# WARNING: PYTHIA6PT works only for processes without FSR!!!!          *
#*********************************************************************
  HERWIG6    = parton_shower
#*********************************************************************
# Renormalization and factorization scales                             *
# (Default functional form for the non-fixed scales is the sum of      *
# the transverse masses of all final state particles and partons. This *
# can be changed in SubProcesses/set_scales.f)                         *
#*********************************************************************
 .true.    = fixed_ren_scale  ! if .true. use fixed ren scale
 .true.    = fixed_fac_scale  ! if .true. use fixed fac scale
 235       = muR_ref_fixed    ! fixed ren reference scale
 235       = muF1_ref_fixed   ! fixed fact reference scale for pdf1
 235       = muF2_ref_fixed   ! fixed fact reference scale for pdf2
#*********************************************************************
# Renormalization and factorization scales (advanced and NLO options)  *
#*********************************************************************
 .true.    = fixed_QES_scale  ! if .true. use fixed Ellis-Sexton scale
 235       = QES_ref_fixed    ! fixed Ellis-Sexton reference scale
 1         = muR_over_ref     ! ratio of current muR over reference muR
 1         = muF1_over_ref    ! ratio of current muF1 over reference muF1
```

```
 1         = muF2_over_ref    ! ratio of current muF2 over reference muF2
 1         = QES_over_ref     ! ratio of current QES over reference QES
#***********************************************************************
# Reweight flags to get scale dependence and PDF uncertainty           *
# For scale dependence: factor rw_scale_up/down around central scale   *
# For PDF uncertainty: use LHAPDF with supported set                   *
#***********************************************************************
 .true.   = reweight_scale   ! reweight to get scale dependence
  0.5     = rw_Rscale_down   ! lower bound for ren scale variations
  2.0     = rw_Rscale_up     ! upper bound for ren scale variations
  0.5     = rw_Fscale_down   ! lower bound for fact scale variations
  2.0     = rw_Fscale_up     ! upper bound for fact scale variations
 .true.   = reweight_PDF     ! reweight to get PDF uncertainty
 10551    = PDF_set_min      ! First of the error PDF sets
 10594    = PDF_set_max      ! Last of the error PDF sets
#***********************************************************************
# Merging - WARNING! Applies merging only at the hard-event level.     *
# After showering an MLM-type merging should be applied as well.       *
# See http://amcatnlo.cern.ch/FxFx_merging.htm for more details.       *
#***********************************************************************
 0         = ickkw            ! 0 no merging, 3 FxFx merging, 4 UNLOPS
#***********************************************************************
#
#***********************************************************************
# BW cutoff (M+/-bwcutoff*Gamma)                                       *
#***********************************************************************
 15  = bwcutoff
#***********************************************************************
# Cuts on the jets                                                     *
# Jet clustering is performed by FastJet.
# When matching to a parton shower, these generation cuts should be    *
# considerably softer than the analysis cuts.                          *
# (more specific cuts can be specified in SubProcesses/cuts.f)         *
#***********************************************************************
   1  = jetalgo   ! FastJet jet algorithm (1=kT, 0=C/A, -1=anti-kT)
 0.7  = jetradius ! The radius parameter for the jet algorithm
  10  = ptj       ! Min jet transverse momentum
  -1  = etaj      ! Max jet abs(pseudo-rap) (a value .lt.0 means no cut)
#***********************************************************************
# Cuts on the charged leptons (e+, e-, mu+, mu-, tau+ and tau-)        *
# (more specific gen cuts can be specified in SubProcesses/cuts.f)     *
#***********************************************************************
   0  = ptl      ! Min lepton transverse momentum
  -1  = etal     ! Max lepton abs(pseudo-rap) (a value .lt.0 means no cut)
   0  = drll     ! Min distance between opposite sign lepton pairs
   0  = drll_sf  ! Min distance between opp. sign same-flavor lepton pairs
   0  = mll      ! Min inv. mass of all opposite sign lepton pairs
  30  = mll_sf   ! Min inv. mass of all opp. sign same-flavor lepton pairs
#***********************************************************************
# Photon-isolation cuts, according to hep-ph/9801442                   *
# When ptgmin=0, all the other parameters are ignored                  *
#***********************************************************************
  20  = ptgmin     ! Min photon transverse momentum
  -1  = etagamma   ! Max photon abs(pseudo-rap)
 0.4  = R0gamma    ! Radius of isolation code
 1.0  = xn         ! n parameter of eq.(3.4) in hep-ph/9801442
 1.0  = epsgamma   ! epsilon_gamma parameter of eq.(3.4) in hep-ph/9801442
 .true.  = isoEM   ! isolate photons from EM energy (photons and leptons)
#***********************************************************************
# Maximal PDG code for quark to be considered a jet when applying cuts.*
# At least all massless quarks of the model should be included here.   *
#***********************************************************************
 4 = maxjetflavor
#***********************************************************************
```

```
# For aMCfast+APPLGRID use in PDF fitting (http://amcfast.hepforge.org)*
#*********************************************************************
 0 = iappl   ! aMCfast switch (0=OFF, 1=prepare APPLgrids, 2=fill grids)
#*********************************************************************
```

A.4 Parameter card for the 5FS

```
######################################################################
## PARAM_CARD AUTOMATICALY GENERATED BY MG5 FOLLOWING UFO MODEL   ####
######################################################################
##                                                                  ##
##  Width set on Auto will be computed following the information    ##
##        present in the decay.py files of the model.               ##
##        See  arXiv:1402.1178 for more details.                    ##
##                                                                  ##
######################################################################

###################################
## INFORMATION FOR LOOP
###################################
Block loop
    1 9.118800e+01 # MU_R

###################################
## INFORMATION FOR MASS
###################################
Block mass
    6 1.725000e+02 # MT
   15 1.777000e+00 # MTA
   23 9.118800e+01 # MZ
   25 1.250000e+02 # MH
## Dependent parameters, given by model restrictions.
## Those values should be edited following the
## analytical expression. MG5 ignores those values
## but they are important for interfacing the output of MG5
## to external program such as Pythia.
  1 0.000000 # d : 0.0
  2 0.000000 # u : 0.0
  3 0.000000 # s : 0.0
  4 0.000000 # c : 0.0
  5 0.000000 # b : 0.0
  11 0.000000 # e- : 0.0
  12 0.000000 # ve : 0.0
  13 0.000000 # mu- : 0.0
  14 0.000000 # vm : 0.0
  16 0.000000 # vt : 0.0
  21 0.000000 # g : 0.0
  22 0.000000 # a : 0.0
  24 80.419002 # w+ : cmath.sqrt(MZ__exp__2/2. + cmath.sqrt(MZ__exp__4/4. - (
    aEW*cmath.pi*MZ__exp__2)/(Gf*sqrt__2)))

###################################
## INFORMATION FOR SMINPUTS
###################################
Block sminputs
    1 1.325070e+02 # aEWM1
    2 1.166390e-05 # Gf
    3 1.180000e-01 # aS

###################################
## INFORMATION FOR YUKAWA
###################################
Block yukawa
```

```
    6  1.725000e+02 # ymt
   15  1.777000e+00 # ymtau

###################################
## INFORMATION FOR DECAY
###################################
DECAY   6  1.491500e+00 # WT
DECAY  23  2.441404e+00 # WZ
DECAY  24  2.047600e+00 # WW
DECAY  25  6.382339e-03 # WH
## Dependent parameters, given by model restrictions.
## Those values should be edited following the
## analytical expression. MG5 ignores those values
## but they are important for interfacing the output of MG5
## to external program such as Pythia.
DECAY  1  0.000000 # d : 0.0
DECAY  2  0.000000 # u : 0.0
DECAY  3  0.000000 # s : 0.0
DECAY  4  0.000000 # c : 0.0
DECAY  5  0.000000 # b : 0.0
DECAY  11  0.000000 # e- : 0.0
DECAY  12  0.000000 # ve : 0.0
DECAY  13  0.000000 # mu- : 0.0
DECAY  14  0.000000 # vm : 0.0
DECAY  15  0.000000 # ta- : 0.0
DECAY  16  0.000000 # vt : 0.0
DECAY  21  0.000000 # g : 0.0
DECAY  22  0.000000 # a : 0.0
```

A.5 Proc card for the 5FS

```
#************************************************************
#*                    MadGraph5_aMC@NLO                     *
#*                                                          *
#*                *                       *                 *
#*                  *        * *        *                   *
#*                    * * * * 5 * * * *                     *
#*                  *        * *        *                   *
#*                *                       *                 *
#*                                                          *
#*                                                          *
#*         VERSION 2.2.2                 2014-11-06         *
#*                                                          *
#*    The MadGraph5_aMC@NLO Development Team - Find us at   *
#*    https://server06.fynu.ucl.ac.be/projects/madgraph     *
#*                                                          *
#************************************************************
#*                                                          *
#*              Command File for MadGraph5_aMC@NLO          *
#*                                                          *
#*     run as ./bin/mg5_aMC  filename                       *
#*                                                          *
#************************************************************
set group_subprocesses Auto
set ignore_six_quark_processes False
set loop_optimized_output True
set gauge unitary
set complex_mass_scheme False
import model sm
define p = g u c d s u~ c~ d~ s~
define j = g u c d s u~ c~ d~ s~
define l+ = e+ mu+
define l- = e- mu-
```

```
define vl = ve vm vt
define vl~ = ve~ vm~ vt~
import model loop_sm-no_b_mass
define p = p b b~
define j = j b b~
generate p p > t t~ h [QCD]
output crosssection_ttH_5F
```

A.6 Run card for the 5FS

```
#***********************************************************************
#                        MadGraph5_aMC@NLO                             *
#                                                                      *
#                     run_card.dat aMC@NLO                             *
#                                                                      *
#  This file is used to set the parameters of the run.                 *
#                                                                      *
#  Some notation/conventions:                                          *
#                                                                      *
#   Lines starting with a hash (#) are info or comments                *
#                                                                      *
#   mind the format:   value    = variable     ! comment               *
#***********************************************************************
#
#*******************
# Running parameters
#*******************
#
#***********************************************************************
# Tag name for the run (one word)                                      *
#***********************************************************************
  tag_2     = run_tag ! name of the run
#***********************************************************************
# Number of LHE events (and their normalization) and the required      *
# (relative) accuracy on the Xsec.                                     *
# These values are ignored for fixed order runs                        *
#***********************************************************************
 10000 = nevents ! Number of unweighted events requested
    -1 = req_acc ! Required accuracy (-1=auto determined from nevents)
    -1 = nevt_job! Max number of events per job in event generation.
                 !  (-1= no split).
#***********************************************************************
# Normalize the weights of LHE events such that they sum or average to *
# the total cross section                                              *
#***********************************************************************
 average = event_norm      ! average or sum
#***********************************************************************
# Number of points per itegration channel (ignored for aMC@NLO runs)   *
#***********************************************************************
 0.01   = req_acc_FO       ! Required accuracy (-1=ignored, and use the
                           ! number of points and iter. below)
# These numbers are ignored except if req_acc_FO is equal to -1
 5000   = npoints_FO_grid  ! number of points to setup grids
 4      = niters_FO_grid   ! number of iter. to setup grids
 10000  = npoints_FO       ! number of points to compute Xsec
 6      = niters_FO        ! number of iter. to compute Xsec
#***********************************************************************
# Random number seed                                                   *
#***********************************************************************
     0    = iseed       ! rnd seed (0=assigned automatically=default))
#***********************************************************************
# Collider type and energy                                             *
#***********************************************************************
```

```
    1   = lpp1     ! beam 1 type (0 = no PDF)
    1   = lpp2     ! beam 2 type (0 = no PDF)
 3500   = ebeam1   ! beam 1 energy in GeV
 3500   = ebeam2   ! beam 2 energy in GeV
#***********************************************************************
# PDF choice: this automatically fixes also alpha_s(MZ) and its evol.  *
#***********************************************************************
 lhapdf    = pdlabel    ! PDF set
 10550     = lhaid      ! if pdlabel=lhapdf, this is the lhapdf number
#***********************************************************************
# Include the NLO Monte Carlo subtr. terms for the following parton    *
# shower (HERWIG6 | HERWIGPP | PYTHIA6Q | PYTHIA6PT | PYTHIA8)         *
# WARNING: PYTHIA6PT works only for processes without FSR!!!!          *
#***********************************************************************
  HERWIG6   = parton_shower
#***********************************************************************
# Renormalization and factorization scales                             *
# (Default functional form for the non-fixed scales is the sum of      *
# the transverse masses of all final state particles and partons. This *
# can be changed in SubProcesses/set_scales.f)                         *
#***********************************************************************
 .true.    = fixed_ren_scale   ! if .true. use fixed ren scale
 .true.    = fixed_fac_scale   ! if .true. use fixed fac scale
 235       = muR_ref_fixed     ! fixed ren reference scale
 235       = muF1_ref_fixed    ! fixed fact reference scale for pdf1
 235       = muF2_ref_fixed    ! fixed fact reference scale for pdf2
#***********************************************************************
# Renormalization and factorization scales (advanced and NLO options)  *
#***********************************************************************
 .true.    = fixed_QES_scale   ! if .true. use fixed Ellis-Sexton scale
 235       = QES_ref_fixed     ! fixed Ellis-Sexton reference scale
 1         = muR_over_ref      ! ratio of current muR over reference muR
 1         = muF1_over_ref     ! ratio of current muF1 over reference muF1
 1         = muF2_over_ref     ! ratio of current muF2 over reference muF2
 1         = QES_over_ref      ! ratio of current QES over reference QES
#***********************************************************************
# Reweight flags to get scale dependence and PDF uncertainty           *
# For scale dependence: factor rw_scale_up/down around central scale   *
# For PDF uncertainty: use LHAPDF with supported set                   *
#***********************************************************************
 .true.    = reweight_scale    ! reweight to get scale dependence
  0.5      = rw_Rscale_down    ! lower bound for ren scale variations
  2.0      = rw_Rscale_up      ! upper bound for ren scale variations
  0.5      = rw_Fscale_down    ! lower bound for fact scale variations
  2.0      = rw_Fscale_up      ! upper bound for fact scale variations
 .true.    = reweight_PDF      ! reweight to get PDF uncertainty
 10551     = PDF_set_min       ! First of the error PDF sets
 10594     = PDF_set_max       ! Last of the error PDF sets
#***********************************************************************
# Merging - WARNING! Applies merging only at the hard-event level.     *
# After showering an MLM-type merging should be applied as well.       *
# See http://amcatnlo.cern.ch/FxFx_merging.htm for more details.       *
#***********************************************************************
 0         = ickkw             ! 0 no merging, 3 FxFx merging, 4 UNLOPS
#***********************************************************************
#
#***********************************************************************
# BW cutoff (M+/-bwcutoff*Gamma)                                       *
#***********************************************************************
 15  = bwcutoff
#***********************************************************************
# Cuts on the jets                                                     *
# Jet clustering is performed by FastJet.
# When matching to a parton shower, these generation cuts should be    *
```

```
# considerably softer than the analysis cuts.                        *
# (more specific cuts can be specified in SubProcesses/cuts.f)        *
#***********************************************************************
   1  = jetalgo   ! FastJet jet algorithm (1=kT, 0=C/A, -1=anti-kT)
 0.7  = jetradius ! The radius parameter for the jet algorithm
  10  = ptj       ! Min jet transverse momentum
  -1  = etaj      ! Max jet abs(pseudo-rap) (a value .lt.0 means no cut)
#***********************************************************************
# Cuts on the charged leptons (e+, e-, mu+, mu-, tau+ and tau-)       *
# (more specific gen cuts can be specified in SubProcesses/cuts.f)    *
#***********************************************************************
   0  = ptl      ! Min lepton transverse momentum
  -1  = etal     ! Max lepton abs(pseudo-rap) (a value .lt.0 means no cut)
   0  = drll     ! Min distance between opposite sign lepton pairs
   0  = drll_sf  ! Min distance between opp. sign same-flavor lepton pairs
   0  = mll      ! Min inv. mass of all opposite sign lepton pairs
  30  = mll_sf   ! Min inv. mass of all opp. sign same-flavor lepton pairs
#***********************************************************************
# Photon-isolation cuts, according to hep-ph/9801442                  *
# When ptgmin=0, all the other parameters are ignored                 *
#***********************************************************************
  20  = ptgmin    ! Min photon transverse momentum
  -1  = etagamma  ! Max photon abs(pseudo-rap)
 0.4  = R0gamma   ! Radius of isolation code
 1.0  = xn        ! n parameter of eq.(3.4) in hep-ph/9801442
 1.0  = epsgamma  ! epsilon_gamma parameter of eq.(3.4) in hep-ph/9801442
 .true.  = isoEM  ! isolate photons from EM energy (photons and leptons)
#***********************************************************************
# Maximal PDG code for quark to be considered a jet when applying cuts.*
# At least all massless quarks of the model should be included here.  *
#***********************************************************************
 5 = maxjetflavor
#***********************************************************************
# For aMCfast+APPLGRID use in PDF fitting (http://amcfast.hepforge.org)*
#***********************************************************************
 0 = iappl    ! aMCfast switch (0=OFF, 1=prepare APPLgrids, 2=fill grids)
#***********************************************************************
```

B Comparison between event samples and measurement

In the subsequent subsections more technical details about the production of the event samples used in chapter 8 are given. Furthermore, the Rivet analysis applied to compare the event samples with the measurement data is shown.

B.1 Sample $t\bar{t}$+0/1/2jets NLO

In the following subsections are the parameter card, the proc card, the run card, and the madspin card are shown which were used to generate the parton-level events with the aMC@NLO matrix element event generator. Additionally, the code fragment used in CMSSW for the Pythia8 event generator is shown.

B.1.1 Parameter card of the $t\bar{t}$+0/1/2jets NLO sample

```
######################################################################
## PARAM_CARD AUTOMATICALY GENERATED BY MG5 FOLLOWING UFO MODEL   ####
######################################################################
##                                                                  ##
##  Width set on Auto will be computed following the information   ##
##         present in the decay.py files of the model.              ##
##         See  arXiv:1402.1178 for more details.                   ##
```

```
##                                                                            ##
################################################################################

######################################
## INFORMATION FOR LOOP
######################################
Block loop
    1 9.118800e+01 # MU_R

######################################
## INFORMATION FOR MASS
######################################
Block mass
    6 1.730000e+02 # MT
   15 1.777000e+00 # MTA
   23 9.118800e+01 # MZ
   25 1.250000e+02 # MH
## Dependent parameters, given by model restrictions.
## Those values should be edited following the
## analytical expression. MG5 ignores those values
## but they are important for interfacing the output of MG5
## to external program such as Pythia.
  1 0.000000 # d : 0.0
  2 0.000000 # u : 0.0
  3 0.000000 # s : 0.0
  4 0.000000 # c : 0.0
  5 0.000000 # b : 0.0
  11 0.000000 # e- : 0.0
  12 0.000000 # ve : 0.0
  13 0.000000 # mu- : 0.0
  14 0.000000 # vm : 0.0
  16 0.000000 # vt : 0.0
  21 0.000000 # g : 0.0
  22 0.000000 # a : 0.0
  24 80.419002 # w+ : cmath.sqrt(MZ__exp__2/2. + cmath.sqrt(MZ__exp__4/4. - (aEW*cmath.pi*MZ__exp__2)/(Gf*sqrt__2)))

######################################
## INFORMATION FOR SMINPUTS
######################################
Block sminputs
    1 1.325070e+02 # aEWM1
    2 1.166390e-05 # Gf
    3 1.180000e-01 # aS

######################################
## INFORMATION FOR WOLFENSTEIN
######################################
Block wolfenstein
    1 2.253000e-01 # lamWS
    2 8.080000e-01 # AWS
    3 1.320000e-01 # rhoWS
    4 3.410000e-01 # etaWS

######################################
## INFORMATION FOR YUKAWA
######################################
Block yukawa
    6 1.730000e+02 # ymt
   15 1.777000e+00 # ymtau

######################################
## INFORMATION FOR DECAY
######################################
```

```
DECAY   6 1.491500e+00 # WT
DECAY  23 2.441404e+00 # WZ
DECAY  24 2.047600e+00 # WW
DECAY  25 6.382339e-03 # WH
## Dependent parameters, given by model restrictions.
## Those values should be edited following the
## analytical expression. MG5 ignores those values
## but they are important for interfacing the output of MG5
## to external program such as Pythia.
DECAY  1 0.000000 # d : 0.0
DECAY  2 0.000000 # u : 0.0
DECAY  3 0.000000 # s : 0.0
DECAY  4 0.000000 # c : 0.0
DECAY  5 0.000000 # b : 0.0
DECAY  11 0.000000 # e- : 0.0
DECAY  12 0.000000 # ve : 0.0
DECAY  13 0.000000 # mu- : 0.0
DECAY  14 0.000000 # vm : 0.0
DECAY  15 0.000000 # ta- : 0.0
DECAY  16 0.000000 # vt : 0.0
DECAY  21 0.000000 # g : 0.0
DECAY  22 0.000000 # a : 0.0
```

B.1.2 Proc card of the $t\bar{t}$+0/1/2jets NLO sample

```
#************************************************************
#*                    MadGraph5_aMC@NLO                     *
#*                                                          *
#*               *                        *                 *
#*                 *        * *        *                    *
#*                   * * * * 5 * * * *                      *
#*                 *        * *        *                    *
#*               *                        *                 *
#*                                                          *
#*                                                          *
#*          VERSION 2.2.1                2014-09-25         *
#*                                                          *
#*    The MadGraph5_aMC@NLO Development Team - Find us at   *
#*    https://server06.fynu.ucl.ac.be/projects/madgraph     *
#*                                                          *
#************************************************************
#*                                                          *
#*              Command File for MadGraph5_aMC@NLO          *
#*                                                          *
#*     run as ./bin/mg5_aMC  filename                       *
#*                                                          *
#************************************************************
set group_subprocesses Auto
set ignore_six_quark_processes False
set loop_optimized_output True
set complex_mass_scheme False
import model loop_sm-ckm_no_b_mass
define p = g u c d s u~ c~ d~ s~
define j = g u c d s u~ c~ d~ s~
define l+ = e+ mu+
define l- = e- mu-
define vl = ve vm vt
define vl~ = ve~ vm~ vt~
define p = p b b~
define j = j b b~
generate p p > t t~ [QCD] @0
add process p p > t t~ j [QCD] @1
add process p p > t t~ j j [QCD] @2
```

```
output tt012j_5f_ckm_NLO_FXFX
```

B.1.3 Run card of the $t\bar{t}$+0/1/2jets NLO sample

```
#*********************************************************************
#                        MadGraph5_aMC@NLO                           *
#                                                                    *
#                      run_card.dat aMC@NLO                          *
#                                                                    *
#  This file is used to set the parameters of the run.               *
#                                                                    *
#  Some notation/conventions:                                        *
#                                                                    *
#   Lines starting with a hash (#) are info or comments              *
#                                                                    *
#   mind the format:   value    = variable     ! comment             *
#*********************************************************************
#
#*******************
# Running parameters
#*******************
#
#*********************************************************************
# Tag name for the run (one word)                                    *
#*********************************************************************
  tag_1     = run_tag ! name of the run
#*********************************************************************
# Number of events (and their normalization) and the required        *
# (relative) accuracy on the Xsec.                                   *
# These values are ignored for fixed order runs                      *
#*********************************************************************
  1500 = nevents ! Number of unweighted events requested
 0.001 = req_acc ! Required accuracy (-1=auto determined from nevents)
   10 = nevt_job! Max number of events per job in event generation.
                 !  (-1= no split).
average = event_norm ! Normalize events to sum or average to the X sect.
#*********************************************************************
# Number of points per itegration channel (ignored for aMC@NLO runs) *
#*********************************************************************
 0.01    = req_acc_FO       ! Required accuracy (-1=ignored, and use the
                            ! number of points and iter. below)
# These numbers are ignored except if req_acc_FO is equal to -1
 5000    = npoints_FO_grid  ! number of points to setup grids
 4       = niters_FO_grid   ! number of iter. to setup grids
 10000   = npoints_FO       ! number of points to compute Xsec
 6       = niters_FO        ! number of iter. to compute Xsec
#*********************************************************************
# Random number seed                                                 *
#*********************************************************************
     0    = iseed       ! rnd seed (0=assigned automatically=default))
#*********************************************************************
# Collider type and energy                                           *
#*********************************************************************
    1    = lpp1     ! beam 1 type (0 = no PDF)
    1    = lpp2     ! beam 2 type (0 = no PDF)
 4000    = ebeam1   ! beam 1 energy in GeV
 4000    = ebeam2   ! beam 2 energy in GeV
#*********************************************************************
# PDF choice: this automatically fixes also alpha_s(MZ) and its evol. *
#*********************************************************************
 lhapdf    = pdlabel    ! PDF set
 260000    = lhaid      ! if pdlabel=lhapdf, this is the lhapdf number
#*********************************************************************
```

```
# Include the NLO Monte Carlo subtr. terms for the following parton    *
# shower (HERWIG6 | HERWIGPP | PYTHIA6Q | PYTHIA6PT | PYTHIA8)          *
# WARNING: PYTHIA6PT works only for processes without FSR!!!!           *
#***********************************************************************
  PYTHIA8   = parton_shower
#***********************************************************************
# Renormalization and factorization scales                              *
# (Default functional form for the non-fixed scales is the sum of       *
# the transverse masses of all final state particles and partons. This *
# can be changed in SubProcesses/set_scales.f)                          *
#***********************************************************************
 F          = fixed_ren_scale  ! if .true. use fixed ren scale
 F          = fixed_fac_scale  ! if .true. use fixed fac scale
 91.188     = muR_ref_fixed    ! fixed ren reference scale
 91.188     = muF1_ref_fixed   ! fixed fact reference scale for pdf1
 91.188     = muF2_ref_fixed   ! fixed fact reference scale for pdf2
#***********************************************************************
# Renormalization and factorization scales (advanced and NLO options)  *
#***********************************************************************
 F          = fixed_QES_scale  ! if .true. use fixed Ellis-Sexton scale
 91.188     = QES_ref_fixed    ! fixed Ellis-Sexton reference scale
 1          = muR_over_ref     ! ratio of current muR over reference muR
 1          = muF1_over_ref    ! ratio of current muF1 over reference muF1
 1          = muF2_over_ref    ! ratio of current muF2 over reference muF2
 1          = QES_over_ref     ! ratio of current QES over reference QES
#***********************************************************************
# Reweight flags to get scale dependence and PDF uncertainty            *
# For scale dependence: factor rw_scale_up/down around central scale    *
# For PDF uncertainty: use LHAPDF with supported set                    *
#***********************************************************************
 .true.     = reweight_scale   ! reweight to get scale dependence
  0.5       = rw_Rscale_down   ! lower bound for ren scale variations
  2.0       = rw_Rscale_up     ! upper bound for ren scale variations
  0.5       = rw_Fscale_down   ! lower bound for fact scale variations
  2.0       = rw_Fscale_up     ! upper bound for fact scale variations
 .true.  = reweight_PDF        ! reweight to get PDF uncertainty
 260001     = PDF_set_min      ! First of the error PDF sets
 260100     = PDF_set_max      ! Last of the error PDF sets
#***********************************************************************
# Merging - WARNING! Applies merging only at the hard-event level.      *
# After showering an MLM-type merging should be applied as well.        *
# See http://amcatnlo.cern.ch/FxFx_merging.htm for more details.        *
#***********************************************************************
 3          = ickkw            ! 0 no merging, 3 FxFx merging
#***********************************************************************
#
#***********************************************************************
# BW cutoff (M+/-bwcutoff*Gamma)                                        *
#***********************************************************************
 15  = bwcutoff
#***********************************************************************
# Cuts on the jets                                                      *
# Jet clustering is performed by FastJet.
# When matching to a parton shower, these generation cuts should be     *
# considerably softer than the analysis cuts.                           *
# (more specific cuts can be specified in SubProcesses/cuts.f)          *
#***********************************************************************
   1  = jetalgo    ! FastJet jet algorithm (1=kT, 0=C/A, -1=anti-kT)
 1.0  = jetradius  ! The radius parameter for the jet algorithm
  10  = ptj        ! Min jet transverse momentum
  -1  = etaj       ! Max jet abs(pseudo-rap) (a value .lt.0 means no cut)
#***********************************************************************
# Cuts on the charged leptons (e+, e-, mu+, mu-, tau+ and tau-)         *
# (more specific gen cuts can be specified in SubProcesses/cuts.f)      *
```

```
#*********************************************************************
  0  = ptl      ! Min lepton transverse momentum
 -1  = etal     ! Max lepton abs(pseudo-rap) (a value .lt.0 means no cut)
  0  = drll     ! Min distance between opposite sign lepton pairs
  0  = drll_sf  ! Min distance between opp. sign same-flavor lepton pairs
  0  = mll      ! Min inv. mass of all opposite sign lepton pairs
 30  = mll_sf   ! Min inv. mass of all opp. sign same-flavor lepton pairs
#*********************************************************************
# Photon-isolation cuts, according to hep-ph/9801442               *
# When ptgmin=0, all the other parameters are ignored               *
#*********************************************************************
  20  = ptgmin    ! Min photon transverse momentum
  -1  = etagamma  ! Max photon abs(pseudo-rap)
 0.4  = R0gamma   ! Radius of isolation code
 1.0  = xn        ! n parameter of eq.(3.4) in hep-ph/9801442
 1.0  = epsgamma  ! epsilon_gamma parameter of eq.(3.4) in hep-ph/9801442
 .true.  = isoEM  ! isolate photons from EM energy (photons and leptons)
#*********************************************************************
# Maximal PDG code for quark to be considered a jet when applying cuts.*
# At least all massless quarks of the model should be included here.   *
#*********************************************************************
 5 = maxjetflavor
#*********************************************************************
```

B.1.4 MadSpin card of the $t\bar{t}$+0/1/2jets NLO sample

```
#************************************************************
#*                          MadSpin                         *
#*                                                          *
#*    P. Artoisenet, R. Frederix, R. Rietkerk, O. Mattelaer *
#*                                                          *
#*    Part of the MadGraph5_aMC@NLO Framework:              *
#*    The MadGraph5_aMC@NLO Development Team - Find us at   *
#*    https://server06.fynu.ucl.ac.be/projects/madgraph     *
#*                                                          *
#************************************************************
#Some options (uncomment to apply)
#
#directory for gridpack mode
set ms_dir ./madspingrid

#initialization parameters
 set Nevents_for_max_weigth 250 # number of events for the estimate of the
    max. weight
# set BW_cut 15                # cut on how far the particle can be off-shell
 set max_weight_ps_point 400  # number of PS to estimate the maximum for each
     event
#
#to properly limit the number of concurrent processes for grid running
set max_running_process 1
#
# specify the decay for the final state particles
 decay t > w+ b, w+ > all all
 decay t~ > w- b~, w- > all all
 decay w+ > all all
 decay w- > all all

#define ell+ = e+ mu+ ta+
#define ell- = e- mu- ta-

# specify the decay for the final state particles
#decay w+ > ell+ vl
#decay w- > ell- vl~
```

```
# running the actual code
launch
```

B.1.5 Code fragment used in CMSSW for the Pythia8 event generator of the $t\bar{t}$+0/1/2jets NLO sample

```
generator = cms.EDFilter("Pythia8HadronizerFilter",
    maxEventsToPrint = cms.untracked.int32(1),
    pythiaPylistVerbosity = cms.untracked.int32(1),
    filterEfficiency = cms.untracked.double(1.0),
    pythiaHepMCVerbosity = cms.untracked.bool(False),
    comEnergy = cms.double(8000.),
    PythiaParameters = cms.PSet(
        pythia8CommonSettingsBlock,
        pythia8CUEP8M1SettingsBlock,
        pythia8aMCatNLOSettingsBlock,
        processParameters = cms.vstring(
            'JetMatching:setMad = off',
            'JetMatching:scheme = 1',
            'JetMatching:merge = on',
            'JetMatching:jetAlgorithm = 2',
            'JetMatching:etaJetMax = 999.',
            'JetMatching:coneRadius = 1.',
            'JetMatching:slowJetPower = 1',
            'JetMatching:qCut = 30.', #this is the actual merging scale
            'JetMatching:doFxFx = on',
            'JetMatching:qCutME = 10.',#this must match the ptj cut in the
    lhe generation step
            'JetMatching:nQmatch = 5', #4 corresponds to 4-flavour scheme (no
     matching of b-quarks), 5 for 5-flavour scheme
            'TimeShower:nPartonsInBorn = 4', #number of coloured particles (
    before resonance decays) in highest multiplicity born matrix element
            'JetMatching:nJetMax = 2', #number of partons in born matrix
    element for highest multiplicity
        ),
        parameterSets = cms.vstring('pythia8CommonSettings',
                                    'pythia8CUEP8M1Settings',
                                    'pythia8aMCatNLOSettings',
                                    'processParameters',
                                    )
    )
)
```

B.2 Samples $t\bar{t}$+0(NLO)/1/2/3jets and $t\bar{t}$+0(NLO)/1(NLO)/2/3jets

In the following subsections the input files used for the generation of the $t\bar{t}$+0(NLO)/1/2/3jets Sherpa and $t\bar{t}$+0(NLO)/1(NLO)/2/3jets Sherpa event samples by making use of the Sherpa GPMC event generator are shown.

B.2.1 Input file of the $t\bar{t}$+0(NLO)/1/2/3jets sample

```
(run){
  % general setting
  EVENTS 1M; ERROR 0.99;
  EVENT_OUTPUT=HepMC_GenEvt[ttbar01NLO23LO]

  % scales, tags for scale variations
  FSF:=1.; RSF:=1.; QSF:=1.;
  SCALES METS{FSF*MU_F2}{RSF*MU_R2}{QSF*MU_Q2};
  CORE_SCALE QCD;
  METS_BBAR_MODE 5;
```

```

  % tags for process setup
  NJET:=3; LJET:=2; QCUT:=30.;

  % me generator settings
  ME_SIGNAL_GENERATOR Comix Amegic LOOPGEN;
  EVENT_GENERATION_MODE Weighted;
  LOOPGEN:=OpenLoops;

  % collider setup
  BEAM_1 2212; BEAM_ENERGY_1 = 4000.;
  BEAM_2 2212; BEAM_ENERGY_2 = 4000.;

  % decays
  HARD_DECAYS On;
  STABLE[24] 0; STABLE[6] 0; WIDTH[6] 0;

  NLO_SMEAR_THRESHOLD 1;
  NLO_SMEAR_POWER 2;
}(run)

(processes){
  Process : 93 93 -> 6 -6 93{NJET};
  Order_EW 0; CKKW sqr(QCUT/E_CMS);
  NLO_QCD_Mode MC@NLO {LJET};
  ME_Generator Amegic {LJET};
  RS_ME_Generator Comix {LJET};
  Loop_Generator LOOPGEN {LJET};
  Max_N_Quarks 6 {5,6,7,8};
  Integration_Error 0.05 {5,6,7,8};
  Scales LOOSE_METS{FSF*MU_F2}{RSF*MU_R2}{QSF*MU_Q2} {5,6,7,8};
  End process
}(processes)

(isr){
  PDF_LIBRARY     = LHAPDFSherpa
  PDF_SET         = cteq6l1
}(isr)
```

B.2.2 Input file of the $t\bar{t}$+0(NLO)/1(NLO)/2/3jets sample

```
(run){
  % general setting
  EVENTS 1M; ERROR 0.99;
  EVENT_OUTPUT=HepMC_GenEvt[ttbar01NLO23LO]

  % scales, tags for scale variations
  FSF:=1.; RSF:=1.; QSF:=1.;
  SCALES METS{FSF*MU_F2}{RSF*MU_R2}{QSF*MU_Q2};
  CORE_SCALE QCD;
  METS_BBAR_MODE 5;

  % tags for process setup
  NJET:=3; LJET:=2,3; QCUT:=30.;

  % me generator settings
  ME_SIGNAL_GENERATOR Comix Amegic LOOPGEN;
  EVENT_GENERATION_MODE Weighted;
  LOOPGEN:=OpenLoops;

  % collider setup
  BEAM_1 2212; BEAM_ENERGY_1 = 4000.;
  BEAM_2 2212; BEAM_ENERGY_2 = 4000.;
```

```

  % decays
  HARD_DECAYS On;
  STABLE[24] 0; STABLE[6] 0; WIDTH[6] 0;

  NLO_SMEAR_THRESHOLD 1;
  NLO_SMEAR_POWER 2;
}(run)

(processes){
  Process : 93 93 -> 6 -6 93{NJET};
  Order_EW 0; CKKW sqr(QCUT/E_CMS);
  NLO_QCD_Mode MC@NLO {LJET};
  ME_Generator Amegic {LJET};
  RS_ME_Generator Comix {LJET};
  Loop_Generator LOOPGEN {LJET};
  Max_N_Quarks 6 {5,6,7,8};
  Integration_Error 0.05 {5,6,7,8};
  Scales LOOSE_METS{FSF*MU_F2}{RSF*MU_R2}{QSF*MU_Q2} {5,6,7,8};
  End process
}(processes)

(isr){
  PDF_LIBRARY     = LHAPDFSherpa
  PDF_SET         = cteq6l1
}(isr)
```

B.3 Rivet analysis

The successive Rivet analysis was used to compare the event samples with the measurement data.

```
// -*- C++ -*-
// Author: F. Schaaf
// Created: 2014-09-02
// Modified by A. Descroix: 20Nov2014

#include "Rivet/Analysis.hh"
#include "Rivet/Rivet.hh"
//#include "Rivet/Projections/FinalState.hh"
#include "Rivet/Projections/FastJets.hh"
#include "Rivet/Projections/IdentifiedFinalState.hh"
#include "Rivet/Tools/ParticleIdUtils.hh"
//#include "Rivet/ParticleName.hh"

#include "HepMC/GenEvent.h"

namespace Rivet {


////////////
// Config //
////////////

// Lepton Cuts
const double MIN_PT_GOOD_ELECTRON = 30*GeV;
const double MIN_PT_GOOD_MUON = 30*GeV;
const double MIN_PT_LOOSE_ELECTRON = 15*GeV;
const double MIN_PT_LOOSE_MUON = 15*GeV;

const double MAX_ETA_GOOD_ELECTRON = 2.4;
const double MAX_ETA_GOOD_MUON = 2.4;
const double MAX_ETA_LOOSE_ELECTRON = 2.5;
```

```
const double MAX_ETA_LOOSE_MUON = 2.5;

// Jet Cuts
const double JET_MIN_PT = 30 * GeV;
const double JET_MAX_ETA = 2.5;
const double JET_MIN_DELTA_R = 0.4;


class CMS_2014_ttbarPlusXJets : public Analysis
{
public:

  CMS_2014_ttbarPlusXJets() : Analysis( "CMS_2014_ttbarPlusXJets" ),
    _nameLength(18), _nJets(20), _nJets_err(20), _nJetsE(20), _nJetsE_err(20)
    , _nJetsMu(20), _nJetsMu_err(20)
  {
  }

private:

  enum Cuts
  {
    TotalEvents=0,
    GoodLepton,
    GoodLepton_Electron,
    GoodLepton_Muon,
    LooseLeptonVeto,
    LooseLeptonVeto_Electron,
    LooseLeptonVeto_Muon,
    NJetsGE4,
    NJetsGE4_Electron,
    NJetsGE4_Muon,
    NBJetsGE2,
    NBJetsGE2_Electron,
    NBJetsGE2_Muon,
    Size
  };

  char** _cutNames;

  size_t* _cuts;

private:

  const size_t _nameLength;

  void init_Names()
  {
    _nonOneWeights=false;
    _cuts = new size_t[Size];

        _cutNames = new char* [Size];

    for (size_t i = 0; i<Size; i++)
    {
            _cutNames[i] = new char[_nameLength];
    }
    sprintf(_cutNames[0], "TotalEvents        ");
    sprintf(_cutNames[1], "GoodLepton         ");
    sprintf(_cutNames[2], "GoodLepton|e       ");
    sprintf(_cutNames[3], "GoodLepton|mu      ");
    sprintf(_cutNames[4], "LooseLeptonVeto    ");
    sprintf(_cutNames[5], "LooseLeptonVeto|e  ");
    sprintf(_cutNames[6], "LooseLeptonVeto|mu");
```

```
    sprintf(_cutNames[7], "nJets>=4          ");
    sprintf(_cutNames[8], "nJets>=4|e        ");
    sprintf(_cutNames[9], "nJets>=4|mu       ");
    sprintf(_cutNames[10],"nBJets>=2         ");
    sprintf(_cutNames[11],"nBJets>=2|e       ");
    sprintf(_cutNames[12],"nBJets>=2|mu      ");
  }

  void init_Projections()
  {
    IdentifiedFinalState ifsLeptons;
    ifsLeptons.acceptIdPair( ELECTRON );
    ifsLeptons.acceptIdPair( MUON );
    ifsLeptons.acceptIdPair( NU_E );
    ifsLeptons.acceptIdPair( NU_MU );
    addProjection( ifsLeptons, "Leptons" );
    const FinalState finalState;
    addProjection( FastJets( finalState, FastJets::ANTIKT, 0.5 ), "Jets" );
  }

  void init_Output()
  {
    for (size_t i = 0; i<Size; i++)
    {
            _cuts[i] = 0;
    }
  }

public:

  void init()
  {
    init_Names();
    init_Projections();
    init_Output();
  }

private:

  std::vector<double> _nJets;
  std::vector<double> _nJets_err;
  std::vector<double> _nJetsE;
  std::vector<double> _nJetsE_err;
  std::vector<double> _nJetsMu;
  std::vector<double> _nJetsMu_err;

  bool _nonOneWeights;

  bool isLepton( Particle const& p )
  {
    int const& absid = abs( p.pdgId() );
    return absid == ELECTRON || absid == MUON || absid == NU_E || absid ==
   NU_MU;
  }

  enum ParticleTypeMatch
  {
    EXACT,
    ALLOW_SYMMETRIC_PARTNER
  };

  bool isParticleType( Particle const& p, int type, const ParticleTypeMatch
    particleTypeMatch = ALLOW_SYMMETRIC_PARTNER )
  {
```

```
    int pid = p.pdgId();
    if( particleTypeMatch == ALLOW_SYMMETRIC_PARTNER )
    {
      pid = abs( pid );
      type = abs( type );
    }
    return pid == type;
  }

  bool isE;
  bool isMu;

  bool analyze_Lepton( const Event& event, const IdentifiedFinalState& leptons, Particle& chosenLepton )
  {
    vector<Particle> goodElectrons;
    vector<Particle> goodMuons;
    vector<Particle> looseElectrons;
    vector<Particle> looseMuons;
    foreach( const Particle& p, leptons.particlesByPt() )
    {
      double pT = p.momentum().pT();
      double absEta = abs( p.momentum().eta() );
      if( isParticleType( p, ELECTRON ) && pT > MIN_PT_GOOD_ELECTRON && absEta < MAX_ETA_GOOD_ELECTRON )
      {
        goodElectrons.push_back( p );
      }
      else if( isParticleType( p, MUON ) && pT > MIN_PT_GOOD_MUON && absEta < MAX_ETA_GOOD_MUON )
      {
        goodMuons.push_back( p );
      }
      if( isParticleType( p, ELECTRON ) && pT > MIN_PT_LOOSE_ELECTRON && absEta < MAX_ETA_LOOSE_ELECTRON )
      {
        looseElectrons.push_back( p );
      }
      else if( isParticleType( p, MUON ) && pT > MIN_PT_LOOSE_MUON && absEta < MAX_ETA_LOOSE_MUON )
      {
        looseMuons.push_back( p );
      }
    }

    // Good Lepton Cut
    bool goodElectron = goodElectrons.size()==1 && goodMuons.size() == 0;
    bool goodMuon = goodMuons.size()==1 && goodElectrons.size() == 0;
    bool goodLepton = goodElectron | goodMuon;
    if (goodLepton)
    {
      _cuts[GoodLepton]++;
    }

    if (goodElectron)
    {
      _cuts[GoodLepton_Electron]++;
    }

    if (goodMuon)
    {
      _cuts[GoodLepton_Muon]++;
    }

```

```
    // loose Lepton Veto
    isE = goodElectrons.size() == 1 && looseElectrons.size() == 1 && looseMuons.size() == 0;
    isMu = goodMuons.size() == 1 && looseElectrons.size() == 0 && looseMuons.size() == 1;
    bool isSelected = isE ^ isMu;

    if (!isSelected)
    {
      return false;
    }

    if( isE )
    {
      _cuts[LooseLeptonVeto_Electron]++;
      chosenLepton = goodElectrons[0];
    }
    if( isMu )
    {
      _cuts[LooseLeptonVeto_Muon]++;
      chosenLepton = goodMuons[0];
    }
    return true;
  }

  bool analyze_CountJets( const Event& event, const Particle chosenLepton )
  {
    vector<FourMomentum> jets;
    int nBJets( 0 );
    int nJetsWrongEta( 0 );
    int nJetsTooCloseToGoodLepton(0);
    foreach( const Jet& j, applyProjection<FastJets>( event, "Jets" ).jetsByPt( JET_MIN_PT ) )
    {
      const double absEta = abs( j.momentum().eta() );
      if( absEta > JET_MAX_ETA )
      {
    nJetsWrongEta++;
    continue;
      }
      if ( deltaR( chosenLepton.momentum(), j.momentum() ) < JET_MIN_DELTA_R )
      {
    nJetsTooCloseToGoodLepton++;
    continue;
      }

      jets.push_back( j.momentum() );
      if( j.containsBottom() )
      {
    nBJets++;
      }
    }

    int nJets = jets.size();

    if (nJets < 4)
    {
      return false;
    }

    _cuts[NJetsGE4]++;
    if (isE) _cuts[NJetsGE4_Electron] ++;
    if (isMu) _cuts[NJetsGE4_Muon] ++;
```

```

    if (nBJets < 2)
    {
      return false;
    }

    double wgt=event.weight();
    double sqWgt=wgt*wgt;

    _nJets[min(10,nJets)] += wgt;
    _nJets_err[min(10,nJets)] += sqWgt;

    if (isE) _nJetsE[min(10,nJets)] += wgt;
    if (isE) _nJetsE_err[min(10,nJets)] += sqWgt;

    if (isMu) _nJetsMu[min(10,nJets)] += wgt;
    if (isMu) _nJetsMu_err[min(10,nJets)] += sqWgt;

    return true;
  }

public:

  void analyze( const Event& event )
  {
    if((!_nonOneWeights) && (event.weight()!=1)) _nonOneWeights=true;

    _cuts[TotalEvents]++;
    const IdentifiedFinalState leptons = applyProjection<IdentifiedFinalState
   >( event, "Leptons" );
    Particle chosenLepton;
    if( !analyze_Lepton( event, leptons, chosenLepton ) )
    {
      vetoEvent;
    }
    _cuts[LooseLeptonVeto]++;

    if (!analyze_CountJets( event, chosenLepton ))
    {
      vetoEvent;
    }
    _cuts[NBJetsGE2]++;
    if (isE) _cuts[NBJetsGE2_Electron] ++;
    if (isMu) _cuts[NBJetsGE2_Muon] ++;
  }

  void finalize_Names()
  {

    for (size_t i = 0; i<Size; i++)
    {
            delete [] _cutNames[i];
    }
    delete [] _cutNames;
    delete [] _cuts;

}

  void finalize_DisplayCuts()
  {
    int count (-1);
    int countIndex( 0 );
    int childCount (0);

```

```
    cout << "[Cut flow without weight]" << endl;
    cout << "--------------------------------------------------------------------" << endl;
    cout << "[#.#] (Cut Descr.|Branch):nEvents ( Parent% /    Total% )" << endl;
    cout << "--------------------------------------------------------------------" << endl;

    for( size_t i=0; i<Size; i++ )
    {
      double percentage = 100.*_cuts[i]/_cuts[TotalEvents];
      double ofParentPercentage = 100. * _cuts[i]/_cuts[countIndex];
      cout.precision( 3 );

      bool isChild = false;
      if (std::string(_cutNames[i]).find('|') != std::string::npos)
      {
    isChild = true;
      }

      if (!isChild)
      {
    count++;
    countIndex = i;
      }

      cout << "[" << count;

      if (isChild)
      {
    cout << "." << childCount;
      }
      else
      {
    cout << "  ";
      }
      cout << "] (" << _cutNames[i] << "): " << setw(6) << _cuts[i] << " (" << setw(7) << ofParentPercentage << "% / " << setw(7) << percentage << "% )" << endl;

      if (!isChild)
      {
    childCount=0;
      }
      else
      {
    childCount++;
      }

    }
    cout << "--------------------------------------------------------------------" << endl;
  }

  void finalize_DisplayJetMultiplicy()
  {
    cout << "[Jet Multiplicy in Merged Channel]" << endl;
    for (int i=4;i<=10;i++)
    {
      cout << "[" << i << "]: " << (long)_nJets[i] << " +- " << (long)sqrt(_nJets_err[i]) << endl;
    }

    cout << "[Jet Multiplicy in E+Jets Channel]" << endl;
```

```
    for (int i=4;i<=10;i++)
    {
      cout << "[" << i << "]: " << (long)_nJetsE[i] << " +- " << (long)sqrt(
    _nJetsE_err[i]) << endl;
    }

    cout << "[Jet Multiplicy in Mu+Jets Channel]" << endl;
    for (int i=4;i<=10;i++)
    {
      cout << "[" << i << "]: " <<(long)_nJetsMu[i] << " +- " << (long)sqrt(
    _nJetsMu_err[i]) << endl;
    }
  }

  void finalize_DisplayResults()
  {
    cout << endl;
    cout << "[Displaying Results]" << endl;
    cout << endl;
    finalize_DisplayCuts();
    cout << endl;
    finalize_DisplayJetMultiplicy();
    cout << endl;
  }

  void finalize()
  {
    if(_nonOneWeights) cout<<endl<<"Warning! This sample has event weights
    different from one! Are you taking it into account?"<<endl<<endl;
    finalize_DisplayResults();
//      finalize_Root();
  }



};

  // The hook for the plugin system
  DECLARE_RIVET_PLUGIN(CMS_2014_ttbarPlusXJets);

}
```